DEVELOPMENT OF NOVEL FRONT CONTACT SILVER PASTES FOR CRYSTALLINE SILICON SOLAR CELLS BASED ON NANOMATERIALS

CHE QUANDE

Ph. D
THE HONG KONG
POLYTECHNIC UNIVERSITY
2013

The Hong Kong Polytechnic University

Department of Building Services Engineering

Development of Novel Front Contact Silver Pastes for Crystalline Silicon Solar Cells Based on Nanomaterials

Che Quande

A thesis submitted in partial fulfillment of the requirements for
the Degree of Doctor of Philosophy

June 2013

CERTIFICATE OF ORIGINALITY

I hereby declare that this thesis is my own work and that, to the best of my knowledge and belief, it reproduces no material previously published or written, nor material that has been accepted for the award of any other degree or diploma, except where due acknowledgement has been made in the text.

I also declare that the intellectual content of this thesis is the product of my own work, even though I may have received assistance from others on style, presentation and language expression.

______________________ (Signed)

Che Quande (Name of student)

Department of Building Services Engineering

The Hong Kong Polytechnic University

Hong Kong, China

June, 2013

ABSTRACT

Crystalline silicon solar cells have attracted significant attention in the past years due to their rich raw materials, low cost and relatively high photo-electric conversion efficiency. Typically, the structure of a crystalline silicon solar cell fabricated on silicon wafer is mainly a *p-n junction*. Metal contacts to both the n- and p-type sides of the junction are used to collect electricity. For commercial crystalline silicon solar cells, metal contacts are usually formed by screen-printing a silver paste which is then densified by a firing treatment process at high temperature.

There are some problems and shortcomings preventing the screen-printed solar cells towards high-efficiency: (i) Due to the significant shrinkage of silver paste during firing treatment, it is difficult to achieve silver electrodes with high aspect ratio. This means that there would be high shading losses caused by a large percentage of front-side metal coverage. (ii) The inferior conductivity of the fired silver paste, which is several times lower than that of pure silver, largely limits the optimization of the metal contacts. In fact, these problems are mainly due to the formulation of the silver paste consisting of a suspension of fine particles of silver and glass frit in organics, which tends to result in non-homogeneous metallization contacts and low conductivity. Therefore, it is necessary to research and develop novel silver pastes based on new components and technologies to overcome the shortages and strive for a breakthrough to get better achievements in the development of high efficiency crystalline silicon solar cells.

The objective of this thesis is to improve the photovoltaic performances of crystalline silicon solar cells by introducing novel front-side silver pastes based on nanomaterials. For better understanding and development of high performance front-side metallization silver pastes for solar cells, all the functional components (i.e. silver particles and glass frit) were prepared in this project. A series of silver pastes based on the as-developed materials were prepared and systematically studied.

Lead-free nano-glass frit powders (NGFPs) were developed for the first time in this project to replace the conventional micron glass frit which tends to result in non-continuous contact formation in Si-Ag alloys. The NGFPs with glass transition temperature (T_g) of 376°C were prepared by sol-gel method from a multicomponent gel in the Bi_2O_3-SiO_2-B_2O_3-Al_2O_3-ZnO system. The X-ray diffraction (XRD) pattern demonstrated that the xerogel was completely converted into amorphous glass after heat treatment at 500°C. To determine the wetting behavior and etching effect of the NGFPs, the test glass paste was prepared and deposited on silicon wafers with SiNx antireflective coating, followed by firing process. Finally, it was found that the NGFPs showed excellent wetting behavior and etching effect on silicon wafers and SiN_x antireflective coating layer. The silver paste containing the as-developed NGFPs was prepared by mixing the NGFPs, silver particles and organic vehicle with the ratio of 4/80/16 (wt%) using a rotary evaporator and a three-roll mixer. In the *I-V* measurement, the fabricated solar cell based on the NGFPs showed higher conversion efficiency (15.7%) than that (14.6%) resulting from the reference sample (solar cell containing conventional micron glass frit).

Besides, spherical silver nanoparticles (SSNPs)-aided silver pastes were developed using the SSNPs as a sintering aid. High-dispersive SSNPs were prepared by the solvothemal method. The silver pastes composed of micron silver particles (70 wt%), the SSNPs with an average size of 50nm (10 wt%), lead free glass frit (4 wt%) and organic vehicle (16 wt%) were screen-printed on single crystalline silicon wafers with SiN_x antireflective coating, followed by firing treatment and tests. The experimental results demonstrated that the SSNPs with high surface energy are favor to the sintering of micron silver particles. Moreover, the size and numbers of pores in the silver thick films were reduced due to the SSNPs's unique sintering behavior, contributing to better conductive network. In the *I-V* measurement, the fabricated solar cell based on the SSNPs-aided silver paste exhibited higher conversion efficiency (16.1%) than that (15.4%) resulting from the reference sample (solar cell containing no SSNPs).

Moreover, silver nanowires (SNWs)-aided silver pastes were also developed by adding the SNWs into micron silver particles. The SNWs were prepared by reducing $AgNO_3$ with ethylene glycol in the presence of Pt seeds and polyvinylpyrrolidone (PVP). Pt nanoparticles as crystal seeds play a crucial effect on the anisotropic growth of silver nanowires. The silver pastes composed of micron silver particles (70 wt%), SNWs (100nm to 200nm wide and 0.5μm to 4μm long, 10 wt%), lead free glass frit (4 wt%) and organic vehicle (16 wt%) were screen-printed on single crystalline silicon wafers with SiNx antireflective coating, followed by firing treatment and tests. The fabricated solar cells based on the SNWs-aided paste generated an open-circuit voltage (V_{oc}) of 621mV, a short-circuit current density (J_{sc}) of 34.3mA/cm^2, a fill factor (FF) of 74.1% and a conversion efficiency (E_{ff}) of 15.8%. The solar cell performance improvement could be attributed to unique electronic property and "bridge-effect" of the one-dimensional (1-D) metal nanostructures.

In addition, to further improve the photovoltaic performances of crystalline silicon solar cells, the agglomeration of silver particles in the front-side paste should be resolved. In this thesis, high-dispersive spherical micron silver particles were developed in hot ethylene glycol. Experimental results demonstrated that the polyol process tends to obtain silver particles with better dispersibility compared with the aqueous reduction system. The silver pastes composed of high-dispersive silver particles with an average size of 0.5μm (80 wt%), lead free glass frit (4 wt%) and organic vehicle (16 wt%) were screen-printed on single crystalline silicon wafers with SiNx antireflective coating, followed by firing and tests. The fabricated solar cell based on the as-developed high-dispersive silver particles generated a conversion efficiency of 16.4%.

In summary, the novel developments and their processes of the developed silver pastes reported in this thesis demonstrate that the optimum formulation for better conductivity and continuous contact formation of the silver front-side paste for crystalline silicon solar cells could be made by addition of silver nanoparticles and adoption of nano-glass frit and high-dispersive silver particles. Moreover, the results provide a basic understanding and development of synthesis of silver particles with various shapes in different sizes and nano-glass frit powders, which have also great potential for applications in conductive inks, adhesives and pastes for electronic devices.

Keywords: crystalline silicon solar cells, silver, glass frit, paste, photovoltaic, nanoparticle, nanowire, nanomaterial, solvothermal, polyol, sol-gel.

PUBLICATIONS DURING PHD STUDY

Journal papers during PhD study:

1. **Quande Che**, Hongxing Yang, Lin Lu, Yuanhao Wang, A new environmental friendly silver front contact paste for crystalline silicon solar cells. Journal of Alloys and Compounds. 2013. **549**: 22-25.
2. **Quande Che**, Hongxing Yang, Lin Lu, Yuanhao Wang, Nanoparticles-Aided Silver Front Contact Paste for Crystalline Silicon Solar Cells. Journal of Materials Science: Materials in Electronics. 2013. **24**: 524-528.
3. **Quande Che**, Hongxing Yang, Lin Lu, Yuanhao Wang, One-Step Synthesis of Hybrid Silver Particles for Front Contact Paste for Crystalline Silicon Solar Cells. Electronic Materials Letters. 2013.**9**: 353-356.
4. **Quande Che**, Hongxing Yang, Lin Lu, Yuanhao Wang, Preparation of Lead-free Nano Glass Frit Powder for Crystalline Silicon Solar Cells. Applied Energy. 2013, **112**: 657-662.
5. **Quande Che**, Hongxing Yang, Lin Lu, Yuanhao Wang. Pt nanoparticles-assisted route for shape-controlled synthesis of branched silver nanowires and their application in silver front contact paste for crystalline silicon solar cells. Chemical Communications. (Under preparation).
6. Yuanhao Wang, Lin Lu, Hongxing Yang, **Quande Che**, Development of high dispersed TiO_2 paste for transparent screen-printable self-cleaning coatings on glass. Journal of nanoparticle research. 2013.**15**: 1384-1389.

Conference papers during PhD study:

1. **Quande Che**, Hongxing Yang, Lin Lu, Yuanhao Wang. Preparation of lead-free glass frit powder for crystalline silicon solar cells. The 4th International Conference on Applied Energy. July 5-8, 2012 Suzhou, China

Patents:

1. **Quande Che**, Hongxing Yang, Lin Lu, Yuanhao Wang. Preparation of a new environmental friendly nano glass frit powder and its application in crystalline silicon solar cells. The Hong Kong Polytechnic University. (Under Preparation)

ACKNOWLEDGEMENTS

This thesis was completed under the guidance and with the help of a considerate number of people. It is my great pleasure that I have now the opportunity to express my sincere gratitude for all of them.

First and foremost, I would like to express my greatest gratitude to my chief supervisor, Professor Yang Hongxing, for his invaluable guidance, supervision, support and overly enthusiasm throughout my research period. Professor Yang has given me a lot of encouragement and valuable suggestions whenever I need help during the whole PhD study.

I would also like to acknowledge my co-supervisor, Dr. Lu Lin, who gave me a lot of helpful advice and kept an eye on the progress of my research work during my PhD study.

I would also like to express my gratitude to all the members in the Renewable Energy Research Group (RERG) for their assistance, accompany and advice throughout my research work.

A special thank to my beloved family for their endless love, understanding, encouragement and support throughout the whole research period. This thesis is dedicated to all of them.

TABLE OF CONTENTS

LIST OF FIGURES

LIST OF TABLES

LIST OF ABBREVIATIONS AND NOTATION

EG: ethylene glycol

FCC: face-centered cubic

FESEM: field-emission scanning electron microscopy

PVP: polyvinylpyrrolidone

RoHS: restriction of Hazardous Substances

SEM: scanning electron microscopy

STC: standard testing conditions, solar radiation of 1000W/m^2 and temperature of 25 °C

TGA/DSC: thermogravimetric analysis/ Differential scanning calorimeter

XRD: x-ray diffraction

d: the value of interplanar spacing

D: the diameter size of silver particles

FF: fill factor

J_{sc}: short-circuit current

V_{oc}: open-circuit voltage

T_g: glass transition temperature

T_m: melting point of a spherical particle with radius r

T_0: melting temperature of the bulk

λ: wave length of X-ray,

β: full width at half maximum of the diffraction peak (FWHM),

θ: diffraction angle

γ_{sl}: solid-liquid interfacial energy

ΔH_m: bulk latent fusion heat.

η: conversion efficiency

CHAPTER 1 INTRODUCTION

1.1 Crystalline silicon solar cells

With the rapid development of world economy, the earth's conventional energy reserves are exhausting fast. It is urgent to find the substitute of non-renewable energy resource. Solar energy is generally regarded as the most promising renewable energy for the future. Among many kinds of solar energy applications, crystalline silicon solar cells have attracted significant attention in the past decades due to their high photo-electric conversion efficiency and reliable large-scale production **[1-6]**.

1.1.1. Basic principle

Typically, the structure of an industrial crystalline silicon solar cell fabricated on p-type silicon wafer is shown in **Figure 1.1**. When photons hit on the silicon solar cell, they will be absorbed by the silicon in the p-layer. The solar energy will be transferred from the photons absorbed in the silicon crystalline lattice to electrons. After receiving the energy which is greater than that of the silicon band gap, the electrons probably leave the silicon atoms, instead of bounding tightly in the covalent bonds. Namely the electrons are excited from the valence band into the conduction band. At the same time, a hole is formed in the covalent band where the atom losing an electron. Finally, the electron-hole pairs are formed in the silicon solar cells. Subsequently, the electron-hole pairs separate under the force of electric filed in the diode which is formed by a thin n-type emitter layer and a thick p-type base substrate. This is well known as a *p-n junction*, as shown in **Figure 1.2**. The current flow generated by converting solar irradiation to electrons can be extracted at the front and back side contact through an external load. To make an efficient silicon solar cell, many methods were used to maximize the conduction, including maximizing absorption, minimizing reflection and recombination. Specifically, the emitter surface is usually textured and at the same time an antireflective coating layer is applied to reduce the optical losses on the front side of silicon solar cells.

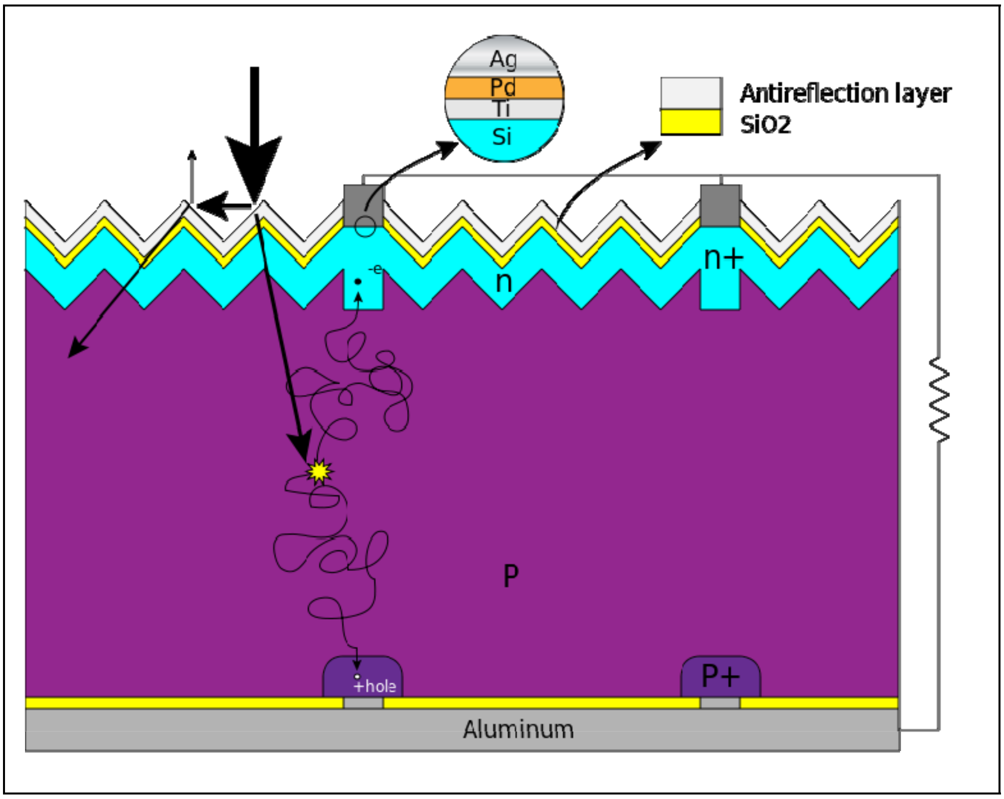

Figure 1.1 Basic structure of a crystalline silicon solar cell and its working mechanism. The photon-generated electron-hole pairs are separated by the force of built-in electric field, and extracted via the metal contact through external load [7]

1.1.2 Current-voltage characteristic

As mentioned above, as an optoelectronic device, a crystalline silicon solar cell works due to the incident irradiation of sunlight on the surface of the semiconductor with a p-n junction. The absorbed photons generate electron-hole pairs, which are separated by the built-in electric field. A voltage is generated at the same time, which is also known as *photovoltaic effect*. Then a current flow will be generated if there is an external load connected to the solar cell. There is no doubt that the most important performance parameter of a silicon solar cell is the energy conversion efficiency, which demonstrates the fraction of the incident sunlight irradiation being converted into electricity. It is usually determined by three important parameters: the open-circuit voltage (V_{oc}), the short-circuit current (J_{sc}) and the fill factor (FF)，as shown in **Figure 1.3**.

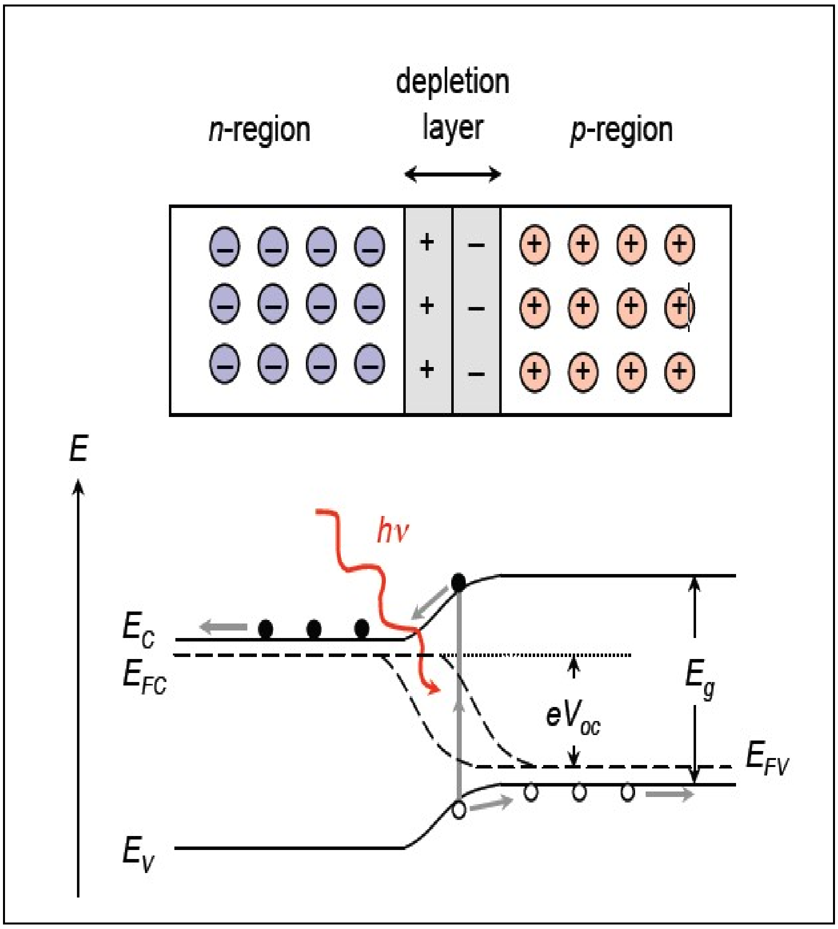

Figure 1.2 Energy band diagram (*P-N junction*) of crystalline silicon solar cells [8]

The energy conversion efficiency (η) of a crystalline silicon solar cell is defined as the ratio of the maximum output P_{max} to the total power of incident sunlight irradiation P_{in}, given by the following equation. It is usually measured at the standard testing conditions (STC): solar radiation of 1000W/m^2 and temperature of 25 °C.

$$\eta = \frac{J_{sc} \cdot V_{oc} \cdot FF}{P_{in}}$$

where P_{in} represents the incident sunlight irradiation on the silicon solar cells. The FF is the indication of the 'squareness' of the voltage-current curve of the silicon solar cells, which is given by the following equation:

$$FF = \frac{V_{mp} I_{mp}}{V_{oc} I_{sc}}$$

where V_{mp} and I_{mp} represent the voltage and current at the maximum power point, respectively.

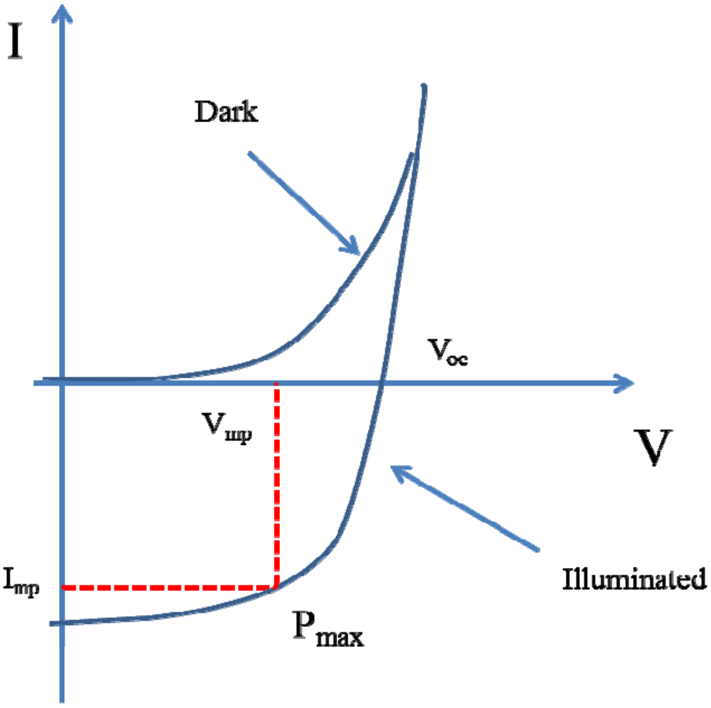

Figure 1.3 *I-V* characteristic of crystalline silicon solar cells under illumination and in the dark [9]

1.1.3 Factors affecting energy conversion efficiency

A large part of the energy from the sun irradiation hitting on a crystalline silicon solar cell is wasted instead of being converted into electrical power. This is mainly ascribed to the natural instincts of materials, which somewhat limit the conversion efficiency of a solar cell. First of all, wavelength of light, i.e. photo energy is a major factor. Due to different wavelengths, many outcomes would be possible when photons hit on silicon solar cells. Only a small part of photons with special wavelengths are absorbed by the silicon and subsequently generate electron-hole pairs. In crystalline silicon, there is a minimum energy required to generate electron-hole pairs, named "bandgap". The photons with the energy higher than the minimum energy can excite electrons from the valence band into the conduction band. Moreover, the excess part of photo energy will be wasted, which means that a photo even with higher energy than the required minimum energy can only generate one electron. Besides, the other photos are either being reflected or being absorbed but cannot generate electron-hole pair, or even pass through the silicon wafer.

In fact, even though the electrons and holes could be generated if the photos have appropriate energy. It does not necessarily to obtain electricity due to the recombination of the pairs before they are separated and conduct into the circuit. There are some other factors effecting conversion efficiency, including natural resistance, temperature, and electrical resistance due to the metal contact and other manufacturing processes. Therefore, these factors mentioned above should be taken into account to obtain high efficiency silicon solar cells, especially the metal contact, which is an important factor.

1.2 Thick film metallization technologies

Metallization contacts play a key role in efficiency-improving and cost-control in solar cell processing. World record photo-electric conversion efficiency of 25% on mono-crystalline silicon has been achieved with photolithography (PL) contacts.

Although PL and metal deposition are the well-established techniques for metallization contacts of crystalline silicon solar cells, they are time-consuming and expensive due to their complicated process and vacuum requirement. As a fast and reliable technique, thick-film metallization has been applied in the silicon solar cell industry for many years due to its simple equipment, easy operation and reliable large-scale production. The current industrially fabricated silicon solar cells are most commonly fabricated using this method to deposit silver paste on silicon wafers to form front-side metallization contacts. Thick film metallization contacts can be obtained by deposing silver pastes or ink on silicon wafers in several ways **[10-28]**. In this subsection the most common processes are presented.

1.2.1 Screen-printing

As a fast and reliable technology, screen-printing has been applied in crystalline silicon solar cells for many years. This technology are most commonly used to deposit silver paste on silicon wafers with antireflective coating to form front metallization contacts for the current industrially fabricated silicon solar cells. Therefore, all solar cells fabricated in this work were metallized using the screen-printing technology.

The basic working principle of screen-printing is not complicated. The silver paste is forced through openings of the emulsion layer on a screen by a squeegee onto the surface of silicon wafers, as shown in **Figure 1.4**. Specifically, silver paste is deposited by screen-printing using certain stainless-steel-wire mesh screen, which is then densified by fire processing in an infrared belt furnace. Then the metallization contacts are formed, which collect the current from the silicon solar cell and transfer it to the silver “busbars” connected to the external load.

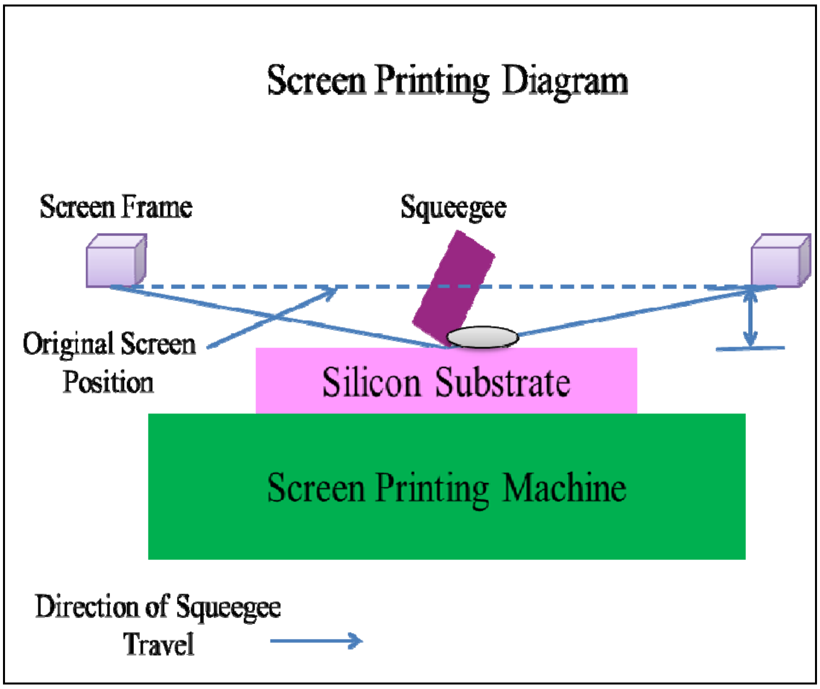

Figure 1.4 Schematic diagram of the screen-printing process for metallization of crystalline silicon solar cells [30]

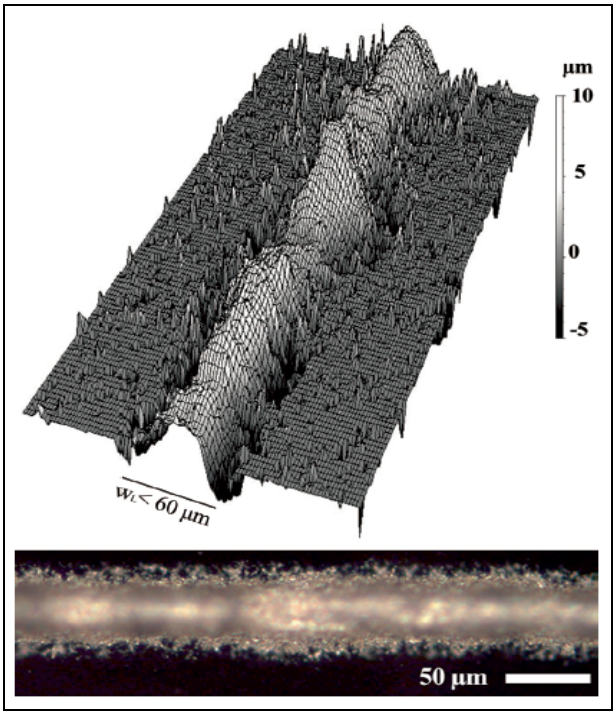

Figure 1.5 3D-topview microscopic graph of a fine electrode deposited by screen-printing on C_z-silicon surface with a width about 50µm [31]

The minimum width of the silver electrodes formed by screen-printing is determined by the wire mesh size of the screen. The minimizing the width is an important factor affecting the light absorption of the silicon solar cells, which consequently influences the conversion efficiency. In order to obtain maximum light absorption and minimum line resistance, it is necessary to optimize the screen design and the formulation of silver paste, which will be discussed in later sections. As for the industrial screen-printed crystalline silicon solar cells, the width of silver electrodes are typically more than 100μm in the last decades **[29]**. However, it has been improved to be about 50μm recently, as shown in **Figure 1.5**.

There are three other factors affecting the photovoltaic performance of the industrial screen-printed silicon solar cells. The first one is the height-to-width aspect ratio. As we discussed above, the front-side silver fingers can cause shading loss. In order to reduce the shading loss, one method is to decrease the width of the silver fingers. However in this case, the line conductivity would also decrease for the same height. Therefore, it is necessary to prepare narrow and high silver fingers, i.e. with high aspect ratio. The second one is the line resistance of the fine silver electrodes which is mainly related to the silver paste, including the purity of compositions, size of particles, and formulations. The third is the contact resistance, which is determined by the firing processing and the composition of glass frit in silver paste. In summary, these are the main issues regarding the preparation of optimal silver pastes to reduce the energy losses.

1.2.2 Stencil-printing

Stencil printing is a technology mainly applied in the printed circuit boards, which is applied on the front metallization of crystalline silicon solar cells in recent years [32, 33]. Compared to the screen-printing, the only difference is only that the stainless steel wire mesh screen is substituted by metal stencils for printing the silver paste on the surface of silicon wafer, as shown in **Figure 1.6**.

The main advantage is that the silver fingers deposited by stencil printing are easy to obtain higher height-to-width aspect ratio compared to screen-printing [34]. However, there are still some problems with the stencil printing for large-scale application, mainly due to the stability of the stencils, especially on the silicon wafers with textured surfaces.

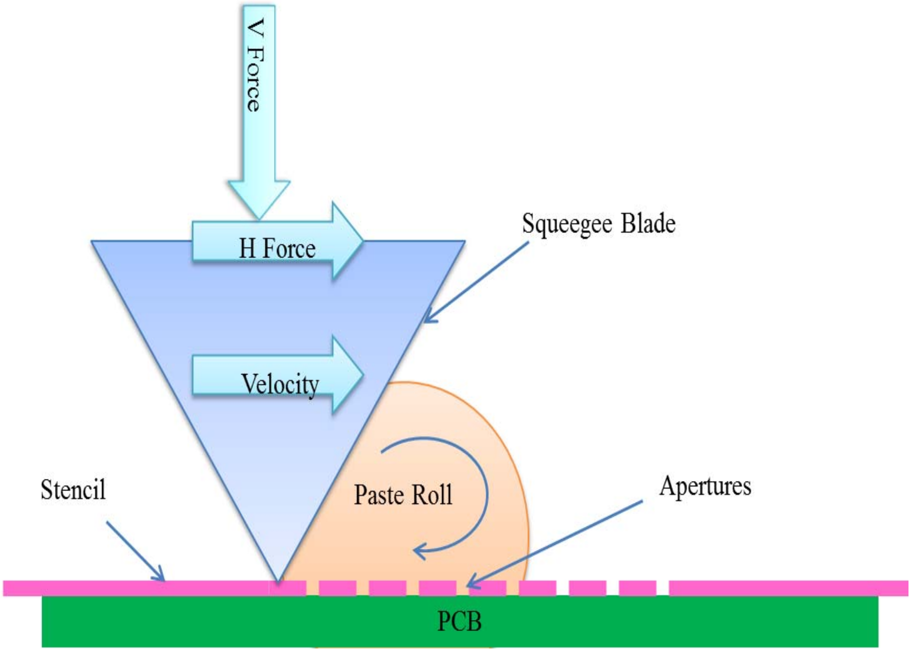

Figure 1.6 Schematic diagram of the stencil-printing process for metallization of crystalline silicon solar cells [35].

1.2.3 Pad-printing

Pad-printing, like screen-printing has already been applied in crystalline silicon solar cells as a reproduction and reliable technology. The Frannhofer ISE has investigated extensively the application of pad-printing in the front-contact metallization of crystalline silicon solar cells [36-38]. The pad-printing process is demonstrated in **Figure 1.7** [39]. Compared to the screen-printing, an advantage of pad-printing is that it has the possibility to print silver paste on uneven silicon materials like EFG [40, 41].

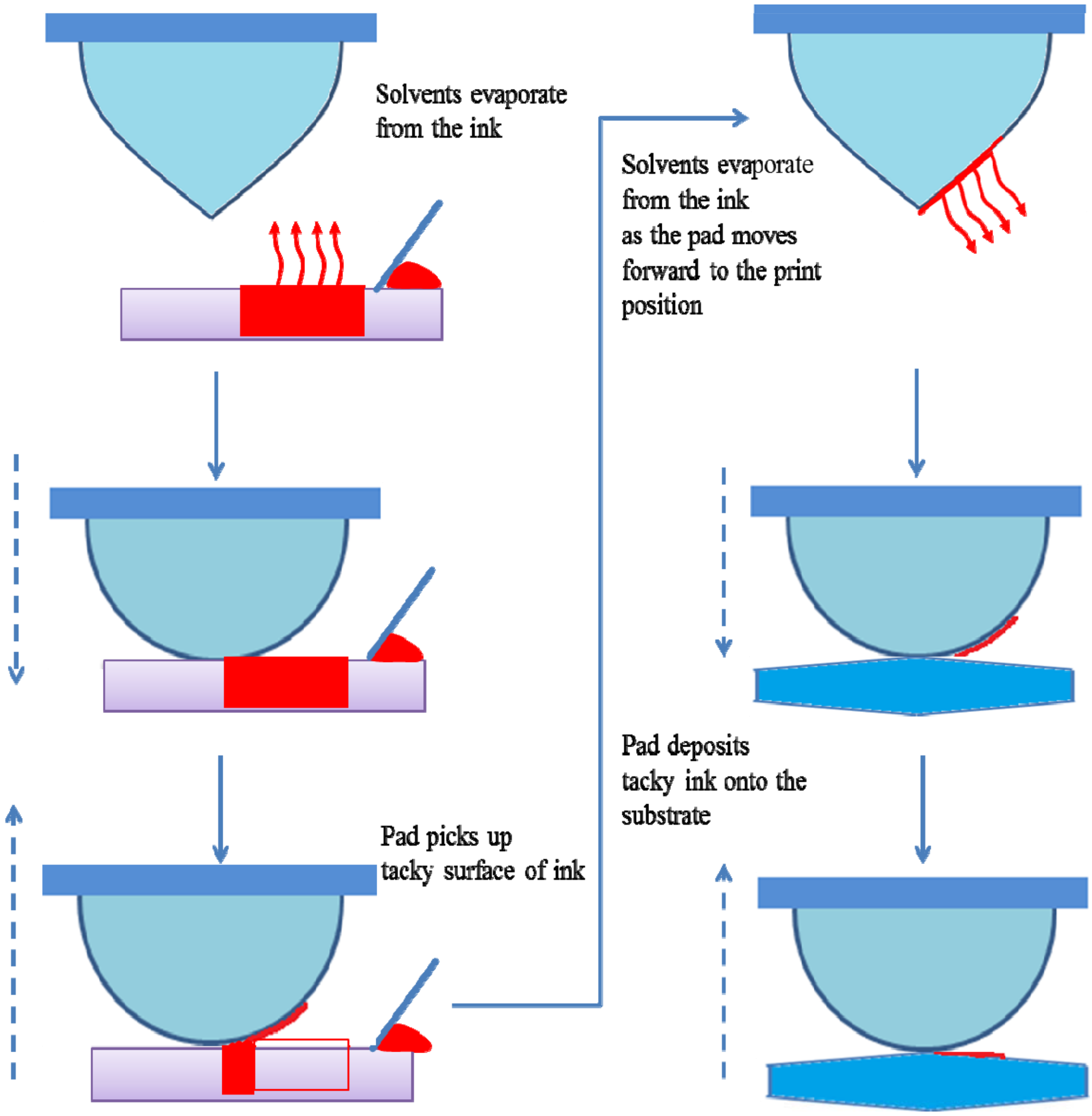

Figure 1.7 Schematic diagram of the pad-printing process for metallization of crystalline silicon solar cells [39].

Moreover, silver fingers with the width less than 50µm can be deposited by pad-printing on front surface of silicon solar cells, as shown in **Figure 1.8**. However, there are still some problems with the pad-printing for large-scale application, mainly due to its inhomogeneity of printing pressure with the increasing of pad size.

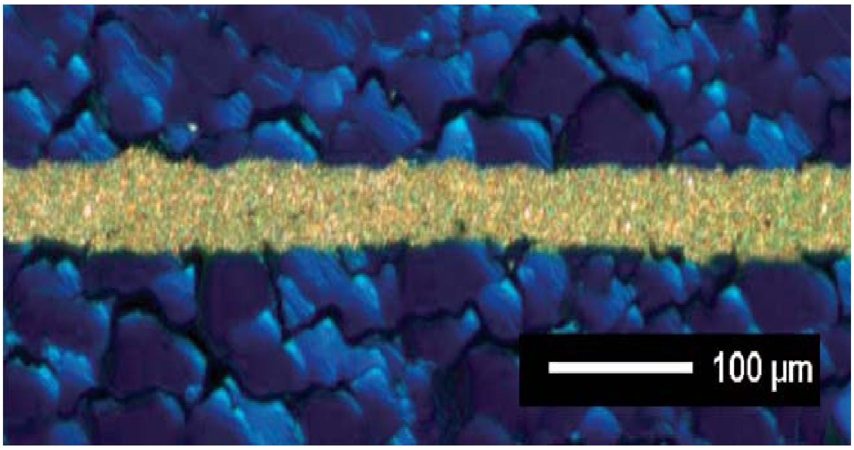

Figure 1.8 Graph of a fine silver finger with a width less than 50µm deposited by pad-printing on the front surface of silicon wafer [41]

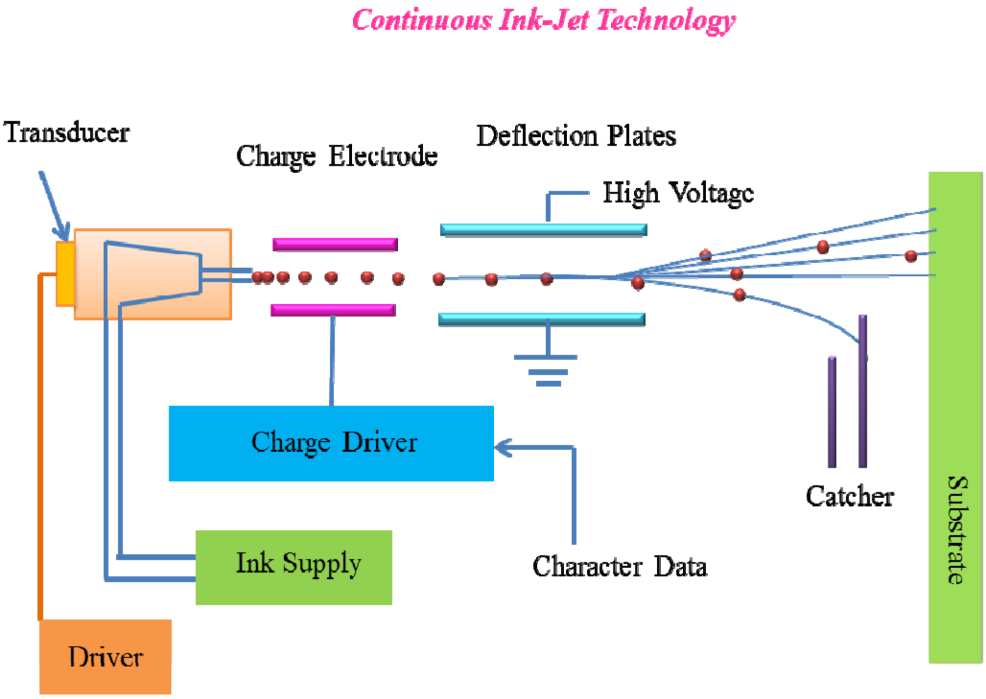

Figure 1.9 Schematic diagram of the ink-jet printing process for metallization of crystalline silicon solar cells [45]

1.2.4 Ink-jet printing

In the past years, as a promising technique for metallization contact of crystalline silicon solar cells, ink-jet printing gained great attention for its various advantages compared to other printing processes such as screen-printing, stencil-printing and pad-printing. The process of ink-jet printing is demonstrated in Figure 1.9. The main advantage of ink-jet printing is that the ultra-fine fingers with a width less than 20 μm can be achievable [42-44]. Besides, it is a non-contact process, which is a great advantage compared to other contact technologies. It can be applied to any substrates regardless of morphology, thickness composition or other properties.

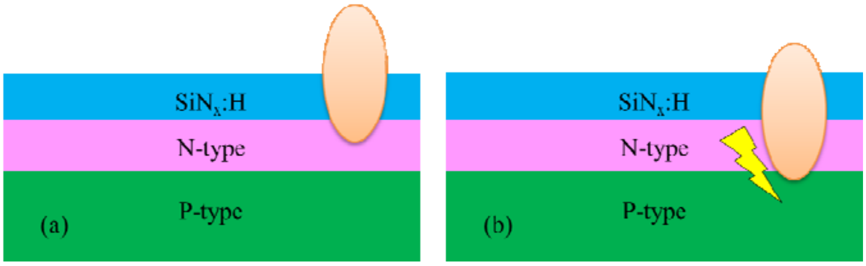

Figure 1.10 The contact between the silver and the N-type silicon (a), and the internal short circuit effect between the P/N junction (b)

1.3 Thick film metallization pastes

1.3.1 Conventional silver front contact paste composition

The silver paste for crystalline silicon solar cells usually contains three principal constituents: silver particles, glass frit powders, and organic binder [46-50]. Among them silver particles and glass frit are the functional materials, both of which are usually micrometer grade. The micromaterials tend to leads to non-homogeneous metallization contact and low conductivity of silver electrodes.

Although the exact formulation of the commercial silver paste is industrial secret, it is generally composed at certain ratio in a typical silver paste, as shown in **Table 1.1**. Silver particles typically represent 70-85% in weight of the paste with a mixture of various shaped particles (predominantly spherical) in micro-size meter, which are responsible for the conductivity. As mentioned above, silver is the best choice for the front contact metallization paste for crystalline silicon solar cells, and has been commercialized by many companies for several years due to its excellent conductivity.

Table 1.1 Typical compositions of silver front contact paste

Components	Silver particles	Glass frit	Organic binder	Solvent
(wt.%)	70-85	2-5	3-15	5-15

The rest of the silver paste compositions, glass frit and resin binder are extremely sensitive to the quality of front metallization contact in crystalline silicon solar cells. The glass frit in the silver front contact paste is regarded as the most important component for obtaining high performances of silicon solar cells with low contact resistance and high conversion efficiency, although it only represents 2-5% in weight in the silver paste. On one hand, as an inorganic binder, the glass frit determines the mechanical performance (adhesion strength) of the silver electrodes to silicon substrate. On the other hand, the glass frit plays a critical role in the sintering process of silver particles and the formation of front metallization contact. Specifically, it serves as a medium for silver particles to recrystalline and form the silver /silicon ohmic contact on the silicon emitter contact during the firing process. The firing process determines the line conductivity of silver fingers and contact resistances **[51]**.

Therefore, in a front contact silver paste for crystalline silicon solar cells, special glass frit with certain chemical composition and thermal property is required. Typically, the glass frit with low glass transition temperature is required, for example, lead borosilicate glass, allowing for the temperature of peaking fire process below 850°C **[52]**. Two examples of different glass frit for silver front contact paste are presented in **Table 1. 2**.

Table 1.2 Compositions of two glass frit examples in silver front contact paste for crystalline silicon solar cells, (wt %) **[53]**

Glass	Paste 1 Phosphate glass based	Paste 2 Borosilicate glass based
Al_2O_3	11.6	14.6
B_2O_3	--	2.1
BaO	0.2	--
CdO	--	0.6
CaO	8.6	0.2
CuO	7.7	0.6
Fe_2O_3	1.4	--
Na_2O	4.1	--
P_2O_5	65.8	4.4
PbO	--	51.8
SiO_2	0.61	25
ZnO	--	0.8

1.3.2 Nanomerials for silver paste

It is well known that nanomaterials exhibit many novel unique properties, which widely broaden the applications of conventional bulk materials. From micro-size to nanoscale, the performance of materials changes significantly. For example, reducing silver particles from micron-size to nanoscale can improve their sintering characteristic, leading to excellent sintering activity at dramatically low temperature. This behavior can be ascribed to the high surface energy of silver nanoparticles. In fact, the melting temperature of a material depends significantly on particle size. The melting point of silver particles decreases with the particle size, especially when the size is less than 50nm, which will be discussed in the later section of this thesis. Except for the unique sintering behavior, silver nanoparticles also exhibit excellent thermal, electrical, optical and catalyzing properties due to their nano-size effects. Therefore, silver nanoparticles have attracted great attention in past years, and been widely applied in the fields of electronics, optoelectronics, biomedicine, catalysis and so on **[54-58].**

In the field of electronics, silver nanoparticles are usually used as the conductive phase to formulate conductive inks, adhesives, and pastes due to their excellent conductivity and sintering characteristics **[59-61]**. Park et al. reported that the printed silver thick film resulting from the silver paste prepared using silver nanoparticles showed high conductivity although it was sintered at low temperature **[62]**. However, most of the current silver nanopastes are usually applied in semiconductor device interconnection or fine electronic circuit pattern formation. To the best of our knowledge, only a handful studies have been conducted on the application of silver nanoparticles in silver front contact paste for crystalline silicon solar cells. As a special silver paste for crystalline silicon solar cells, which is sintered at high temperature, namely near 850°C, it is worthy of being investigated for low-temperature sintering and high conductivity. Furthermore, the agglomeration of silver nanoparticles is a key issue for their application in silver paste. It tends to form inhomogeneous thick film metallization, which in turn results in inferior conductivity and poor photovoltaic performance of solar cells. Therefore, it is necessary to solve the agglomeration behaviour of silver nanoparticles for high performance silver front contact paste. Except for silver nanoparticles, one-dimensional (1-D) silver materials, such as nanorods, nanotubes and nanowires have drawn much attention for their unique electronic performance and great potential application in conductive paste for electronic devices [63-65]. It was reported that silver nanowires improved the system containing micron silver particles by a small amount addition, in which silver nanowires tend to act as bridges to form linkages between micron silver particles, increasing the contact opportunities of particles [66]. In this thesis, the synthesis of silver particles and nanowires would be studied, as well as their application in silver front contact paste, to develop novel silver paste based on nanomaterials for crystalline silicon solar cells.

Therefore, it could be preliminarily deduced that the crystalline silicon solar cells fabricated using silver front contact paste containing silver nanoparticles tend to show better sintering behaviour and higher photovoltaic performance than those of solar cells resulting from silver paste containing single micron silver particles.

In addition, as a crucial component in silver front contact paste, the current glass frit in silver front contact paste are usually micrometer grade, which tends to result in non-continuous contact formation in Si-Ag alloys. It is reported that the silver front contact paste prepared using the glass frit with a smaller mean size tends to result in a higher photo-electrical conversion efficiency [67]. However, although there are many reports on preparation of glass frit for silver front contact paste, many shortcoming and problems exist due to their less experience or complicated experimental conditions for optimizing the formulation of silver paste. The current reported glass frit for silver front contact paste is usually made by the conventional melting route, which have many drawbacks, hindering the optimization of the silver paste. To overcome the drawbacks of the conventional glass frit, the goal of this study is to develop nano glass frit for the first time for silver front contact paste. More details will be presented later in this thesis.

1.3.3 Firing process and sintering theory

After screen-printing, the crystalline silicon solar cells need to be fired in a conveyor infrared belt furnace in an industrial process environment to form the metallization contact. The firing treatment basically includes three steps as follows: at the first step, all the solvents are dried to evaporate, which is done at about 150 °C. The purpose of this step is to prevent the formation of gas bubbles and subsequent cracking in the films during high temperature firing, which leads to cracking of the thick films. In the second step, the resin binders are burn out at temperature of about 350 °C; during the final step, silver electrodes forms and adheres to the silicon wafers, which is done at about 850 °C. The temperature profile of the firing process is demonstrated in **Figure 1.11**.

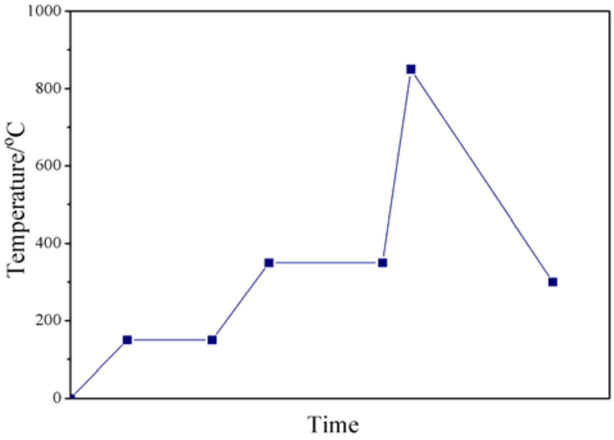

Figure 1.11 Schematic diagram of the temperature profile of silicon solar cells during firing process in a conveyor infrared belt furnace

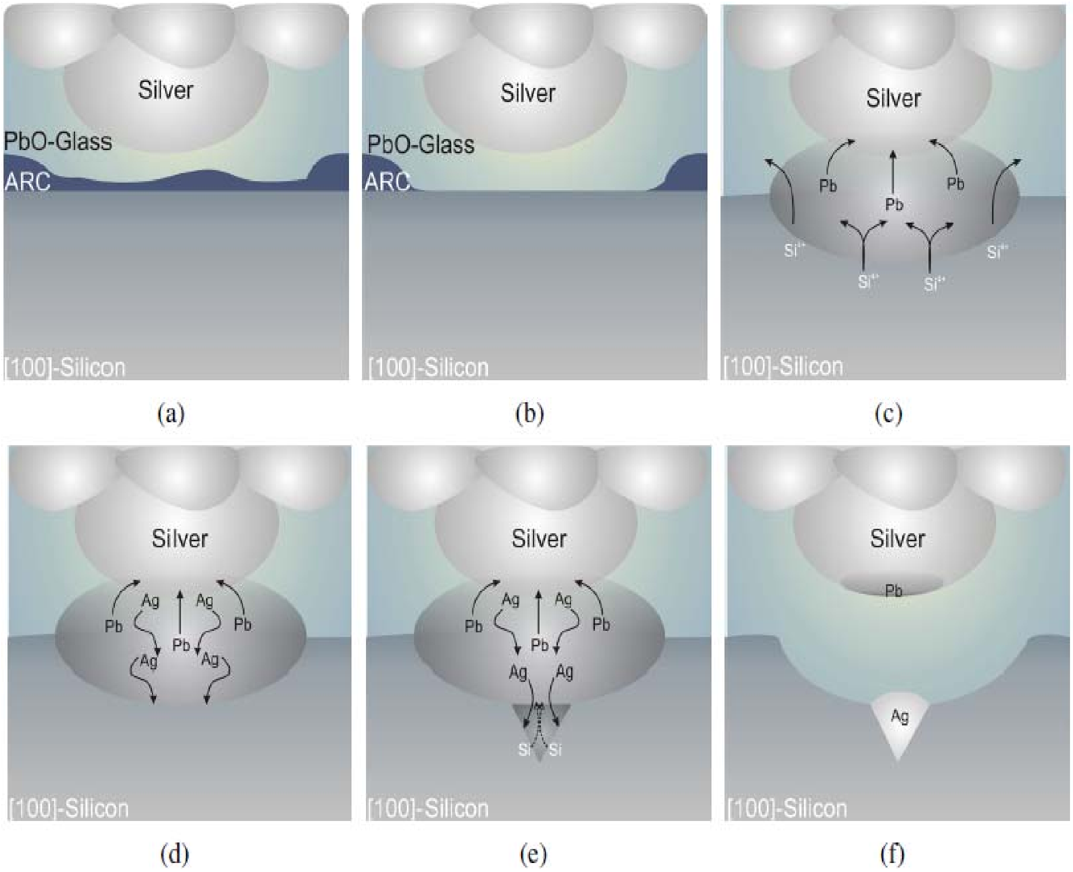

(a) (b) (c)

(d) (e) (f)

Figure 1.12 Model of the formation of front metallization contact as published by Schubert, demonstrating the sintering mechanism of silver paste [75]

During high temperature sintering process, the viscosity of glass frit with low glass transition temperature decreases sharply, and soon the glass frit is changed into fluid phase. It is assumed that during this process, silver, even and silicon are dissolved in the glass phase [68-72]. With the cooling down of glass phase, silver particles start to grow into silicon and form several small silver pyramids finally at the silicon emitter [73]. At the same time silicon recrystallizes epitaxially. It is also assumed that the liquid glass etches silicon wafer via redox reactions, and the Si functions as a reducing agent [74]. The microstructure of the emitter layer determines the contact quality, especially contact resistance and adhesion strength. Therefore, the wetting behavior and etching effect of the glass frit powder on silver particles and silicon wafer are important to form a good metallization contact. Schubert studied the mechanism of metallization contact formation of silicon solar cells based on PbO glass frit, which is illustrated by a model, as shown in **Figure 1.12** **[75]**. Similar results were reported by Hilali et al. **[76].**

1.4 Motivation and objectives

For wide application of crystalline silicon solar cells, it is necessary to reduce the fabrication cost. Undoubtedly, increasing the conversion efficiency of solar cells is one of the most effective methods to reduce the cost. As mentioned above, thick silver films are widely used for the metallization front contact in crystalline silicon solar cells for their many advantages. Besides, they play a key role in improving conversion efficiency of solar cells. Therefore, optimizing the front metallization contact of solar cells becomes a hot research topic for its great potential to improve the conversion efficiency of crystalline silicon solar cells.

At present, there are some problems and shortcomings preventing the screen-printed solar cells from achieving high-efficiency: (i) Due to the significant shrinkage of silver paste during firing process, it is difficult to achieve silver electrodes with high aspect ratio by screen-printing technique. This means that there would be high shading losses caused by large percentage coverage of the front-side silver fingers. (ii) The inferior conductivity of the fired silver paste, which is several times lower than that of pure silver, largely limits the optimization of the metal contacts. In fact, these problems are mainly due to the formulation of the silver paste consisting of a suspension of fine particles of silver and glass frit in organics, which tends to result in non-homogeneous metallization contacts and low conductivity. Therefore, it is necessary to research and develop novel silver pastes based on new components and technologies to overcome the shortages and strive for a breakthrough to get better achievements in the development of high efficiency crystalline silicon solar cells.

The objective of this thesis is to improve the photovoltaic performances of crystalline silicon solar cells by developing novel front-side silver pastes based on nanomaterials. For better understanding and development of high performance front-side metallization silver pastes for solar cells, all the functional components (i.e. silver particles and glass frit) will be developed in this project. A series of silver pastes based on nanomaterials will be prepared and systematically studied.

The objectives of this thesis are summarized as follows:

(1) Develop the front contact silver paste for crystalline silicon solar cells based on lead free glass frit powders to overcome lead pollution.

(2) Develop the front contact silver paste for crystalline silicon solar cells based on nano-glass frit to achieve low resistance and high conversion efficiency.

(3) Develop the front contact silver paste for crystalline silicon solar cells based on high-dispersive silver particles to obtain homogenous continuous thick film and high conversion efficiency.

(4) Increase line conductivity of silver electrodes by introducing silver nanoparticles and silver nanowires synthesized by the solvothermal method.

(5) Improve the overall performances of crystalline silicon solar cells by optimizing the formulations of the silver front contact paste.

1.5 Methodology

As mentioned above, there are three main components in the silver front contact paste for crystalline silicon solar cells: silver particles, glass frit powders and organic vehicles. Silver particles and glass frit are the functional materials, serving as conductive phase and inorganic binder, respectively. In this study, all the key functional materials will be synthesized by ourselves for better understanding and development of optimal silver paste. Furthermore, nanomaterials will be synthesized and introduced into the silver paste to improve the sintering characteristic of silver paste. Meanwhile, the products will be compared with the conventional silver paste based on micron materials to optimize the formulations of silver paste. **Figure 1.13** shows the overall research methodology and flow chart of this study.

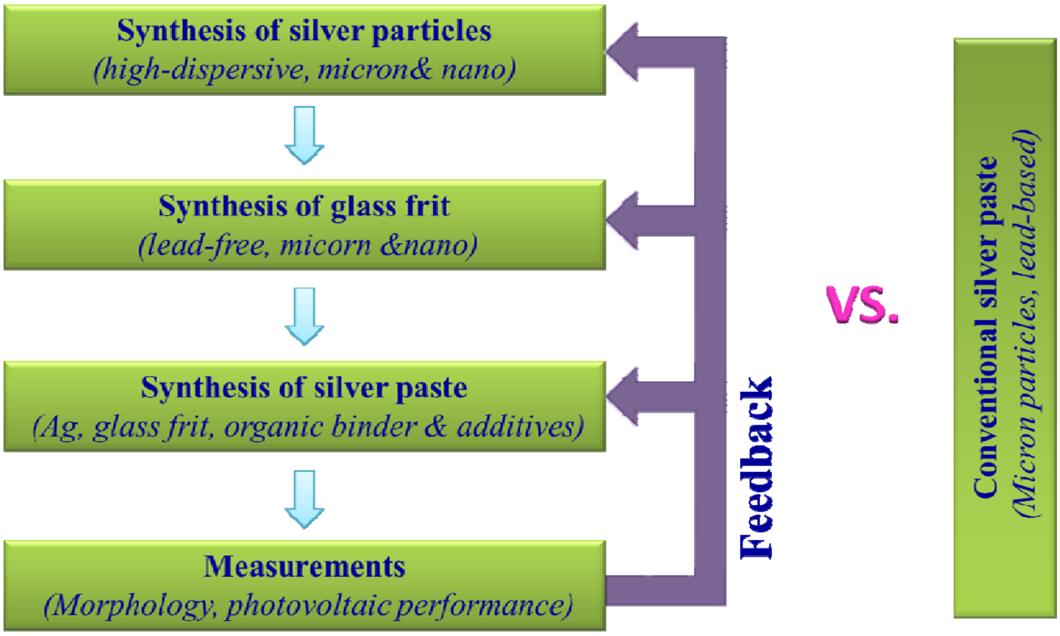

Figure 1.13 The research methodology and flow chart of this study

Specifically, silver particles will be synthesized both in micron meter and nanometer. Traditional liquid-solution chemical reduction method and polyol process will be chosen to synthesize micron silver particles. Silver nanoparticles will be synthesized by the solvothermal method. Similarly, lead-free glass frit powders both in micron meter and nano meter will be synthesized by traditional melt cooling route and sol-gel method, respectively. Then the silver paste will be prepared by mixing the as-prepared silver particles, glass frit powders and organic vehicles using the rotary evaporation method. The performances of fabricated crystalline silicon solar cells based on the silver pastes will be feedback to each step for optimization. Meanwhile, the developed silver paste will be compared with the commercially available conventional silver paste usually based on micron particles and lead-based glass frit powders. Finally, the optimal silver front contact paste for crystalline silicon solar cells will be obtained.

References

[1] J. Zhao, A. Wang, P. Campbell, and M. A. Green, A 19.8% efficient honeycomb multicrystalline silicon solar cell with improved light trapping. *IEEE Transactions On Electron Devices*, 1999. **46**: 1978-83.

[2] M. Tanaka, S. Okamoto, S. Tsuge, and S. Kiyama, Development of HIT solar cells with more than 21% conversion efficiency and commercialization of highest performance hit modules, *in Proceddings of the 3rd World Conference on Photovoltaic Energy Conversion (WCPEC '03)*, Osaka, Japan, May 2003. 955-58

[3] M.J. Hossain, T.K. Saha, N. Mithulananthan, and H.R. Pota, Robust control strategy for PV system integration in distribution systems. *Applied Energy*, 2012. **99**: 355-62.

[4] D. Pysch, A. Mette, A. Filipovic, and S. W. Glunz, Comprehensive analysis of advanced solar cell contacts consisting of printed fine-line seed layers thickened by silver plating. *Progress in Photovoltaics*, 2008. **17**: 101-114.

[5] F. Sarhaddi, S. Farahat, H. Ajam, A. Behzadmehr, and M. Mahdavi Adeli. An improved thermal and electrical model for a solar photovoltaic thermal (PV/T) air collector. *Applied Energy*, 2010. **87**:2328-39.

[6] G. Kumaravelu, M. M. Alkaisi, and A. Bittar, Surface texturing for silicon solar cells using reactive ion etching technique. *Proceedings of the 29th IEEE Photovoltaic specialists conference*, New Orleans, Louisiana, USA, 2002. 258-61.

[7] Wikipedia: Silicon Solar cell structure and mechanism.
http://en.wikipedia.org/wiki/User:Cyferz

[8] S. M. Sze. Semiconductor devices, physics and technology. John Wiley & Sons, New York, 2nd edition, 2002

[9] M.M. Hilali, Understanding and development of manufacturable screen printed contacts on high sheet-resistance emitters for low-cost silicon solar cells. Georgia Institute of Technology. P24.

[10] P. J. Holmes, and R. G. Loasby, Handbook of thick film technology. Glasgow: Electrochemical Publications Ltd, 1976.

[11] R. Mertens, M. Eyckmans, G. Cheek, M. Honore, and R. Van Overstraten, Critical processing parameter optimization for screen-printed semicrystalline silicon solar cells, *Proceedings of the 17th IEEE Photovoltaic Specialists Conference*, Orlando, FL, USA, 1 May 1984. 1347-51.

[12] M. Alemán, A. Streek, P. Regenfuβ, A. Mette, R. Ebert, H. Exner, S. W. Glunz, and G. Willeke, Laser micro-sintering as a new metallization technique for silicon solar cells. *Proceedings of the 21st European Photovoltaic Solar Energy Conference*, Dresden, Germany, 2006. 705-08.

[13] F. Huster, M. Spiegel, P. Fath, E. Bucher, T. Denner, and K. Schanz, Progress of the roller-printing metallisation technique towards an industrially compatible alternative to screen printing. *16th EC PVSEC*, Glasgow, Great Britain, 2000. 1385-88.

[14] D. Jordan and J. P. Nagle, New generation of high-efficiency solar cells: development, processing and marketing, *Progress in Photovoltaics: Research and Applications*, 1994. **2**:171-76.

[15] T. Petch, P. Regenfuβ, R. Ebert, L. Hartwig, S. Klötzer, T. Brabant, and H. Exner, Industrial laser micro sintering, *Rapid Prototyping Journal*, 2004. **11**: 18-25.

[16] A.S. Ionkin , B.M. Fish , Z.R. Li , M. Lewittes , P.D. Soper, J.G. Pepin, and A.F. Carroll, Screen-printable silver pastes with metallic nano-zinc and nano-zinc

alloys for crystalline silicon photovoltaic cells. *Applied Materials and Interfaces*, 2011. **3**: 606-11.

[17] D.M. Huljic, S. Thhormann, R. Preu, R. Lüdemann, and G. Willeke, Pad printing front contacts for c-Si solar cells-a technological and economical evaluation. *Proceedings of the 29th IEEE PVSC*, New Orleans, Louisiana, 2002. 126-29.

[18] D. Kim, S. Hwang and H. Kim, Effect of the thermal properties of frits on the electrical properties of screen-printed silicon solar cells. Journal of the Korean Physical Society, 2009. 55: 1046-50.

[19] F.C. Krebs, Fabrication and processing of polymer solar cells: A review of printing and coating techniques. *Solar Energy Materials and Solar Cells,* 2009. **93**:394-412.

[20] G. Yao, J. Zhao, and J. E. Cotter, Metal stencil-printed selective emitter silicon solar cell fabrication on C_Z wafer. *20th EC PVSEC*, Barcelona, Spain, 2005. 749-52.

[21] A. Rohatgi, D. S. Kim, K. Nakayashiki, V. Yelundur, and B. Rounsaville, High-efficiency solar cells on edge-defined film-fed grown (18.2%) and string ribbon (17.8%) silicon by rapid thermal processing, *Applied Physics Letters*, 2004. **84**: 145-47.

[22] S.W. Glunz, J. Dicker, M. Esterie, M. Hermie, J. Iserberg, F. Kamerewerd, J. Knobloch, D. Kray, A. Leimenstoll, F. Lutz, D. Oβwald, R. Preu, S. Rein, E. Schäffer, C. Schetter, H. Schmidhuber, H. Schmidt, M. Steuder, C. Vorgrimler, and G. Willeke, High-efficiency silicon solar cells for low illumination applications. *Proceedings of the Photovoltaic Specialists Conference*, New Orleans, 2002. 450-53.

[23] P.N. Vinod, SEM and specific contact resistance analysis of screen-printed Ag contacts formed by fire-through process on the shallow emitters of silicon solar cell. Journal of Materials Sciences: Materials in Electronics. 2009. **20**: 1026-32.

[24] W. Neu, A. Kress, W. Jooss, P. Fath, and E. Bucher, Low-cross multicrystalline back-contact silicon solar cells with screen printed metallization. *Solar Energy Materials and Solar Cells*, 2002. **74**:139-46.

[25] L. Pirozzi, G. Arabito, F. Artuso, V. Barbarossa, U. Besi-Vetrella, S. Loreti, P. Mangiapane, and E. Salza, Selective emitters in buried contact silicon solar cells: some low-cost solutions, *Solar Energy Materials and Solar Cells*, 2001. **65**: 287-95.

[26] V. Gazus, K. Feldrapp, R. Auer, R. Brendel, and M. Schultz, Dry processing of silicon solar cells in a large area microwave plasma reactor. *Solar Energy Materials and Solar Cells*, 2002.**77**:277-84.

[27] M. Jeong, S.E. Park, D.H. Kim, J.S. Lee, Y.C. Park, K.S. Ahn, and C.J. Choi, Transmission electron microscope study of screen-printed Ag contacts on crystalline Si solar cells. *Journal of The Electrochemical Society*, 2010. **157**: H934-36.

[28] N.B. Mason, O. Schultz, R. Russel, S.W. Glunz, and W. Warta, 20.1% efficient large area cell on 140 micron thin silicon wafer. *Proceedings of the 21st European Photovoltaic Solar Energy Conference EU PVSEC*, Dresden, Germany, 2006. 521-23.

[29] M.A. Green, and S.R. Wenham, Silicon Cells: Single Junction. One Sun, Terrestrial, Single & Multi-Crystalline. In: Partain. L., Ed., Solar Cells and Their Applications, Wiley, New York, 1995.

[30] A. Ryan, and H. Lewis, Manufacturing an environmentally friendly PCB using existing industrial processes and equipment. *Robotics and Computer-Integrated Manufacturing*, 2007. **23**: 720-26.

[31] D. Erath, A. Filipovic, M. Retzlaff, A.K. Goetz, F. Clement, D. Biro, and R. Preu, Advanced screen printing technique for high definition front side metallization of crystalline silicon solar cells, *Solar Energy Materials and Solar Cells*, 2010. **94**:57-61.

[32] H.H. C. de Moor, J. Hoornstra, A. W. Weeber, A. R. Burgers, and W. C. Sinke, Printing High and Fine Metal Lines Using Stencils, *14th European PVSEC,* Barcelona, Spain, 1997.

[33] H. H. C. de Moor, A. W. Weeber, J. Hoornstra, and W. C. Sinke, Fine-line screen printing for silicon solar cells, *6th workshop on the Role of Impurities and Defects in Silicon Device Processing*, Snowmass Colorado, 1996.154-70.

[34] J. Hoornstra, S. Roberts, H. de Moor, and T. Bruton, First experiences with double layer stencil printing for low cost production solar cells. *2nd WPVSC*, Vienna, Austria, 1998.1527-30.

[35] R. Durairaj, G.J. Jackson, N.N. Ekere, G. Glinski, and C. Bailey, (2002) Correlation of solder paste rheology with computational simulations of the stencil printing process. *Soldering & Surface Mount Technology*, 2002. **14**:11-17.

[36] P. Hahne, Innovative Printing Technologies: Screen Printing - Pad Printing, Der Siebdruck, Lübeck. 2001.

[37] A. Mette, New Concepts for Front Side Metallization of Industrial Silicon Solar Cells. Fraunhofer-Institute for Solar Energy and System. 2007.

[38] D. M. Huljic, E. Hirth, R. Lüdemann, and G. Willeke, Large area crystalline silicon solar cells with pad printed front side metallisation, *17th European Photovoltaic Solar Energy Conference,* Munich, Germany, 2001.1582-85.

[39] P. Hahne, E. Hirth, I.E. Reis, K. Schwichtenberg, W. Richtering, F.M. Horn, and Udo Eggenweiler, Progress in thick-film pad printing technique for solar cells. *Solar Energy Materials & Solar Cells*. 2001. **65**: 399-407.

[40] P. Hahne, I. Reis, E. Hirth, D.M. Huljic, and R. Preu, Pad printing-a novel thick-film technique of fine-line printing for solar cells. *2nd WPVSC*, Vienna, Ausria, 1998.1646-49.

[41] D. M. Huljic, S. Thormann, S. Thormann, R. Preu, R. Ludemann, and G. Willeke, Pad printed front contacts for c-Si solar cells - a technological and economical evaluation. *29th IEE PVSC*, New Orleans, USA, 2002. 126-29.

[42] M. Y. Ghannam, J. Poortmans, and J. F. Nijs, Quantitative comparison between the performance of buried contact and of screen-printed contact industrial silicon solar cells, *Kuwait Journal of Science and Engineering*, 1998. **25**: 363-77.

[43] D. Biro, D. Erath, U. Belledin, J. Specht, D. Stüwe, A. Lemke, M. Aleman, N. Mingirulli, J. Rentsch, R. Preu, R. Schlosser, B. Bitnar, and H. Neuhaus, Inkjet printing for high definition industrial masking processes for solar cell production. *17th IPVSEC Conference,* Fukuoka, Japan, 2007.

[44] K. Murata, Super-fine ink-jet printing for nanotechnology. *3rd World Conference on Photovoltaic Energy Conversion,* Osaka, Japan, 2003.346-49.

[45] W.T. Pimbley, Drop formation from a liquid jet analysis considered as a boundary value problem. *IBM Journal of Research and Development*. 1984. **29**: 148-56.

[46] J.H. Kim, H.Y. Koo, Y.N. Ko, and Y.C. Kang, Characteristics of bi-based glass frit having similar mean size and morphology to those of silver powders at high firing temperatures. *Journal of Alloys and Compound*, 2010.**497**: 259-66.

[47] M.M. Hilali, S. Sridharan, C. Khadilkar, A. Shaikh, A. Rohatig, and S. Kim, Effect of glass frit chemistry on the physical and electrical properties of thick-film Ag contacts for silicon solar cells. *Journal of Electronic Materials*, 2006.**35**: 2041-47.

[48] K.K. Hong, S.B. Cho, J.S. You, J.W. Jeong, S.M. Bea, and J.Y. Huh, Mechanism for the formation of Ag crystallites in the Ag thick-film contacts of crystalline Si solar cells. *Solar Energy Materials and Solar Cells*, 2009. **93**:898-904.

[49] S.J. Jeon, S.M. Koo, and S.A. Hwang, Optimization of lead-and cadmium-free front contact silver paste formulation to achieve high fill factors for industrial screen-printed Si solar cells. *Solar Energy Materials and Solar Cells*, 2009. **93**:1103-09.

[50] D. Kim, S. Shim, S. Hwang, and H. Kim, Electrical properties of screen printed silicon solar cell dependent upon thermophysical behavior of glass frits in Ag pastes. *Japanese Journal of Applied Physics*, 2009. **48**: 05EC06

[51] G. Schubert, F. Huster, and P. Fath, Physical understanding of printed thick-film front contacts of crystalline Si solar cells-Review of existing models and recent developments. *Solar Energy Materials and Solar Cells*, 2006.**90**: 3399-406.

[52] M. de Wild-Scholten, K. Wambach, E. Alsema, and A. Jäger-Waldau, Implications of European environmental legislation for photovoltaic systems. 20th EC PVSEC, Barcelona, 2005. 3143-47.

[53] K. Firor, and S. Hogan, Effects of processing parameters on thick film inks used

for solar cell front metallization, *Solar Cells*, 1981.**5**: 87-100.

[54] Y. Li, Y. Wu, and B.S. Ong, Facile Synthesis of Silver Nanoparticles Useful for Fabrication of High-Conductivity Elements for Printed Electronics. *Journal of the American Chemical Society*. 2005. **127**: 3266-67.

[55] Y. Qin, Silver-containing alginate fibres and dressings. *International Wound Journal*, 2005. **2**: 172-76.

[56] I. Chopra, The increasing use of silver-based products as antimicrobial agents: a useful development or a cause for concern? *Journal of Antimicrobial Chemotherapy*, 2007. **59**: 587-90.

[57] J.K. Schluesener, and H.J. Schluesener, Naosilver: application and nover aspects of toxicology. *Archives of Toxicology*, 2013. **87**: 569-76.

[58] N. Pradhan, A. Pal, and T. Pal, Silver nanoparticle catalyzed reduction of aromatic nitro compounds. Colloids and surface A: physicochemical and engineering aspects. 2002. **196**: 247-57.

[59] D. Kim, and J. Moon, Highly conductive ink jet-printed films of nanosilver particles for printable electronics. *Electrochemical and Solid-State Letters*, 2005. **8**: J30-J33.

[60] D. Chen, X. Qiao, X. Qiu, and J. Chen, Synthesis and electrical properties of uniform silver nanoparticles for electronic applications. *Journal of Materials Science*, 2009. **44**: 1076-1081.

[61] M. Nakamoto, M. Yamamoto, Y. Kashiwagi, T. Tsujimoto, and Y. Yoshida, A variety of silver nanoparticle pastes for fine electronic circuit pattern formation. 6th International Conference on Polymers and Adhesives in Microelectronics and Photonics, Odaiba, Tokyo. 2007.

[62] K. Park, D. Seo, and J. Lee, Conductivity of silver paste prepared from nanoparticles. *Colloids and Surface A: Physicochemical and Engineering Aspects*, 2008. **313-314**: 351-54.

[63] D.L. Chen, and L. Gao, Large-scale growth and end-to-end assembly of silver nanorods by PVP-directed polyol process. *Journal of Crystal Growth*, 2004. **264**: 216-22.

[64] Y. Wu, J. Xiang, C. Yang, W. Lu, and C.M. Lieber, Single-crystal metallic nanowires and metal/semiconductor nanowire heterostructures. *Nature*, 2004. 430: 61-65.

[65] J. I. Pascual, J. Mendez, J. Gomez-Herrero, A.M. Baro, N. Garcia, U. Landman, W.D.Luedtke, E.N. Bogachek, and H.P.Cheng, Properties of metallic nanowires-from conductance quantization to localization. *Science*, 1995. **267**: 1793-95.

[66] C. Chen, L. Wang, R.L. Li, G.H. Jiang, H.J. Yu, and T. Chen, Effect of silver nanowires on electrical conductance of system composed of silver particles. *Journal of Materials Science*, 2007. **42**: 3172-76.

[67] Jeon SJ, Koo SM, Hwang SA. Optimization of lead- and cadmium-free front contact silver paste formulation to achieve high fill factors for industrial screen-printed Si solar cells. *Solar Energy Mater Sol Cells*. 2009. **93**: 1103-09.

[68] M. Prudenziati, L. Moror, B. Morten, and F. Sirotti, Ag-based thick film front metallization of silicon solar cells. *Active and Passive Electrical Compounds*, 1989. **13**: 133-50,

[69] C. Khadilkar, S. Sridharan, T. Pham, A. Shaikh, and S. Kim, Characterization of front contact in a silicon solar cell. *Technical Digest of the International PVSEC-14*, Bangkok, Thailand, 2004. 443-44.

[70] D. M. Huljic, C. Ballif, A. Hessler-Wyser, and G. Willeke, Microstructural analysis of Ag thick-film contacts on n-type silicon emitters. *3rd WCPEC*, Osaka, Japan, 2003.83-86.

[71] G.C. Cheek, R. P. Mertens, R. V. Overstraeten, and L. Frisson, Thick-film metallization for solar cell applications, *Transactions on Electron Devices*, 1984.**31**: 602-09.

[72] C. Ballif, D. M. Huljic, A. Hessler-Wyser, and G.Willeke, Nature of the Ag-Si interface in screen-printed contacts: a detailed transmission electron microscopy study of crosssectional structures. *29th IEEE PVSC*, 2002. 360-63.

[73] C. Ballif, D. M. Huljic, G. Willeke, and A. Hessler-Wyser, Silver thick-film contacts on highly doped n-type silicon emitters: Structural and electronic properties. *Applied Physics Letters*, 2003. **82**: 1878-80.

[74] R. J. S. Young and A. F. Carroll, Advances in front-side thick film metallization for silicon solar cells. *16th EC PVSEC*, Glasgow, Great Britain, 2000, VD3.63.

[75] G. Schubert, Thick film metallisation of crystalline silicon solar cells. Universität Konstanz: Konstanz. 2006. P142.

[76] M.M. Hilali, A. Rohatgi, and B. To, A review and understanding of screen-printed contacts and selective-emitter formation. *14th workshop on crystalline silicon solar cells and modules*, Colorado, USA, 8-11 Augest, 2004.

CHAPTER 2 EXPERIMENTAL METHODS

2.1 Characterization tools

2.1.1 Scanning electron microscopy (SEM)

The scanning electron microscope is widely used for analyzing microscopy of materials for its versatility and abundant information. In this study, a high-resolution JEOL Model JSM-6490 was used, as shown in **Figure 2.1**, which is a high-performance scanning electron microscope, with a resolution of 3.0 nm at electron energy of 12keV.

Figure 2.1 The scanning electron microscopy (JEOL Model JSM-6490)

In this study, the SEM was used to obtain microscopy information, including top-view images as well as cross-section images of the thick-film metallization contact to determine whether the thick film is continuous and homogenous or not, and analyze the contact microstructures. Besides, it was used to analyze the size, dispersiblity, and shape of silver particles synthesized in this work, as well as glass frit powders. A thin coating layer of gold was deposited on the surface of samples to increase the resolution of images by a sputter coater, as shown in **Figure 2.2**.

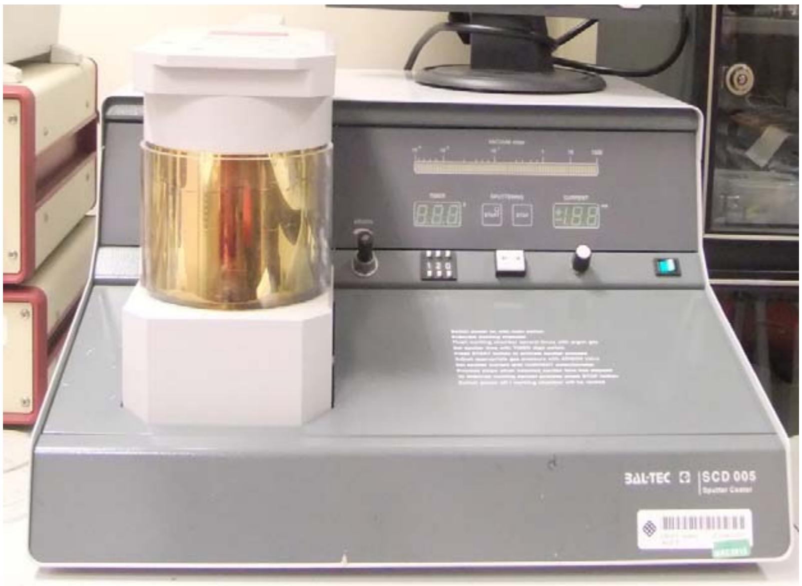

Figure 2.2 The sputter coater for depositing thin coating layer of gold

2.1.2 X-ray diffraction (XRD)

The X-ray Diffractometer (Rigaku SmartLab), as shown in **Figure 2.3**, was used in this study to obtain the phase information of silver particles and glass frit powders. The Rigaku SmartLab, with Cu Ka radiation at a tube voltage of 45 kV and a tube current of 200 mA, is a novel high-resolution x-ray diffractometer, which is extraordinary for its attached SmartLab Guidance software. The user can be well guided by the intelligent user interface through the intricacies. Moreover, the Smartlab has numerous applications for a wide range of materials, including fine powders, bulk materials, thin films and even fluid.

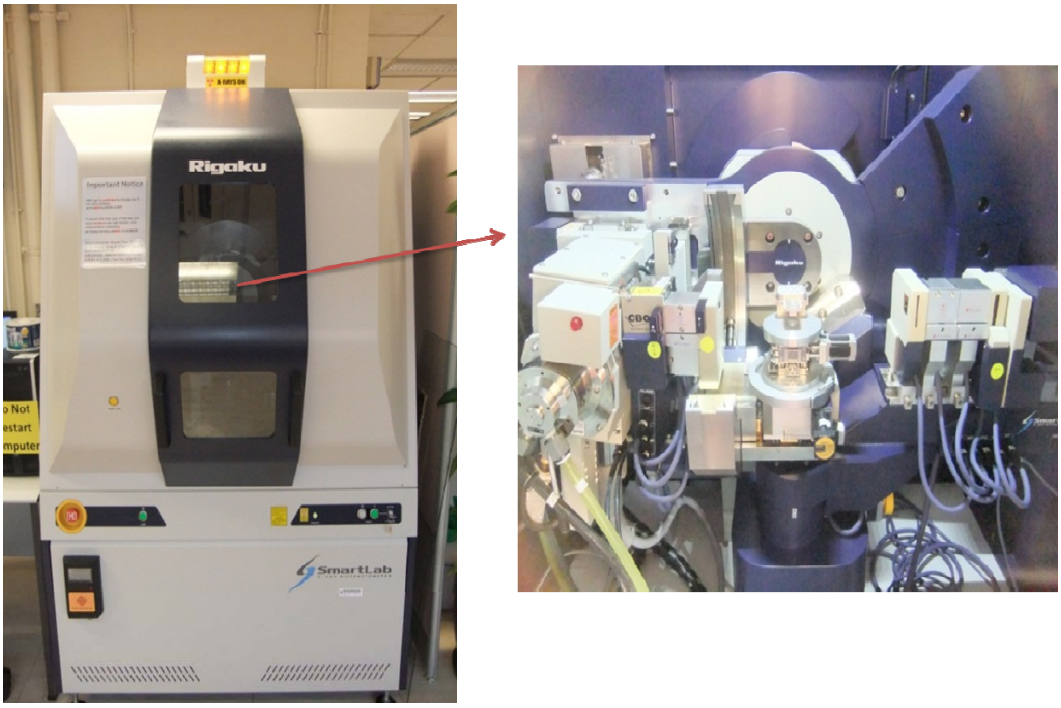

Figure 2.3 The X-ray Diffractometer (Rigaku SmartLab)

2.1.3 Thermogravimetric analysis/ Differential scanning calorimeter (TGA/DSC)

The Thermogravimetric analysis/ Differential scanning calorimeter (TGA/DSC, Netzch STA 449C, Jupiter), as shown in **Figure 2.4**, was used in this study to record the TGA/DSC curves of silver paste, glass gel and glass frit powders. The temperature range is from 25°C to 1500°C, with the max heating rate of 40°C/min. From the TGA curve, abundant information of samples can be obtained, including mass change, corrosion/oxidation, decomposition temperature, reaction kinetics, and composition determination. While from the curve of the DSC, the following information of samples can be obtained, including specific heat, transition enthalpies, melting temperature, glass transition temperature, phase diagrams, purity determination, decomposition effect, and so on.

Figure 2.4 The thermogravimetric analysis/ Differential scanning calorimeter

2.2 Fabrication tools

2.2.1 Synthesis of silver particles

Spherical micron-/submicron silver particles are prepared by the traditional chemical reduction method and the polyol process, respectively, using the reduction equipment as shown in **Figure 2.5**. The main difference of these two methods is the different reaction medium, aqueous phase and organic phase, respectively. Moreover, reasonable metal source, reducing agent and dispersant should be chosen for reduction reaction. Besides, to prepare satisfactory silver particles, a series of experiments should be carried out to study the effecting factors, including concentrations of the agents, dropping rate, PH value, reaction time and so on. Finally the production is filtrated and washed for characterization and application in silver paste for crystalline silicon solar cells.

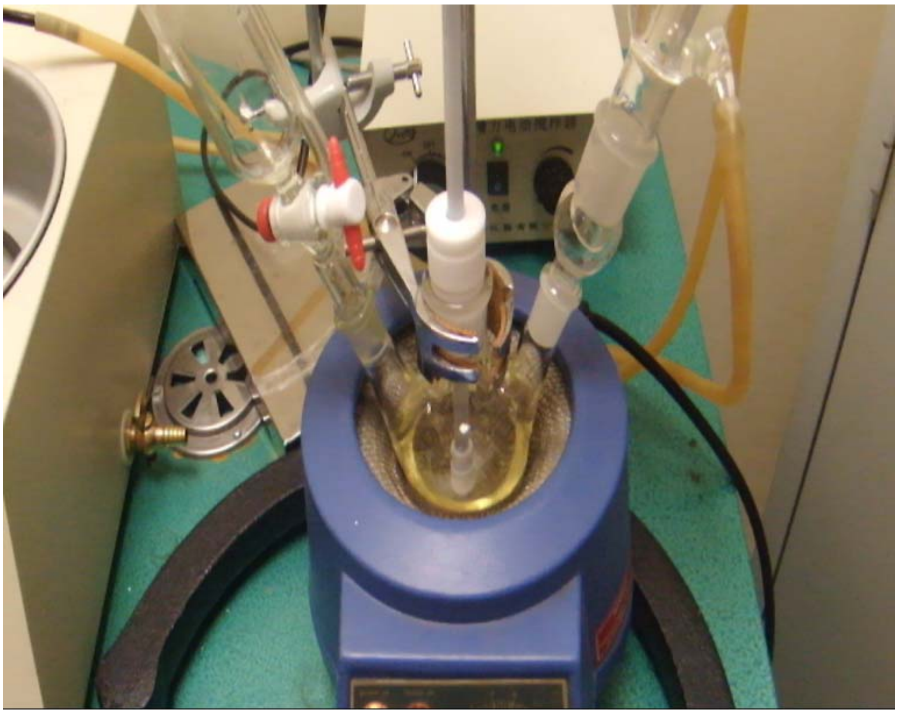

Figure 2.5 Experimental equipment for preparing micron silver particles

Figure 2.6 Autoclave for preparing silver nanoparticles

Nano silver particles are prepared by solvothermal method using the stainless steel autoclave, as shown in **Figure 2.6**. Solvothermal synthesis is a process of preparing chemical compounds, which is similar to hydrothermal method. As a normal liquid solution-based chemical process, solvothermal method is widely used to synthesize various nanomaterials for many advantages. The size, shape, and distribution of nanoparticles can be well controlled and altered by changing the experimental parameters, such as reaction time, reaction temperature, and agent type. Size and morphology of silver nanoparticles are important for their application in silver paste. So I try to synthesize silver nanoparticles using the solvothermal method, and study the size, shape and growth control and its application in silver paste for crystalline silicon solar cells.

2.2.2 Glass frit preparation

Micron glass frit powders are prepared by the conventional melt cooling route, as shown in the follow flowchart in **Figure 2.7**. There are three steps as follows: at the first step, a stoichiometric mixture of oxide powders such as Bi_2O_3, H_3BO_3, SiO_2, Al_2O_3, and ZnO are well mixed in a ball mill for several hours, then the mixture are melted in an aluminum crucible at 1200°C for two hours in a high temperature electric resistance furnace. In the second step, the molten glass are removed from the furnace and poured into the deionized water, rapidly cooling to room temperature. After milling again in a ball mill for several hours, the fine glass frit with micro-size meter is obtained. At present, the glass frit powders for silver paste for crystalline silicon solar cells are usually prepared by this method. In fact, there are many disadvantages for this method. The worst is the impurity of glass frit. During the high temperature melting process, the glass frit is easily contaminated with external impurity. As we know, even the minority of impurity is fatal for silicon solar cells, which would become recombination center for “minority carrier” in silicon wafer.

Therefore, in this work, I try to prepare high-purity glass frit for silver paste by sol-gel method for high performance solar cells.

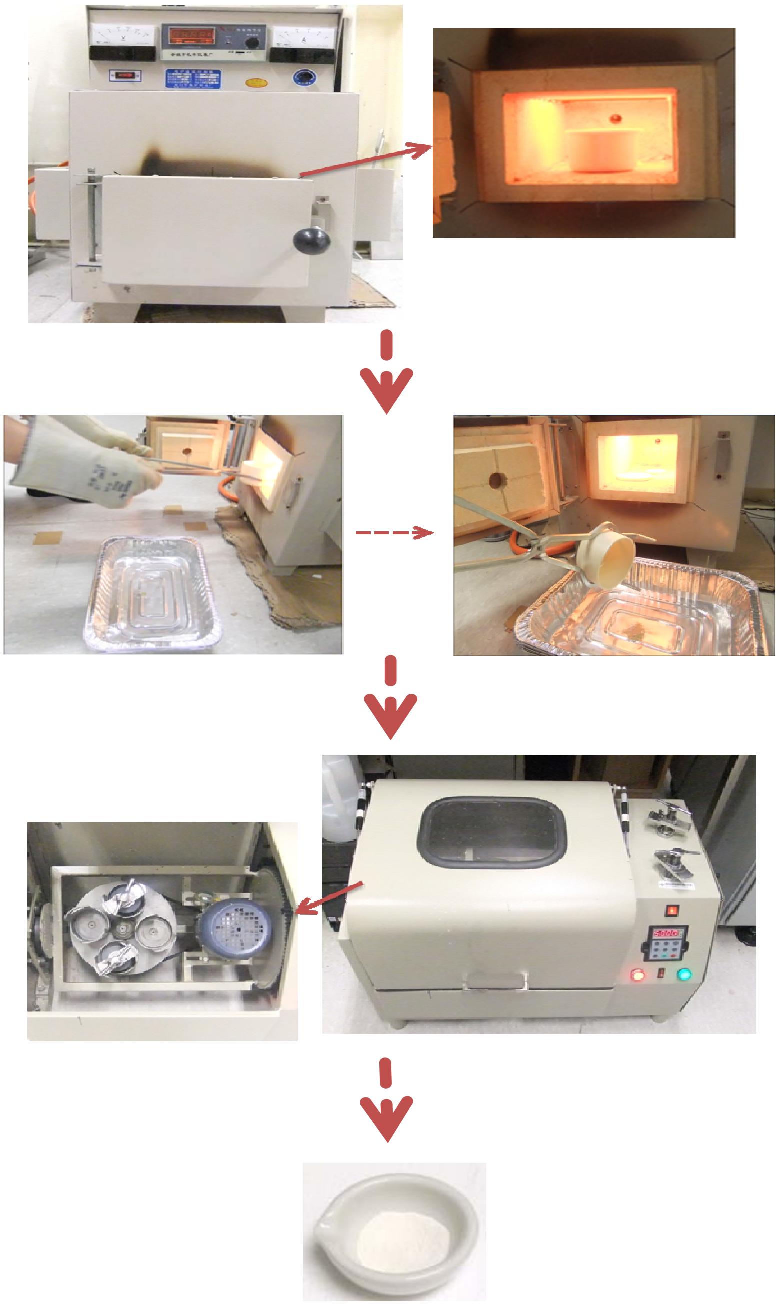

Figure 2.7 Flowchart for preparing micron glass frit powders by the conventional melt cooling route

Nano glass frit powders for silver paste for crystalline silicon solar cells are prepared by the sol-gel process. The sol-gel method has been used for a long time to prepare glass powders for its many potential advantages over to the conventional melting route. First, glass frit can be obtained at much lower temperature than the melt cooling route, thus to reduce pollutions and energy cost. It is well known that high temperature is required in the conventional melt cooling route for preparing glass frit, and several-hours heating is needed to make sure that the glass is molten homogeneously. Apparently, it is a high energy-consumption process. Moreover, at high temperature the glass frit is easily contaminated by the crucible corrosion and the impurities from the melting furnace. Second, as the compositions are mixed in a single-phase liquid, namely molecular mixing, the glass frit prepared by sol-gel process should be homogenous.

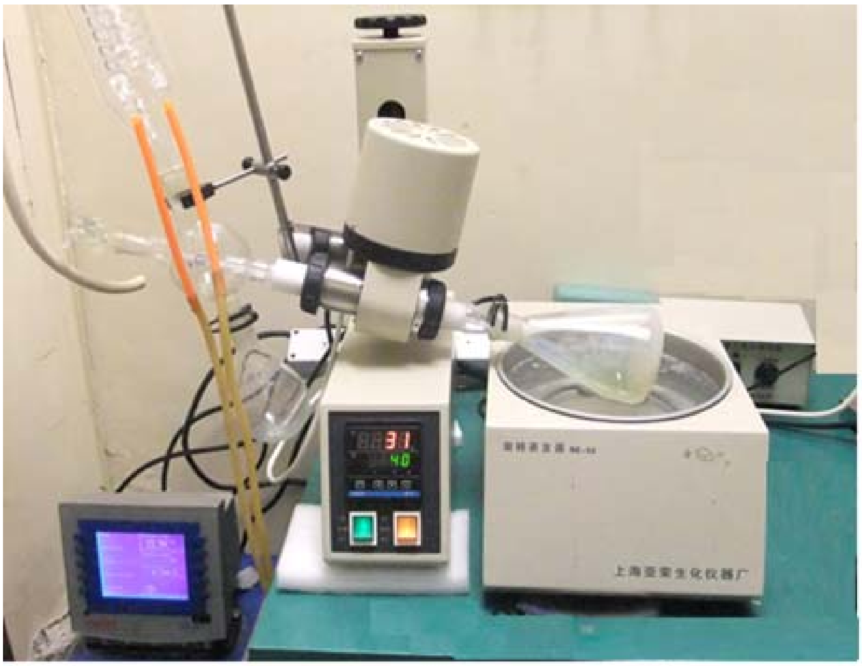

Figure 2.8 Rotary evaporator for preparing silver paste for silicon solar cells

2.2.3 Silver paste preparation

The silver paste for crystalline silicon solar cells are prepared by the rotary evaporation method. Specifically, silver particles, glass frit powders and organic vehicle (ethyl celluloses and terpineol) are mixed at a certain ratio in ethyl alcohol. The contents are concentrated in a rotary evaporator (RE-52) at about 40°C, as shown in **Figure 2.8**. After few hours, the ethyl alcohol can be eliminated, and the preliminary products are finalized by a three-roller-mill grinder (S65), as shown in **Figure 2.9**. The three-roller-mill grinder has widely been used in paste materials, including inks, adhesive and so on. The mill roller is usually made of high hardness alloy, which is also equipped with a cooling device for continuous operation.

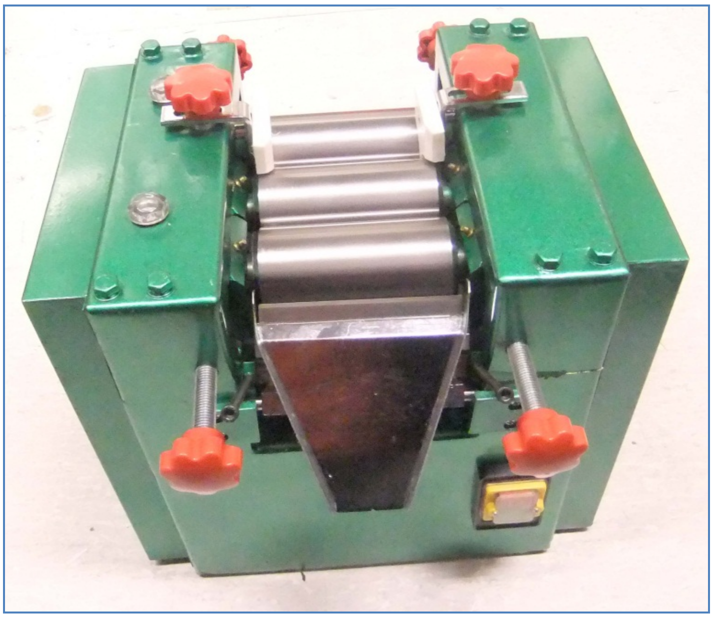

Figure 2.9 Three-roller mill for preparing silver front contact paste for crystalline silicon solar cells

2.2.4 Screen-printing machine

Silver electrodes can be formed by screen-printing silver pastes on crystalline silicon wafers with antireflective coating, using a screen-printing machine, followed by firing process in a conveyor infrared furnace. At present, most of the industrial crystalline silicon solar cells are commonly made by this technology to deposit silver paste on silicon wafer to form front contact silver electrodes, as well as aluminum back surface field. In our laboratory, we use the semi-automatic screen-printing machine (SYP2230) to prepare front-side silver fingers, as shown in **Figure 2.10.** It is versatile and conveniently handled. The screen area is adjustable, which is convenient for preparing crystalline silicon solar cells with different sizes.

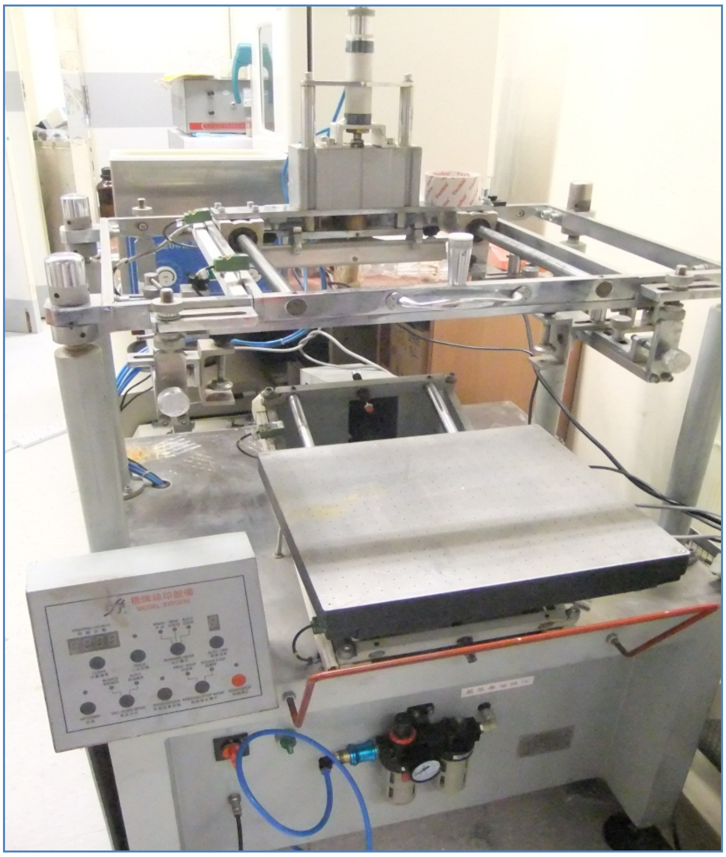

Figure 2.10 The screen-printing machine for preparing silver front contact paste for crystalline silicon solar cells

CHAPTER 3 DEVELOPMENT OF LEAD-FREE SILVER FRONT CONTACT PASTE

3.1 Introduction

The silver front contact pastes for crystalline silicon solar cells usually contain three principal constituents: silver particles, glass frit powders, and organic binder [1-4]. Among them the glass frit could be deemed as the most important component that influences the quality of metallization contacts in solar cells. Although the glass frit only holds 2-5% in mass in a silver front contact paste, it plays a critical role in the front-side metallization contact formation. The glass frit not only acts as an inorganic binder, which determines the adhesion strength of silver electrode to crystalline silicon substrate, but also serves a medium for silver to recrystalline on the silicon emitter contact interface, forming an Ag/Si ohmic contact during firing process, which determines the final resistances of the electrodes and solar cells [5]. Therefore, in a front-side silver paste for crystalline silicon solar cells, the glass frit with special chemical composition and thermal properties is required to achieve excellent electrical and mechanical performance.

Today, most of the commercial silver pastes for crystalline silicon solar cells are lead-based, usually in form of lead oxide [6-9]. In recent years more and more attention is paid to the research and application of the lead-free silver paste due to the restriction of the use of certain hazardous substances (RoHS) executed by European Union for electric devices [10]. Several research studies have been conducted on the lead-free silver paste for crystalline silicon solar cells. Bi-based glass turned out to be the most promising substitute for lead-based glass for a front-side silver paste [11-16]. Kim et al. [12] prepared the Bi-based glass frit with glass transition temperature of

442°C by spray pyrolysis, which improved the adhesion strength of the front metallization contact. Although there are many reports on preparation of glass frit for silver front contact paste, many shortcomings and problems exist due to their less experience or experimental conditions for optimizing the formulation silver paste. For example, the size and size distribution are important factors influencing the continuity and compactness of the thick film, which are not profoundly investigated. Therefore, it is essential to optimize the glass frit in silver paste for high electrical and mechanical properties. In this chapter, lead-free glass frit powders for silver front contact paste for crystalline silicon solar cells have been prepared by the conventional melting route.

For better understanding and development of lead-free silver paste for crystalline silicon solar cells, both the glass frit and silver particles would be synthesized in this work. Typically, the silver particles in silver front contact paste are usually spherical in micron size. Guo et al. [17] prepared silver particles with mean size of 1.15 μm by reducing silver nitrate with ascorbic acid and investigated the preparation and dispersive mechanism of silver particles. Besides, spherical silver particles with average particle size of about 1-2 μm for silicon solar cell electrical paste were prepared by traditional chemical reduction method [18]. In this work, the traditional chemical reduction method was chosen to synthsize silver particles because it is cheap and easy for industrialization.

Finally, the silver front contact pastes are prepared by mixing the as-prepared silver particles, glass frit and organic binders at certain ratio using the rotary evaporation method. The purpose of this section is to optimize the silver paste based on the lead-free glass frit to achieve high-performance crystalline silicon solar cells.

3.2 Experiment materials and equipment

3.2.1 Experiment materials

All the materials used in the experiments are listed in **Table 3.1.**

Table 3.1 Experiment materials

Name	Remark	Manufactory
Silver nitrate	AR.	China National Pharmaceutical Group Industry Corporation Ltd
Ammonia	AR. 28+%	Xilong Chemical Co., Ltd
Ascorbic acid	AR.	Xilong Chemical Co., Ltd
Polyvinylpyrrolidone	AR. PVP40, MW= 40000	Xilong Chemical Co., Ltd
Anhydrous ethyl alcohol	AR.	Xilong Chemical Co., Ltd
Acetone	AR.	Tianjin Fuchen Chemical Reagent Factory
Hydrochloric acid	AR.	Tianjin Fuchen Chemical Reagent Factory
Nitric acid	AR.	Tianjin Chemical Reagent Ltd.
Acetic acid	AR.	Tianjin Chemical Reagent Ltd.
Bismuth (III) oxide	AR.	China National Pharmaceutical Group Industry Corporation Ltd
Silicon dioxide	AR.	China National Pharmaceutical Group Industry Corporation Ltd
Boric acid	AR.	China National Pharmaceutical Group

		Industry Corporation Ltd
Aluminum oxide	AR.	China National Pharmaceutical Group Industry Corporation Ltd
Zinc oxide	AR.	China National Pharmaceutical Group Industry Corporation Ltd
Ethylene glycol	AR.	Xilong Chemical Co., Ltd
Terpineol	AR.	Xilong Chemical Co., Ltd

3.2.2 Equipment

All the equipment used in the experiments is listed in **Table 3.2.**

Table 3.2 Equipment list

Name of instrument	Instrument model	Manufactory
Rotary evaporator	RE-52	Shanghai Yarong Biochemical Apparatus Factory
Electric Stirrer	JJ-1	Shanghai Meipu Instrument Equipment Co., Ltd
Semi-automatic screen printing machine	SYP2230	Shenzhen Qiaopai Screen Machine Factory
Electric heating air-blowing drier	101-2	Shanghai Guangdi Instruments Equipment Co., Ltd
Magnetic Stirring Apparatus	78-1	Changzhou Aohua Instruments Equipment Co., Ltd
Electric heating mantle	EM 100	Electromantle, England

Ultrasonic generator	KQ3200E	Kunshan Ultrasonic Electronic Equipment co., ltd
Electronic balance	ES120	Shenzhen Zhicheng Electronic Balance Co., Ltd
High-temperature electric resistance furnace	SX_2-4-13	Longkou Electric Furnace Factory
Laboratory pH meter	PHB-5	Shanghai Hongji Instruments Equipment Co., Ltd
All-directional planetary ball mill	PMQW0.4L	Nanjing Shunchi Technology Development Co. Ltd
Oilless compressor	EWS24	Zhejiang Jonway Machinery & Electric Manufacture Co., Ltd
Three-roller mill	S65	Changzhou Wujin Xingye Mechanical Equipment Co., Ltd
Thermostat oil bath cauldron	$HH-S_1$	Changzhou Aohua Instruments Equipment Co., Ltd

3. 3 Preparation of micron silver particles

3.3.1 Mechanism

Currently, there are many methods of synthesizing silver particles, such as microwave plasma [19], spray pyrolysis [20], radiation reduction method [21] electrolysis [22], mechanical chemical synthesis [23], and so on. However, the chemical liquid-phase reduction method is regarded as a practical method for many advantages, such as easy operation, few experimental apparatus, and easy to scale up for industriliazation. Therefore, the traditional liquid-phase chemical reduction method was chosen to synthesize silver particles in this work. Specifically, the metal precursor was reduced by the reducing agent in the apparatus as shown in previous chapter. Moreover, reasonable metal source, reducing agent and dispersant would be taken into account. **Figure 3.1** indicates the reaction principles for synthesizing silver particles.

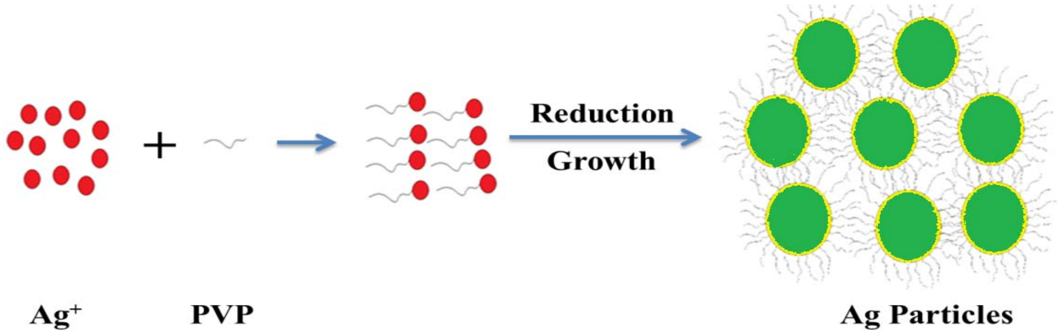

Figure 3.1 The reaction principles for synthesizing silver particles by the traditional chemical reduction method

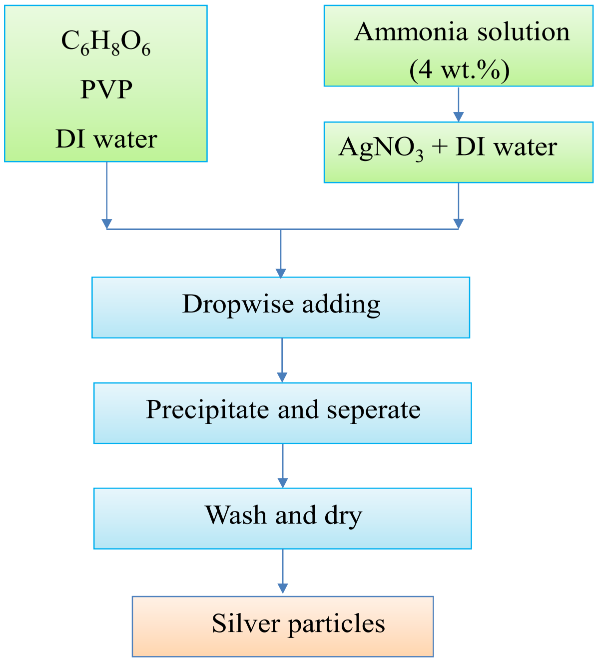

Figure 3.2 Flowchart for synthesizing silver particles by the traditional chemical reduction method

In this work, silver nitrate ($AgNO_3$), ascorbic acid ($C_6H_8O_6$) and polyvinylpyrrolidone (PVP) were used as the metal precursor, reducing agent and dispersant, respectively. Besides, to prepare satisfactory silver particles, a series of experiments were carried out to study the effecting factors, including concentrations of the agents, PH value, reaction time and so on. There are four steps for synthesizing silver particles in my work as follows:

(i) $C_6H_8O_6$ and PVP were dissolved in the deionized water at room temperature and the solution A was obtained.

(ii) Aqueous solution of silver nitrate was made up by dissolving a certain amount of $AgNO_3$ in the deionized water, followed by adding 4 wt% ammonia solution until a clear solution (B) was obtained.

(iii) Then solution A was added into the solution B drop by drop under stirring at a sufficiently low dropping rate to well control the reduction rate. After the addition finished, the solution was further stirred and heated for one hour at a constant temperature of 45°C.

(iv) The resulting precipitates were separated from the solution, washed many times by deionized water and ethanol, followed by a drying process in a vacuum drying oven at 60°C for several hours. The final silver particles were obtained.

3.3.2 Characterization

The morphology of the as-prepared silver particles was observed by the scanning electron microscopy. **Figure 3.3** is the SEM image of the silver particles synthesized by the chemical reduction method under the optimal experimental condition, using silver nitrate as the metal source, ascorbic acid as the reducing agent and PVP as the dispersant agent. From the SEM, it is demonstrated that the silver particles are quasi-spherical in shape, with an average size of 1.2μm, which basically can satisfy the requirement for application in silver front contact paste for crystalline silicon solar cells. Certainly, it is necessary to measure the photovoltaic performance of the fabricated silicon solar cells using the silver paste based on the as-prepared silver particles to analyze and assess whether the as-developed silver particles are suitable for silver front contact paste or not.

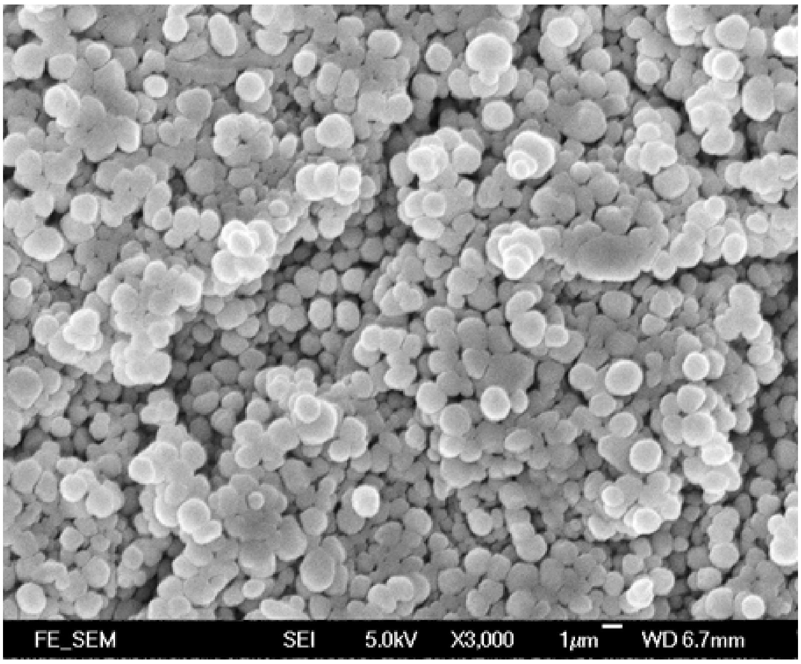

Figure 3.3 SEM image of the silver particles synthesized by the traditional liquid-solution chemical reduction method.

It is important to note that the PVP plays a critical role in the morphology of silver particles. Zhang studied the PVP protective mechanism of silver particles synthesized by chemical reduction method **[24]**, and reported that the PVP/$AgNO_3$ ratio of 1.5 was favorable for synthesis of quasi-spherical silver particles. Similar phenomenon has been observed in this work. Besides, he proposed the protective mechanism of PVP in the silver nitrate reduction system on the basis of the following reactions **[24]**:

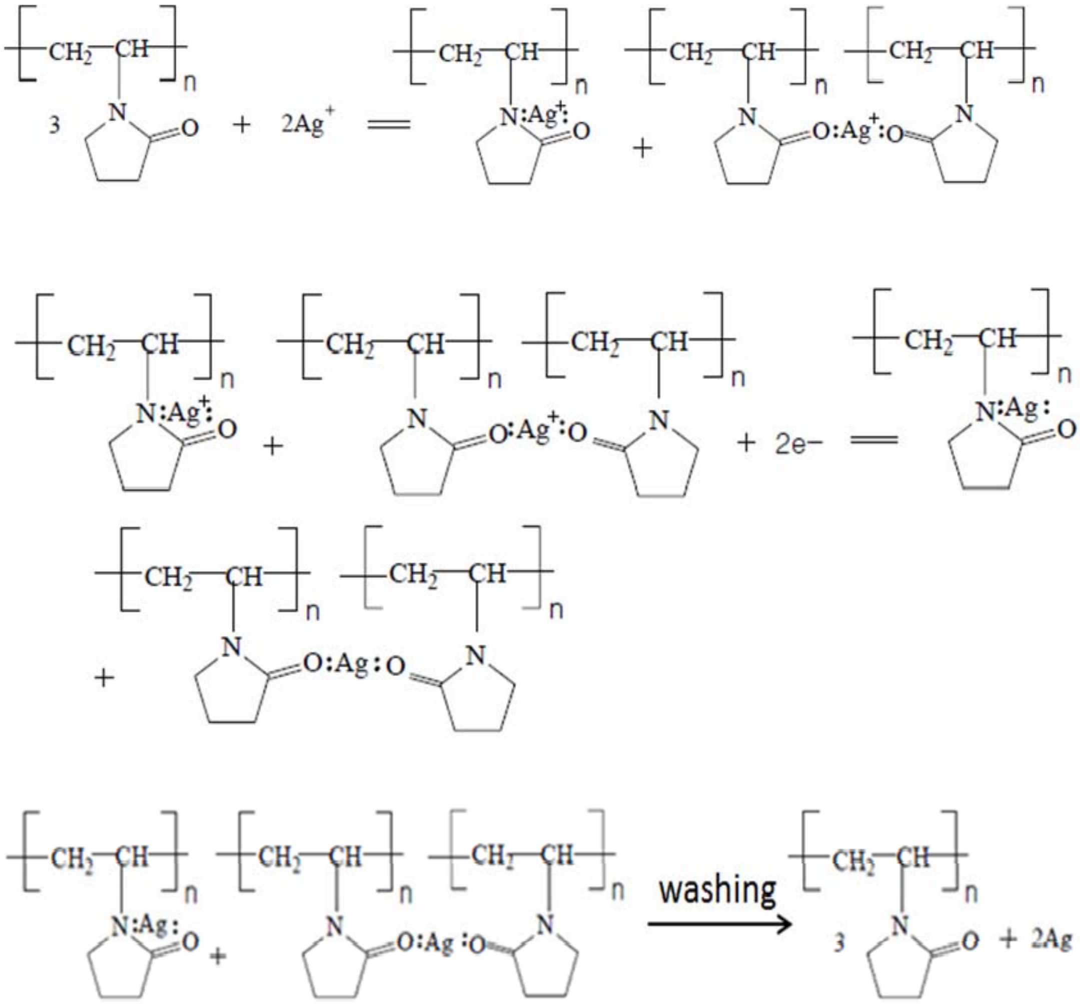

The only drawback is that there is, to a small degree, agglomeration behavior between the silver particles, although the PVP as a protective agent was added into the reduction system. It could be preliminarily ascribed to the natural essence of aqueous system. In fact, to prevent the silver particles from agglomeration, the PVP as a protective agent was usually added in the chemical reduction system. However, it would bring new problems for the application of silver particles in silver paste. For example, it would reduce the size of silver particles, and reduce the solid content of silver paste. All these issues would be discussed and further solved in other chapters.

Figure 3.4 shows the x-ray diffraction pattern of the as-prepared silver particles synthesized by the chemical reduction method. An index process of the diffraction pattern was done and the *Miller indices* to each peak were identified. There are five strong peaks found in the diffraction pattern, which are identical to those of the FCC silver. Besides, there are no crystallographic impurities. Moreover, the silver particles were well crystallized, which could be identified by the high-intensity peaks.

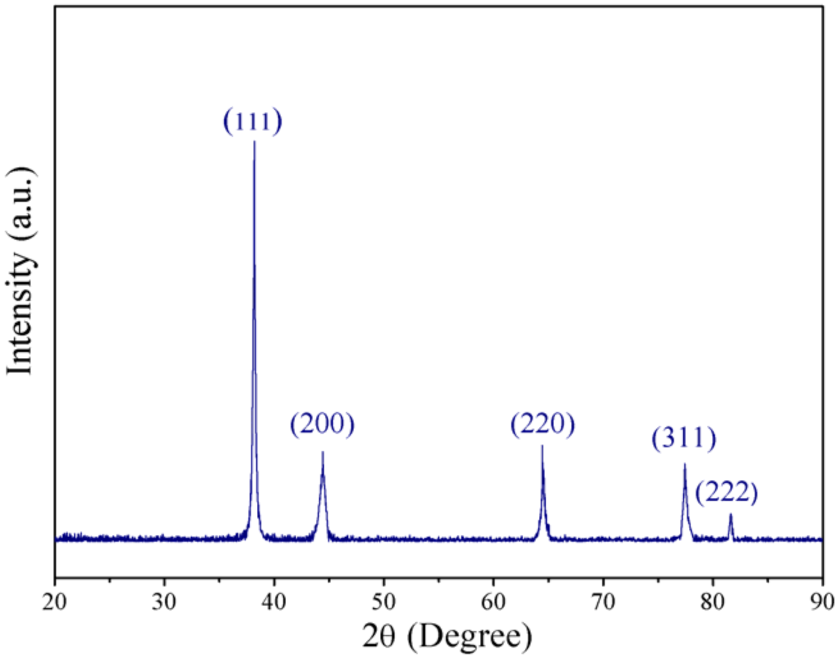

Figure 3.4 X-ray diffraction pattern of silver particles synthesized by the chemical reduction method

3.4 Preparation of micron lead-free glass frit powders

3.4.1 Preparation

At present, the glass frit powders for silver front contact paste for crystalline silicon solar cells are usually prepared by the conventional melting route. The specific manufacturing flowchart is elaborated in Chapter 2. One of the advantages of this method is that it is easy to realize industrial production. Before our further research, and for better understanding and development of high-performance products, it is highly desirable to look into the conventional preparation method of glass frit powders. Therefore, in this section, the conventional melting route method is chosen to prepare lead-free micron glass frit powders.

Specifically, for a typical experiment, there are three steps as follows: at the first step, a stoichiometric mixture of oxide powders including Bi_2O_3, H_3BO_3, SiO_2, Al_2O_3, and ZnO were homogenously mixed in a ball mill for several hours, and then the mixture were melted in an aluminum crucible at 1200°C for two hours in a high temperature electric resistance furnace. In the second step, the molten glass was removed from the furnace and poured into the deionized water, rapidly cooling to room temperature. After milling again in a ball mill for several hours, followed by sieving, the final micron glass frit with micro-size meter was obtained. The flowchart for preparing the glass frit by the conventional melt cooling route is shown in **Figure 3.5**. Moreover, the temperature profile of the molten glass frit during the melt process in a high-temperature electric resistance furnace is presented, as shown in **Figure 3.6**.

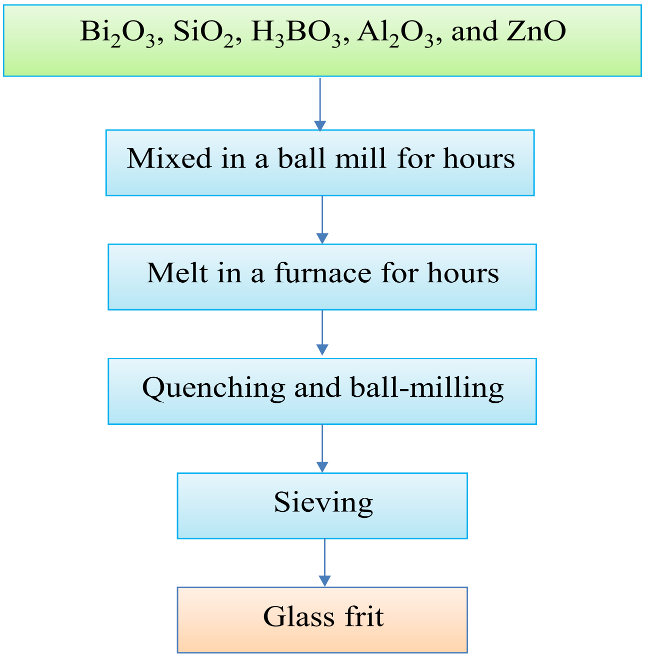

Figure 3.5 Flowchart for preparing glass frit by the conventional melt cooling route

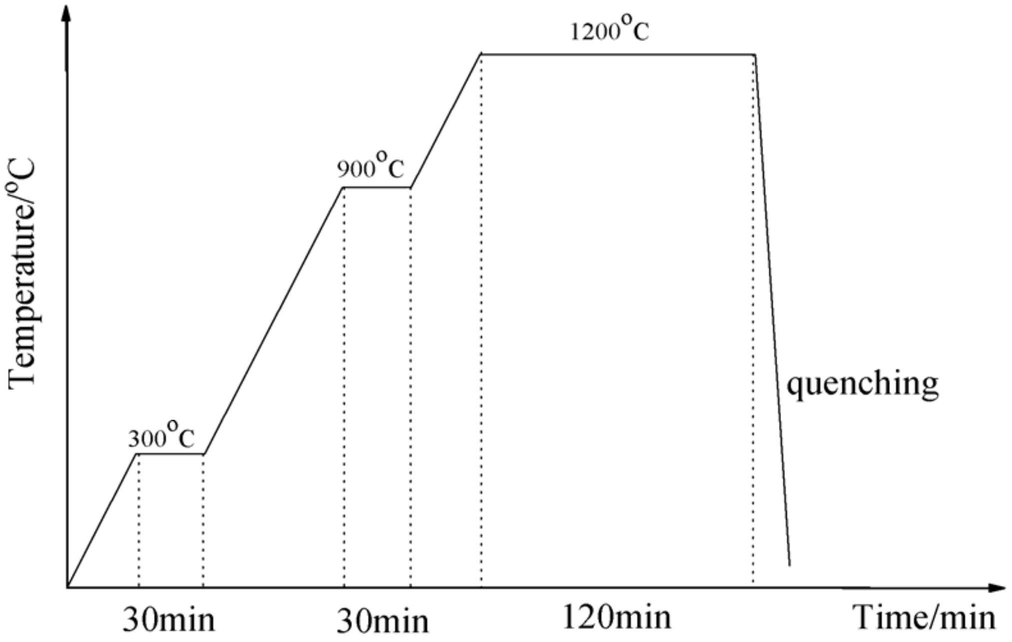

Figure 3.6 Temperature profile of the molten glass frit during melt process in a high-temperature electric resistance furnace

3.4.2 Characterization

Figure 3.7 shows the XRD pattern of the as-prepared Bi-Si-B-Al-Zn-O glass frit prepared by the traditional melting route. The amorphous state of the glass frit was identified by the result of X-ray diffraction, without any sharp peaks, and only broad peak can be found at around 28°. The broad peak is the typical feature of amorphous state materials, such as glass and organic polymer. After melting in the furnace, sharp quenching process is required for preventing crystallization.

The average size of the glass frit powders was 0.5-2μm, which can be seen from the SEM micrograph of the glass frit powders, as shown in **Figure 3.8**. This size dimension is similar to the commercial products used in silver paste for crystalline silicon solar cells. However, it is reported that smaller glass frit size leads to better

PV performance. Therefore, it is necessary to optimize the glass frit, which will be studied in next chapter.

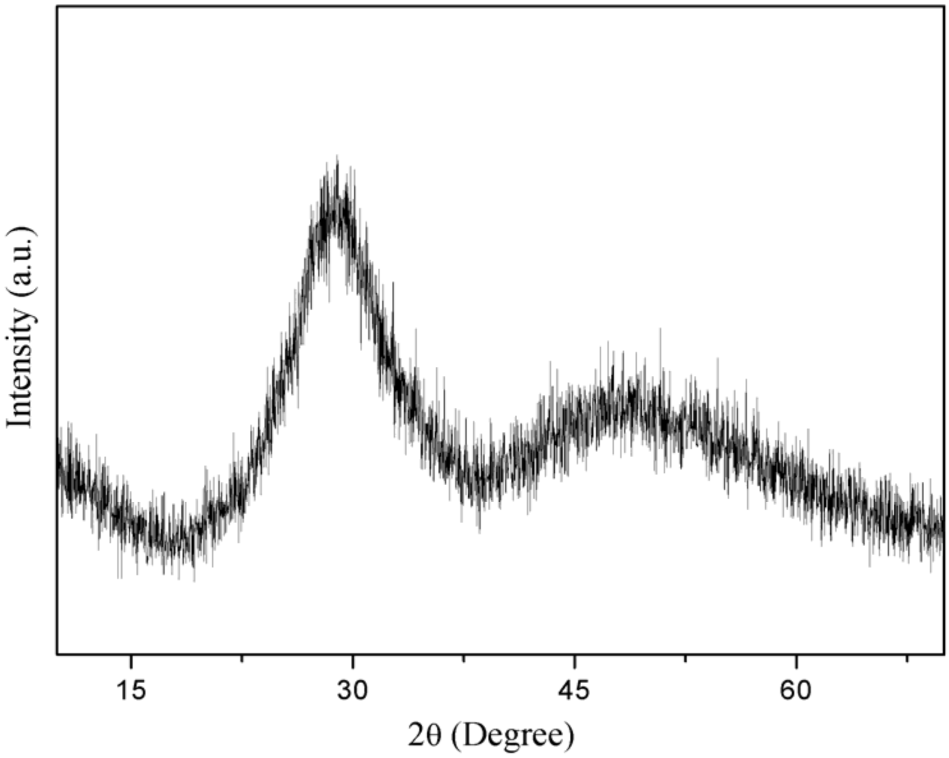

Figure 3.7 XRD pattern of the lead-free glass frit prepared by the traditional melt cooling route

Figure 3.9 shows the DSC curve of the glass frit powders prepared by the traditional melting route. It was noticed that the T_g of the glass frit powder is 385°C. The glass transition temperature of the glass frit plays a crucial role in the electrical and mechanical properties of the silver thick films. Hilali studied the effect of T_g on front contact, and indicated that the lower T_g results in better metallization contact with lower contact resistance under certain firing scheme **[25]**, which can be explained by that the glass frit with lower T_g flows easily during firing process, which allows the glass frit interacting with silver particles for longer time, and consequently dissolving more silver particles, resulting in larger and more silver crystallites at the silicon emitter interface, which can improve the possibility of encountering thin glass layer for tunnelling.

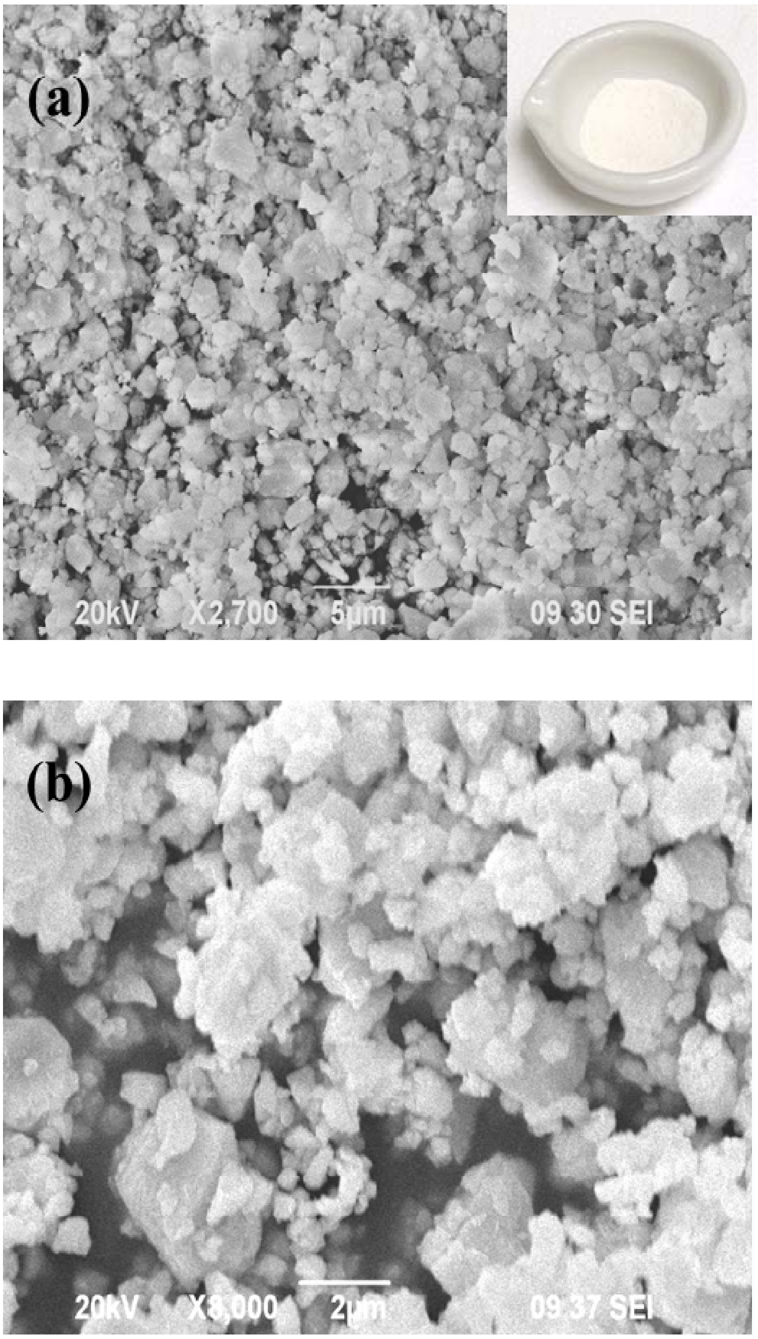

Figure 3.8 SEM micrographs of Bi–Si–B–Al–Zn–O glass frit powders prepared by the traditional melting route: (a) low resolution, where the inset shows the photograph of glass frit sample in a mortar; (b) high resolution.

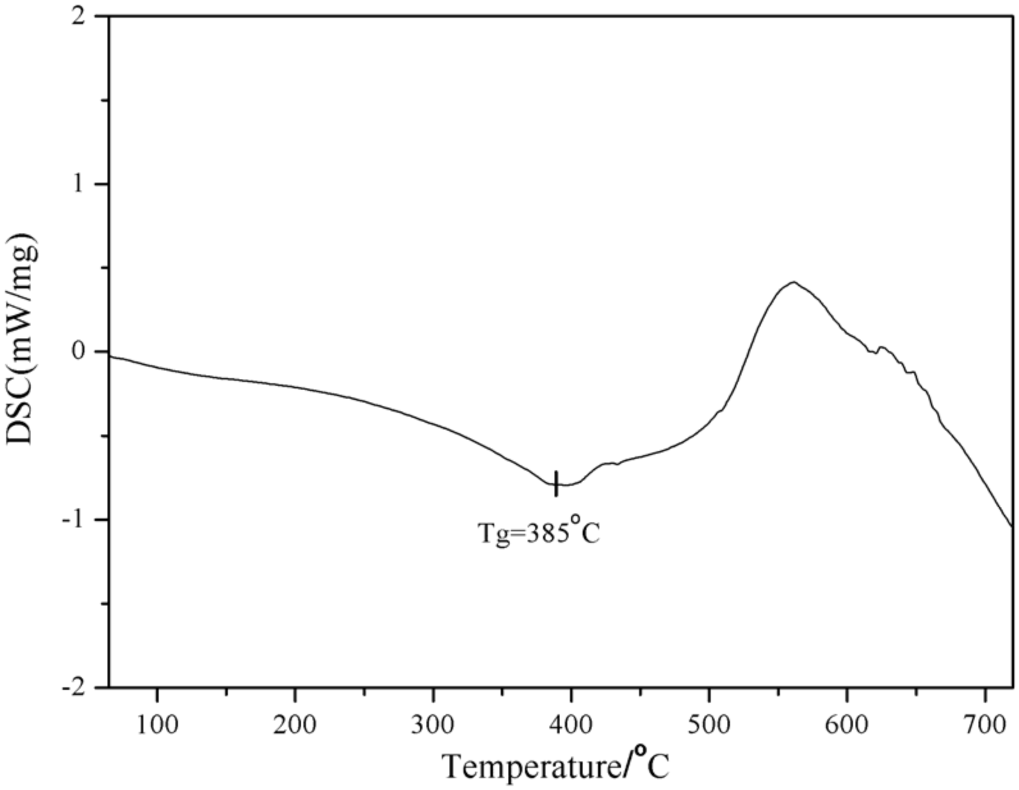

Figure 3.9 DSC curve of the Bi–Si–B–Al–Zn–O glass frit powders prepared by the traditional melting route

3. 5 Preparation of lead-free silver paste

3.5.1 Compositions

The silver front contact paste for crystalline silicon solar cells was prepared by the rotary evaporation method. Specifically, the as-prepared silver particles, lead-free glass frit powders and organic vehicle (ethyl celluloses and terpineol) are mixed at a certain ratio in ethyl alcohol. Other additives were also necessary to modify the rheology of the silver paste. Subsequently, the contents were concentrated in a rotary evaporator at about 40°C. After few hours ethyl alcohol was eliminated, and the preliminary product was finalized by a three-roller mill grinder. The composition of the silver paste was shown in **Table 3.3**. The final silver paste is shown in **Figure 3.11**. Silver electrodes were formed by screen-printing the as-prepared silver paste on crystalline silicon wafers with antireflective coating, using a screen-printing machine, followed by a firing process in a conveyor infrared furnace. After that, the fabricated solar cells were measured.

Table 3.3 Compositions of the as-prepared silver pastes

Paste ID	Silver particles	Glass frit	Organic vehicle	Ratio (wt%)
A	As-prepared	Bi-based	ethyl celluloses + terpineol	80/4/16
B	As-prepared	Pb-based	ethyl celluloses + terpineol	80/4/16

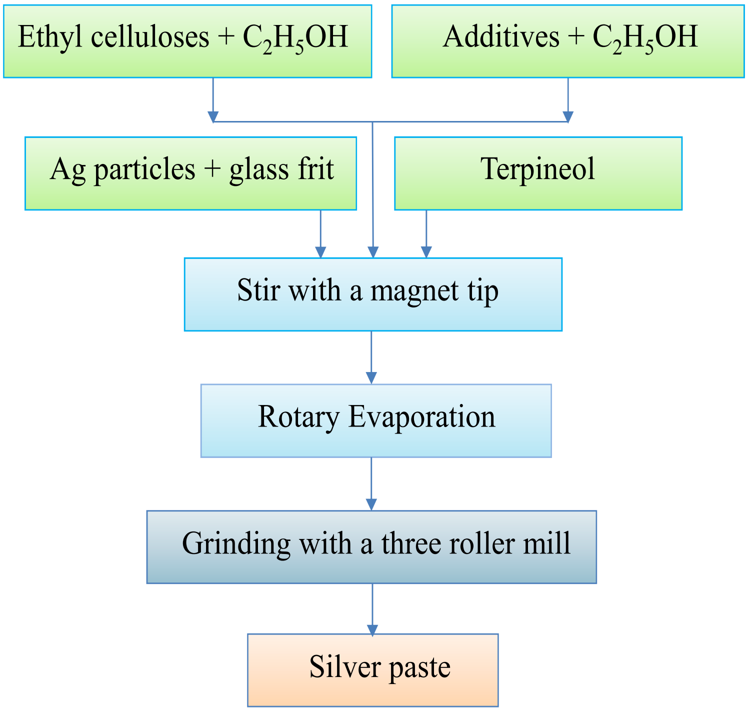

Figure 3.10 Flowchart for preparing silver front contact paste by the rotary evaporation method, using the as-prepared lead-free glass frit

Figure 3.11 Photograph of the as-prepared silver front contact paste using the lead-free glass frit for crystalline silicon solar cells

3.5.2 Characterization

As mentioned before, the wetting behavior and etching effect of glass frit powders on silver particles, anti-reflecting coating layer and silicon wafer are important to form high quality front contact metallization, which in turn determines the final photovoltaic performances of crystalline silicon solar cells. It mainly affects the contact resistance and the adhesion strength of silver electrodes to silicon wafers. If the wetting behavior and etching effect of glass frit are not efficient, the adhesion strength would be poor, as well as the contact conductivity. Therefore, the most important property need to be measured is the wetting behavior and etching effect. The key point which should be taken into consideration is the cross-section microstructure of the front contact resulting from the lead-free silver paste.

Here the morphology of the front thick film contact was characterized, which was formed using by screen-printing the silver paste based on the as-prepared Bi-based glass frit, followed by a firing process.

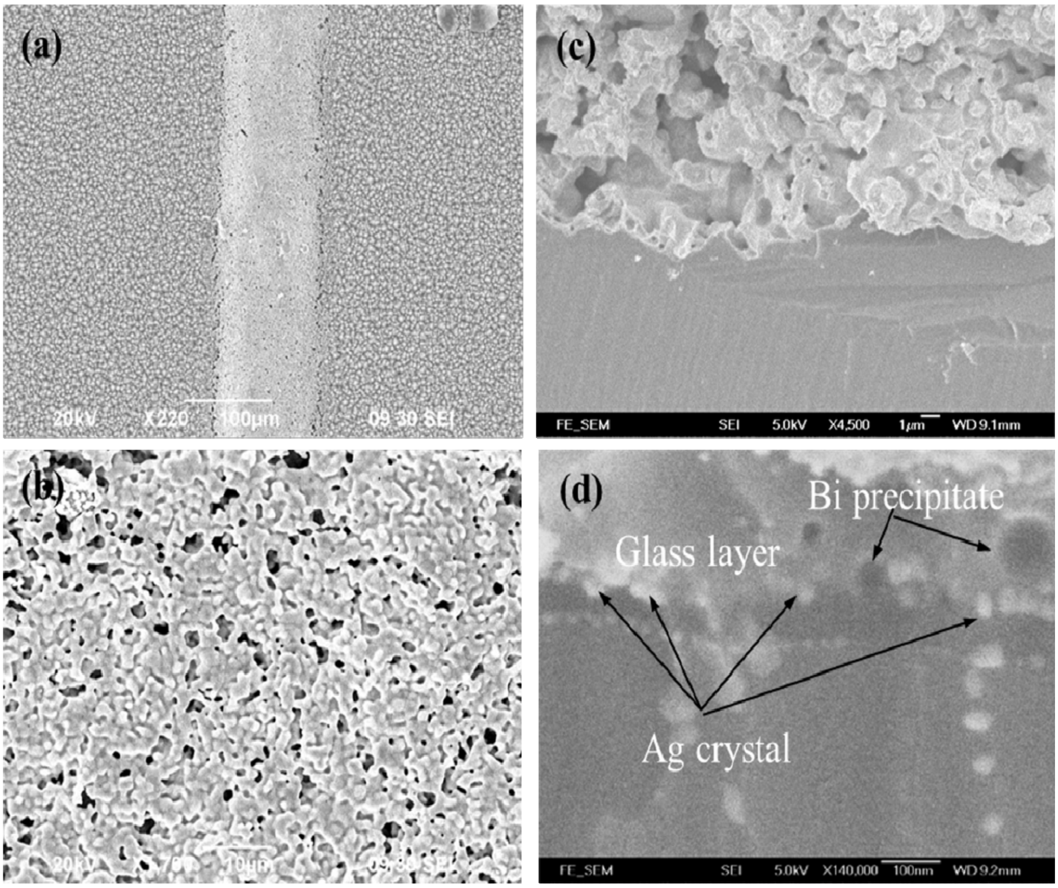

Figure 3.12 SEM top views of the silver electrode (a, b), and cross-section images (c, d) resulting from the Bi-based silver paste

Figure 3.12 shows the SEM top views of the silver electrode (a, b), and cross-section images (c, d). First, it is noticed that the silver thick film was dense, although a few pores can be found which may be ascribed to the natural sintering behavior of micro silver particles, or the slight agglomeration of silver particles prepared by the chemical reduction method. Besides, Bi-precipitates, small silver crystallites and a thin glass layer were formed, which are typical features of the front metallization contact, as shown in Figure **3.12 (d)**. Therefore, it can be said that the wetting behavior and etching effect of the Bi-based glass frit on silver particles, silicon nitride layer and silicon wafer are efficient. Note that similar results were found in the Pb-based silver thick film contact of crystalline silicon solar cells **[26]**. Therefore, it is preliminarily concluded that the as-prepared Bi-based glass frit is efficient as the substitute of the conventional Pb-based glass frit for the application in silver front contact paste for crystalline silicon solar cells. Certainly, the result should be further identified by the photovoltaic performance measurement of solar cells. Moreover, it can be seen that with the help of the glass frit powders during firing process, silver particles were sintered well, which is also important to form a homogenous continuous thick film metallization contact.

In fact, the front contact formation involves a series of complex chemical reductions during the firing process. It is assumed that at the initial stage, silver and even silicon are dissolved in the liquid glass phase. With the cooling down of the glass phase, silver particles start to grow into silicon and form small silver pyramids finally at the silicon emitter. It is also assumed that the liquid glass etches silicon wafer via redox reactions, functioning as a oxidizing agent. To illustrate the chemical reactions between the glass frit powders and silicon wafers, and the mechanism of front contact formation, a model was presented, from the silver/silicon interface contact structure, as shown in **Figure 3.13**, which was similar to the formation of the front contact resulting from the Pb-based silver paste **[26]**. Before the firing process, the silver paste consisting of the micron silver particles, Bi-based glass frit powders and organic vehicles is deposited on a silicon wafer with silicon nitride coating layer by screen-printing (**Figure 3.13(a)**). At the first stage of firing process, all the solvents and organic binder are evaporated and combusted. Then the viscosity of the glass frit decreases rapidly and becomes fluid soon to wet silver particles, and etch SiN_x layer and silicon wafer. The silver particles are dissolved in the glass phase and recrystalline on the silicon emitter surface, and finally small silver pyramids are formed (**Figure 3.13(b)**), as well as a thin glass layer and small metal precipitates formed on the emitter interface. The reactions of the glass frit on the SiN_x layer and silicon wafer can be explained by the following redox reactions:

$$2Bi_2O_{3\text{-}glass} + 3SiN_x \longrightarrow 4Bi + 3SiO_2 + 3x/2N_2 \qquad (1)$$

$$2Bi_2O_{3\text{-}glass} + 3Si \longrightarrow 4Bi + 3\ SiO_2 \qquad (2)$$

The resulting productions should be Bi-precipitates and SiO_2. In a word, the glass frit determines largly the quality of the metallization contact in crystalline silicon solar cells. Certainly, to further determine the perfomnce of the silver paste containing the as-prepared lead-free glass frit powders, the photovoltaic perfromances of the solar cells should be measured.

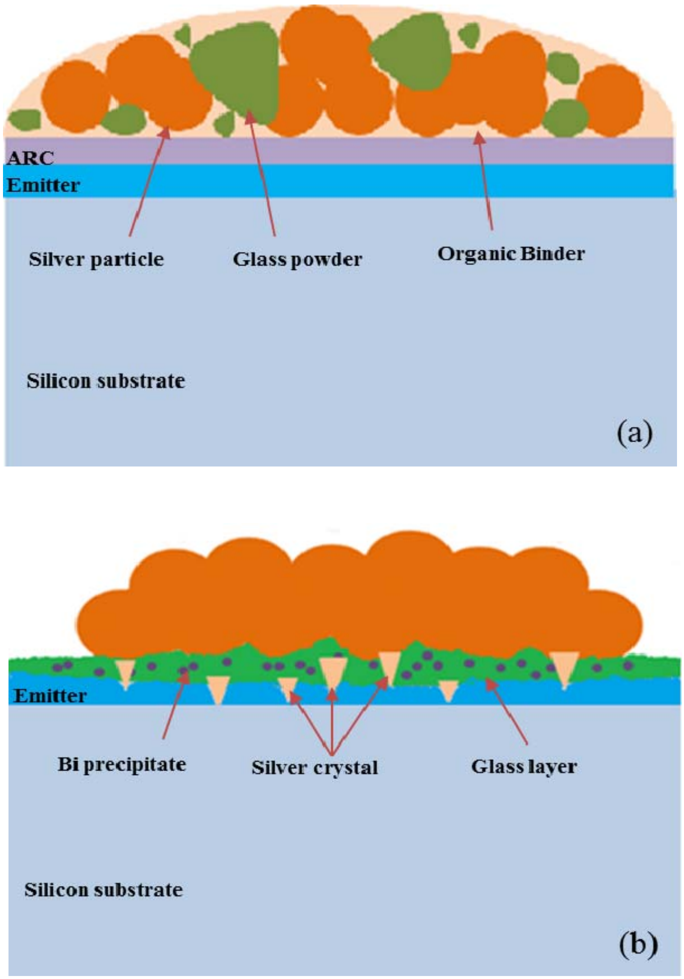

Figure 3.13 Schematic diagrams of the silver electrode, showing the mechanism of the metallization contact formation: (a) before firing process; (b) after firing process

The photovoltaic performance of the fabricated crystalline silicon solar cells resulting from the Bi-based silver paste (denoted as paste A) is shown in **Figure 3.14**. It can be seen that the fabricated silicon solar cells generated an open-circuit voltage (V_{oc}) of 618mV, a short-circuit current density (J_{sc}) of 34.3mA/cm^2, a fill factor (FF) of 72.5% and a conversion efficiency (E_{ff}) of 15.4%.

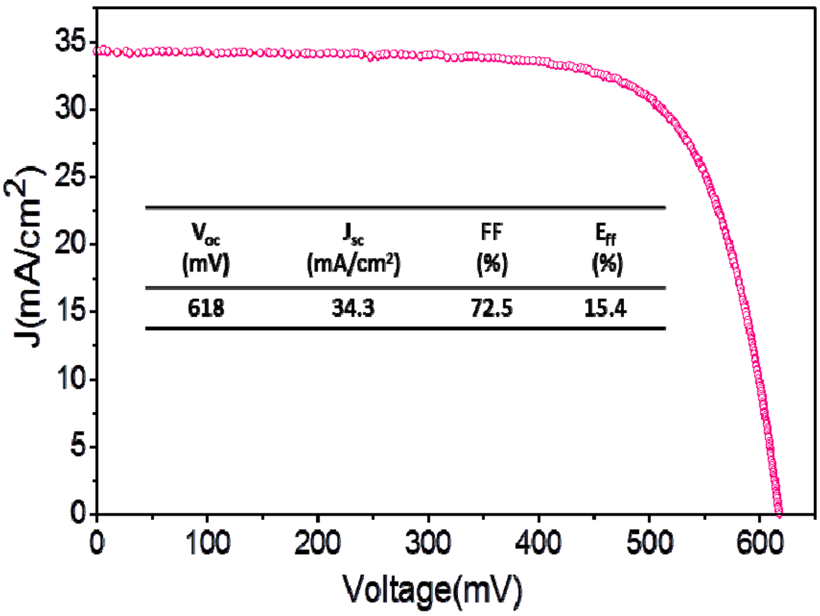

Figure 3.14 I-V performance of the fabricated crystalline silicon solar cells based on the as-prepared Bi-based glass frit powders, under AM 1.5 (1000W/m^2)

For comparison, an additional reference silver paste was prepared by mixing the as-prepared silver particles, commercial Pb-based glass frit and organic vehicle at the same ratio with the Paste A, denoted as paste B, whose composition was shown in **Table 3.2**. The current-voltage curve of the fabricated crystalline silicon solar cells based on the silver paste B is shown in **Figure 3.15**. It can be seen that the fabricated silicon solar cell generated an open-circuit voltage (V_{oc}) of 610mV, a short-circuit current density (J_{sc}) of 33.9mA/cm^2, a fill factor (FF) of 70.3% and a conversion efficiency (E_{ff}) of 14.5%. The fabricated crystalline silicon solar cell containing the as-prepared Bi-based glass frit as an inorganic binder exhibited higher electrical conversion efficiency compared with that of the solar cell fabricated resulting from the commercial lead-based glass frit. All other factors being equal except for the glass frit used in this work, this improvement should be attributed to the better metallization contact resulting from the Bi-based glass frit powders. For better understanding and development of high-performance silver front contact paste, it is really necessary to investigate the difference between these two kinds of glass frits. On basis of this consideration, the basic properties of the commercial Pb-based galss frit were also measured, including morphology and the typical feature of glass material-glass transition temperature.

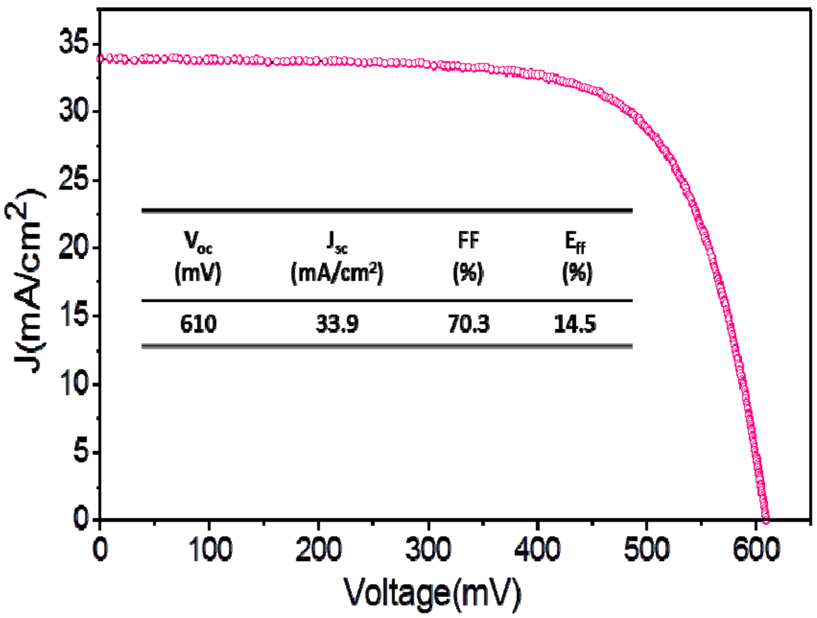

Figure 3.15 I-V performance of the fabricated crystalline silicon solar cells based on the commercial Pi-based glass frit powders, under AM 1.5 (1000W/m^2)

Figure 3.16 shows the SEM micrograph of the commercial Pb-based glass frit powders. It can be seen that from the SEM that the average size of the powders is 1-2μm, which is similar to the as-prepared lead-free glass powders, as shown in **Figure 3.8**. Whereas, it is noticed that the as-prepared lead-free glass frit exhibits better size distribution and better dispersibility than those of the commercial Pb-based glass frit.

All these are favor to obtain better front contact. Except for the size effect, as we discussed before, another important property of the glass frit is the T_g. Therefore, the T_g of the commercial Pb-based glass frit was also tested. **Figure 3.17** shows the DSC curve of the commercial Pb-based glass frit powders. From **Figure 3.17**, it can be seen that the T_g of the Pb-based glass frit is 440°C, which is higher than that of the as-prepared Bi-based glass frit. It is reported that lower T_g leads to better performance of front contact. On basis of what is discussed above, it is evident that the as-prepared Bi-based glass frit with better size distribution and lower T_g results in better photovoltaic performance of the fabricated crystalline silicon solar cells.

Moreover, it can be concluded that good front metallization contact of crystalline silicon solar cells can be achieved by using the as-developed Bi-based glass frit powders as an inorganic binder in the silver paste. Therefore, the as-prepared Bi-based glass frit is a promising substitute of the currently conventional Pb-based glass frit in silver front contact paste for crystalline silicon solar cells.

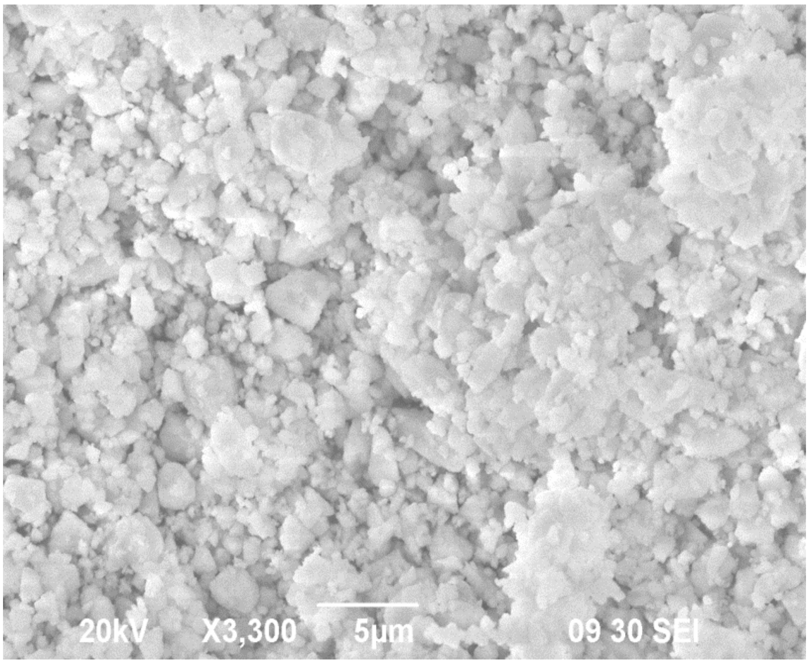

Figure 3.16 SEM image of the commercial lead-based glass frit powders

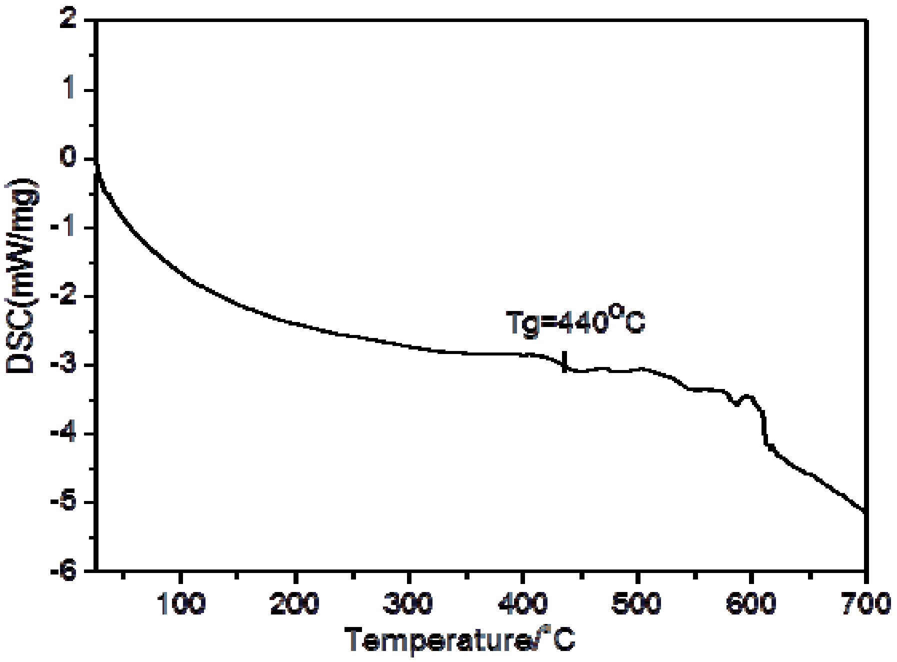

Figure 3.17 DSC curve of the commercial lead-based glass frit powders

3. 6 Conclusions

In summary, for better understanding and development of the novel silver front contact based on lead-free glass frit and nanomaterials, the preparation of conventional silver front contact pastes based on micron materials have been further developed. Frist, as the conduction phase in silver front contact paste, micro spherical silver particles were synthesized by the chemical reduction method, using silver nitrate as the metal source, ascorbic acid as the reducing agent and PVP as the dispersant agent. The morphology and phase structure of the as-prepared silver particles were observed by the SEM and XRD, respectively. From the SEM, it is demonstrated that the silver particles are quasi-spherical in shape, with an average size of 1.2μm, which can basically satisfy the requirement for application in silver front contact paste for crystalline silicon solar cells. Besides, the XRD pattern indicated that the silver particles were well crystallized with no crystallographic impurities. The only drawback is that there is, to a small degree, agglomeration behavior between the silver particles, although the PVP as a protective agent was added into the system. Future work is essential to optimize the disperisbility of silver particles. Second, as the inorganic binder in the silver front contact paste, micron lead-free (Bi-Si-B-Al-Zn-O) glass frit powders were prepared by the conventional melting route. The amorphous state of the glass frit was identified by the X-ray diffraction, with a broad peak found at around 28^o, while no sharp peaks were found. The glass transition temperature is 385°C. Consequently, the front contact silver paste was prepared using the as-prepared silver particles, lead-free glass frit and organic vehicle (ethyl celluloses and terpineol) by the rotary evaporation method. For comparison, the silver paste containing the commercial Pb-based glass frit was also prepared. The experimental results indicated that the fabricated crystalline silicon solar cell containing the as-prepared Bi-based glass frit as an inorganic binder exhibited higher electrical conversion efficiency compared with that of the solar cell fabricated resulting from the commercial lead-based glass frit. All other factors being equal except for the glass frit used in this work, this improvement should be attributed to the better metallization contact resulting from the Bi-based glass frit powder with better dispersibility and lower T_g than those of the commercial Pb-based glass frit. It can be concluded that good front metallization contact of crystalline silicon solar cells can be achieved by using the as-developed Bi-based glass frit powders as an inorganic binder in the silver paste. Therefore, the as-prepared Bi-based glass frit is a promising substitute of the currently conventional Pb-based glass frit in silver front contact paste for crystalline silicon solar cells.

References

[1] J.H. Kim, H.Y. Koo, Y.N. Ko, and Y.C. Kang, Characteristics of Bi-based glass frit having similar mean size and morphology to those of silver powders at high firing temperatures. *Journal of Alloys and Compounds*, 2010. **497**: 259-66.

[2] M.M. Hilali, S. Sridharan, C. Khadilkar, A. Shaikh, A. Rohatig, and S. Kim, Effect of glass frit chemistry on the physical and electrical properties of thick-film Ag contacts for silicon solar cells. *Journal of Electronic Materials*, 2006. **35**:2041-7.

[3] K.K. Hong, S.B. Cho, J.S. You, J.W. Jeong, S.M. Bea, and J.Y. Huh, Mechanism for the formation of Ag crystallites in the Ag thick-film contacts of crystalline Si solar cells. *Solar Energy Materials and Solar Cells*, 2009. **93**:898-904.

[4] S.J. Jeon, S.M. Koo, and S.A. Hwang, Optimization of lead- and cadmium-free front contact silver paste formulation to achieve high fill factors for industrial screen-printed Si solar cells. *Solar Energy Materials and Solar Cells*, 2009.**93**:1103-09.

[5] G. Schubert, F. Huster, and P. Fath, Physical understanding of printed thick-film front contacts of crystalline Si solar cells-Review of existing models and recent developments. *Solar Energy Materials and Solar Cells*, 2006.**90**: 3399-406.

[6] J. Hoornstra, G. Schubert, K. Broek, F. Granek, and C. LePrince, *Proc. 31st IEEE Photovoltaic Specialists Conf.*, Orlando, Florida , 2005. 1293.

[7] M. M. Hilali, B. To, and A. Rohatgi, Proc. *14th Workshop on Crystalline Silicon Solar Cell & Modules: Materials and Processes*, Winter Park, Colorado, 2004. 109.

[8] K.K. Hong, S.B. Cho1, J.Y. Huh, H.J. Park, and J.W. Jeong, Role of PbO-Based Glass Frit in Ag Thick-Film Contact Formation for Crystalline Si Solar Cells. *Metals and Materials International*, 2009. **15**: 307-12.

[9] B. Sopori, V. Mehta, P. Rupnowski, J. Appel, M. Romero, H. Moutinho, D. Domine, B. To, R. Reedy, M. Al-Jassim, A. Shaikh, N. Merchant, C. Khadilkar, D. Carlson, and M. Bennet, *Proc. 17th Workshop on Crystalline Silicon Solar Cells & Modules: Materials and Processes*, Vail, Colorado, 2007. 93.

[10] European directive RoHS, 2002/95/EC.

[11] D.S. Seo, S.H. Park, and J.K. Lee, Sinterability and conductivity for sliver paste with Pb-free frit, *Current Applied Physics*, 2009. **9**: S72-74.

[12] J.H. Kim, H.Y. Koo, Y.N. Ko, and Y.C. Kang, Characteristics of Bi-based glass frit having similar mean size and morphology to those of silver powders at high firing temperatures. *Journal of Alloys and Compounds*, 2010. **497**: 259-66.

[13] Y.P. Zhang, Y.X. Yang, J.H. Zheng, W. Hua, and G.R. Chen, Thermal properties of glass frit and effects on Si solar cells. *Materials Chemistry and Physics*, 2009. **114**: 319-22.

[14] J. Hoornstra, G. Schubert, K. Broek, F. Granek, and C. LePrince, Lead free metallisation paste for crystalline silicon solar cells: from model to results. *in: Proceedings of the 31st IEEE Photovotaic Specialists Conference*, Florida, 2005. 651-54.

[15] M. Bahr, S. Kim, S. Sridharan, C. Khadilkar, J. Lossen, and S. Dauwe, On lead and cadmium free metallizations for industrial solar cells and modules. *in: Proceedings of the 21st European Photovoltaic Solar Energy Conference*, Dresden, Germany, 2006. 859-64.

[16] J.H. Yi, H.Y. Koo, J.H. Kim, Y.N. Ko, Y.J. Hong, Y.C. Kang, H.M. Lee, Pb-free glass frits prepared by spray pyrolysis as inorganic binders of Al electrodes in Si solar cells. *Journal of Alloys and Compounds*, 2011. **509**:6325-31.

[17] G.Q. Guo, W.P. Gan, J. Luo, F. Xiang, J.L. Zhang, H. Zhou, and H. Liu, Preparation and dispersive mechanism of highly dispersive ultrafine silver powder. *Applied Surface Science*, 2010. **256**: 6683-87.

[18] L. Zhao, X.L. Qi, and H. Wang, Synthesis and characterization of spherical and mono-disperse micro-silver powder used for silicon solar cell electronic paste. *Advanced Powder Technology*. 2012. **23**: 250-55.

[19] J.L.H. Chau, M.K. Hsu, C.C. Hsieh, and C.C. Kao, Microwave plasma synthesis of silver nanopowders, *Materials Letters*, 2005. **59**: 905-08.

[20] Z.H. Liu, Z.Y. Liu, Q.H. Li, H.P. Wu, and D.M. Zhang, Morphology control of microsized spherical silver powder prepared by spray pyrolysis. *The Chinese Journal of Nonferrous Metals*, 2007. **17**: 149-55.

[21]Y. Zhou, L. Hao, Y. Hu, Y. Zhu, and Z. Chen, Synthesis of nanowires and coral-shaped nanostructures of Ag by an ultraviolet photo-reduction technique at room temperature. *Chemistry Letters*, 2001, **30**: 1192-93.

[22] M.Z. Si, Y. Fang, J.L. Peng, and P.X. Zhang, Nano-silver colloids prepared by electrolysis and research on its SERS activity. *Spectroscopy and Spectral Analysis*, 2007. 27: 948-52.

[23] J. Keskinen, P. Ruuskanen, M. Karttunen, and S.P. Hannula, Synthesis of silver powder using a mechanochemical process. *Applied Organometallic Chemistry*, 2001.**15**: 393-95.

[24] Z. Zhang, B. Zhao, and L. Hu, PVP protective mechanism of ultrafine silver powder synthesized by chemical reduction processes. *Journal of Solid State Chemistry*, **1996**. **121**: 105-10.

[25] M.M. Hilali, A. Rohatgi, and B. To A review and understanding of screen-printed contacts and selective- emitter formation. *14th workshop on crystalline silicon solar cells and modules*, Colorado, USA. 8-11 Augest. 2004

[26] K.K. Hong, S.B. Cho, J.S. You, J.W. Jeong, S.M. Bea, and J.Y. Huh. Mechanism for the formation of Ag crystallites in the Ag thick-film contacts of crystalline Si solar cells. *Solar Energy Materials and Solar Cells*, 2009. **93**: 898-904.

CHAPTER 4 DEVELOPMENT OF NANO GLASS FRIT BY SOL-GEL MATHOD

4.1 Introduction

As discussed in the previous chapter, most of the commercially available silver front contact pastes for crystalline silicon solar cells contain lead, usually in form of lead oxide incorporated in the glass frit powders [1-3]. Many researchers indicated that crystalline silicon solar cells prepared using lead-free glass frit, for example bismuth glass, can also achieve high photovoltaic performances [4-6]. Our previous experimental result was also a case in point. Nevertheless, either Pb-based or Bi-based glass frit for silver front contact paste, is usually prepared by conventional route at high temperature, namely higher than 1000°C, featured with large energy consumption and heavy pollution. Zhang et al. prepared lead-boron-silicate glass frit for crystalline silicon solar cells by the traditional melting route [7]. In his experiment, regent grade chemicals were used as the starting raw materials to obtain glass. After being melted in an alumina crucible at the temperature of 1000 ~ 1250°C and poured into deionized water, the glass frit were obtained. Kim et al. prepared Bi_2O_3-ZnO-SiO_2-B_2O_3-Al_2O_3-CaO glass frit powder for silicon solar cells with T_g of 442°C by the spray pyrolysis method [8]. The average size of the glass frit powders obtained at 1400°C is 0.87μm.

In fact, there are also many other drawbacks for these methods. The most obvious is the impurity of glass frit. During the high temperature melting process, the glass frit is easily contaminated with external impurity. As we know, even the minority of impurity is fatal for silicon solar cells, which would become recombination center for the "minority" in silicon wafer. Moreover, the size of conventional glass frit powders is generally large (more than 1μm). As reported in Ref. **[9]**, the size of glass frit plays a key role in the solar cell performance. Jeon et al. studied the size effect on the front contact metallization formation and photovoltaic performances of the fabricated solar cells, and concluded that the silver front contact paste prepared using the glass frit powders with a smaller mean size tends to result in a higher photo-electrical conversion efficiency **[9]**. To overcome these drawbacks of the conventional glass frit, the goal of this study is to prepare lead-free glass frit powders in nano meter, and minimize the preparation temperature requirement as low as possible.

The sol-gel method has been used for a long time to prepare glass powders for its many potential advantages over to the conventional melting route. First, glass frit can be obtained at much lower temperature than the melt cooling route. It is well known that high temperature is required in the conventional melt cooling route for preparing glass frit, and the temperature must be kept for several hours to make sure the glass be molten homogeneously, which is a high-energy consumption process, while the sol-gel method is a low temperature process. Second, the sol-gel method can reduce external pollutions. As for the conventional melting route, the glass frit is easily contaminated by the crucible corrosion and the impurities from the melting furnace. Moreover, as the compositions are mixed in a single-phase liquid, namely molecular mixing, the glass frit prepared by a sol-gel process should be homogenous.

Specifically, the sol-gel process is a wet-chemical technique, which is used primarily for preparing materials starting from a precursor solution. There are many successful cases for preparing nano glass frit powders by the sol-gel process **[10-14]**. M. Taira et al. prepared SiO_2-Al_2O_3 glass powders by the sol-gel process for dental applications **[15]**. As far as we know, there are no precedent reports to prepare glass frit powders by the sol-gel process for crystalline silicon solar cells. In this study, we tried to prepare lead-free nano glass frit for silver front contact paste by sol-gel process, and optimized the formulation to obtain higher photovoltaic performance than that resulting from solar cells based on conventional micron glass frit.

4.2 Experimental materials and equipment

4.2.1 Experimental materials

All the materials used in the experiments are listed in **Table 4.1.**

Table 4.1 Experiment materials

Name	Remark	Manufactory
Ethyl orthosilicate	TEOS, AR.	China National Pharmaceutical Group Industry Corporation Ltd
Ammonia	AR. 28+%	Xilong Chemical Co., Ltd
Aluminum nitrate nonahydrate	AR.	China National Pharmaceutical Group Industry Corporation Ltd
Bismuth(III) nitrate pentahydrate	AR.	China National Pharmaceutical Group Industry Corporation Ltd
Zinc nitrate hexahydrate	AR.	China National Pharmaceutical Group Industry Corporation Ltd
Boric acid	AR.	China National Pharmaceutical Group Industry Corporation Ltd
Anhydrous ethyl alcohol	AR.	Xilong Chemical Co., Ltd

Acetone	AR.	Tianjin Fuchen Chemical Reagent Factory
Hydrochloric acid	AR.	Tianjin Fuchen Chemical Reagent Factory
Acetic acid	AR.	Tianjin Chemical Reagent Ltd.
Bismuth (III) oxide	AR.	China National Pharmaceutical Group Industry Corporation Ltd
Silicon dioxide	AR.	China National Pharmaceutical Group Industry Corporation Ltd
Boric acid	AR.	China National Pharmaceutical Group Industry Corporation Ltd
Aluminum oxide	AR.	China National Pharmaceutical Group Industry Corporation Ltd
Zinc oxide	AR.	China National Pharmaceutical Group Industry Corporation Ltd
Ethylene glycol	AR.	Xilong Chemical Co., Ltd
Terpineol	AR.	Xilong Chemical Co., Ltd

4.2.2 Equipment

All the equipment used in the experiments is listed in **Table 4.2.**

Table 4.2 Equipment list

Name of instrument	Instrument model	Manufactory
Rotary evaporator	RE-52	Shanghai Yarong Biochemical Apparatus Factory

Semi-automatic screen printing machine	SYP2230	Shenzhen Qiaopai Screen Machine Factory
Electric heating air-blowing drier	101-2	Shanghai Guangdi Instruments Equipment Co., Ltd
Magnetic Stirring Apparatus	78-1	Changzhou Aohua Instruments Equipment Co., Ltd
Ultrasonic generator	KQ3200E	Kunshan Ultrasonic Electronic Equipment co., ltd
Electronic balance	ES120	Shenzhen Zhicheng Electronic Balance Co., Ltd
Laboratory pH meter	PHB-5	Shanghai Hongji Instruments Equipment Co., Ltd
All-directional planetary ball mill	PMQW0.4L	Nanjing Shunchi Technology Development Co. Ltd
Oilless vacuum pump	AP-550V	Institute of Microelectronics of Chinese Academy of sciences
Oilless compressor	EWS24	Zhejiang Jonway Machinery & Electric Manufacture Co., Ltd
Three-roller mill	S65	Changzhou Wujin Xingye Mechanical Equipment Co., Ltd

4. 3 Preparation of nano glass frit by sol-gel method

4.3.1 Mechanism

Figure 4.1 shows the principle for synthesizing nano glass frit powders by the sol-gel method. In a sol-gel process, there are typical two main steps: hydrolysis and condensation of alkoxide precursor, such as TEOS. The chemical reactions of metal alkoxide $M(OR)_x$ involves in the process can be demonstrated as follows:

$$MOR + H_2O \rightarrow MOH + ROH \qquad (1)$$

$$MOH+ROM \rightarrow M\text{-}O\text{-}M+ROH \qquad (2)$$

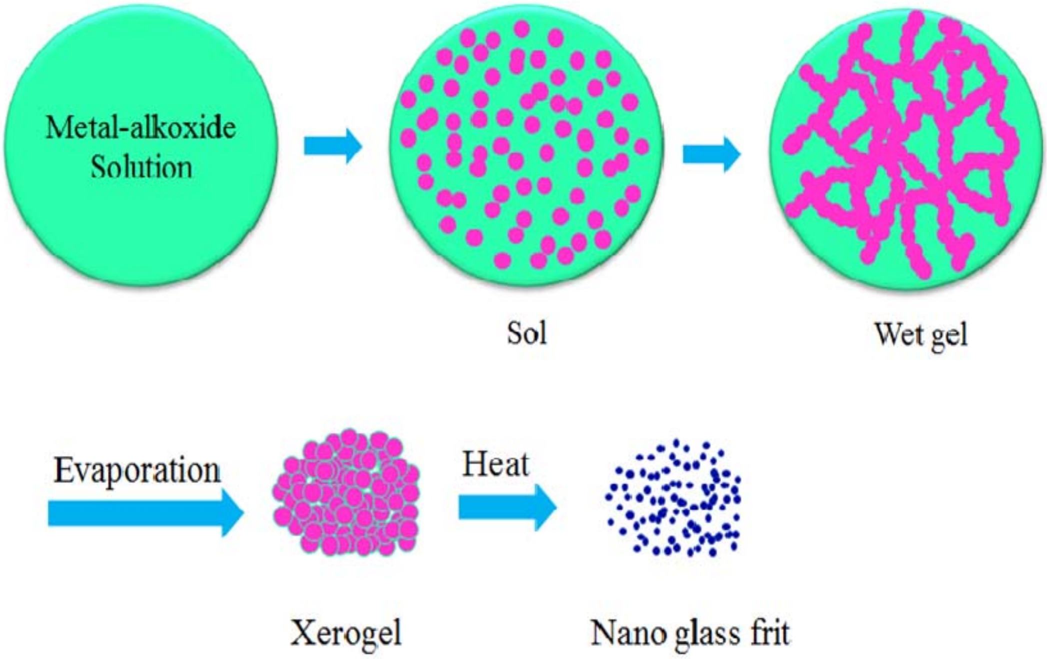

Figure 4.1 Schematic representation of synthesis of nano glass frit powders by the sol-gel process

In this wok, ethyl orthosilicate, aluminum nitrate nonahydrate, bismuth(III) nitrate pentahydrate, zinc nitrate hexahydrate and boric acid were used as metal precursor. The nano glass frit for silver front contact paste was obtained from a multicomponent gel in the Bi_2O_3-SiO_2-B_2O_3-Al_2O_3-ZnO system. **Figure 4.2** shows the flowchart for preparing the glass frit by sol-gel process. In a typical experiment, there are four steps for synthesizing the nano glass powders in our work as follows: 8ml TEOS was mixed with 50ml C_2H_5OH and stirred at room temperature for at least two hours with a magnetic stirrer and finally the solution A was obtained. Next, the solution B consisting of 50 ml C_2H_5OH and 3ml $NH_3 \cdot H_2O$ was added into the solution A and the mixed solution was obtained. At the same time, $Al(NO_3)_3$ and $Zn(NO_3)_2$, dissolved by C_2H_5OH, was added into the mixed solution. $Bi(NO_3)_3$ and HBO_3, dissolved by $C_3H_8O_3$, was added into the mixed solution, and finally the solution C was obtained. After drying the solution C in open air for several hours at 60°C, transparent gel can be obtained, followed by drying under vacuum at 160-200°C for several hours to eliminate the volatile materials. To obtain amorphous glass frit powder, the xerogel needs to be heated at around 500°C for several hours.

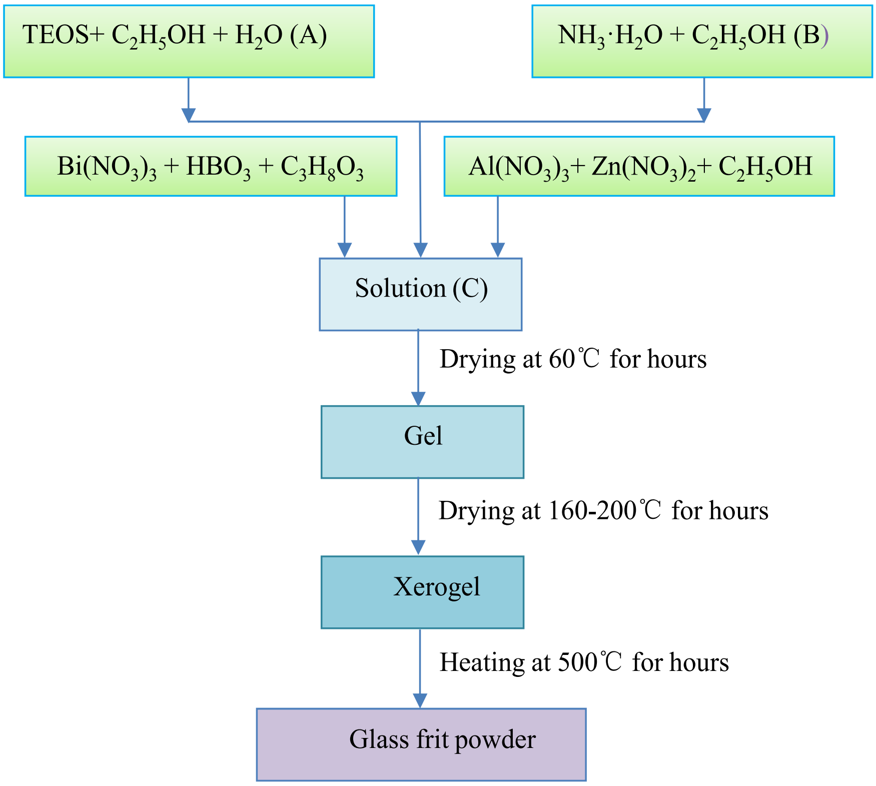

Figure 4.2 Flowchart for synthesizing lead-free nano glass frit by sol-gel method

4.3.2 Characterization

After drying the transparent Bi-B-Si-Al-Zn-O gel under vacuum at 160-200°C for several hours, the xerogel was obtained. To determine the heat treatment temperature, the thermal property of the xerogel was measured. **Figure 4.3** shows the TGA curve of the xerogel. It can be seen that a significant weight loss was observed from 200°C to 350°C, which should be associated with the combustion of precursors. The weight remained constant after 500°C, indicating that the organics were almost eliminated completely at 500°C. According to the thermal analysis of the xerogel, the temperature of 500°C was preliminary selected for heat treatment to obtain glass frit powders.

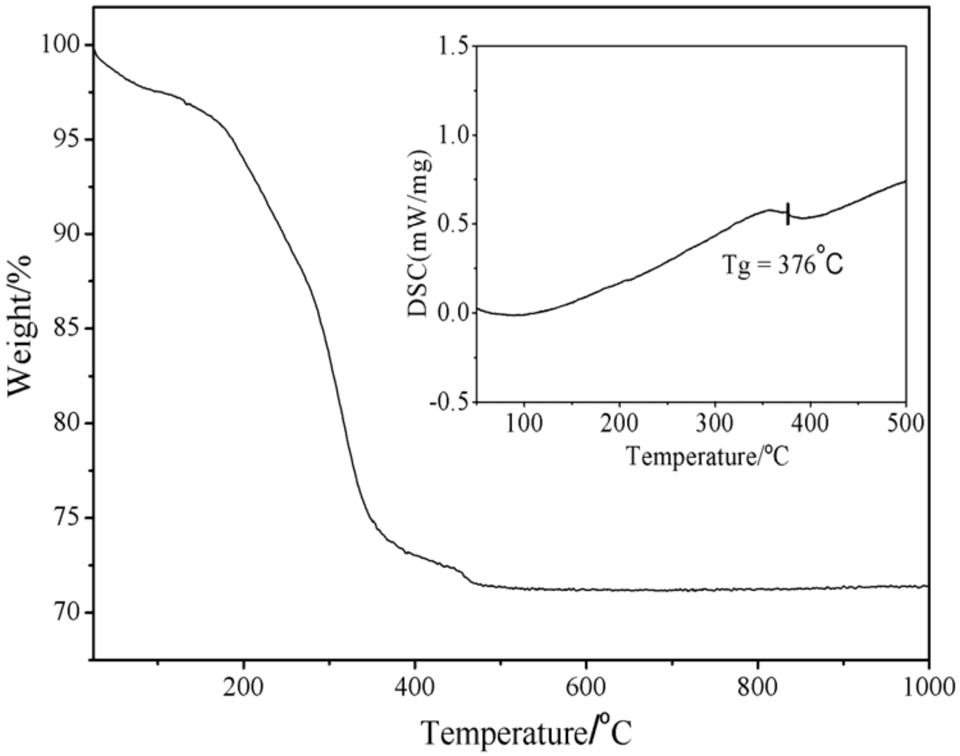

Figure 4.3 TGA curve of the Bi-Si-B-Al-Zn-O xerogel, where the inset shows the DSC curve of the nanosized glass frit powders prepared by sol-gel process

The amorphous state of the powders needs to be justified. Via the X-ray diffraction study, the phase structure of the powders after heat treatment was observed. **Figure 4.4 (a)** shows the XRD result of the powders. It is demonstrated that the xerogel has been converted into amorphous glass frit after heat treatment at 500°C. For comparison, a glass frit sample with the same composition was prepared by the conventional melt cooling route. **Figure 4.4 (b)** shows the X-ray diffraction result of the powders. It is noticed that both the glass frit exhibited broad diffraction peaks at about 27^{o} in the XRD patterns, indicating the amorphous state. Therefore, the heat treatment temperature of 500°C for obtaining nano glass frit was reasonable.

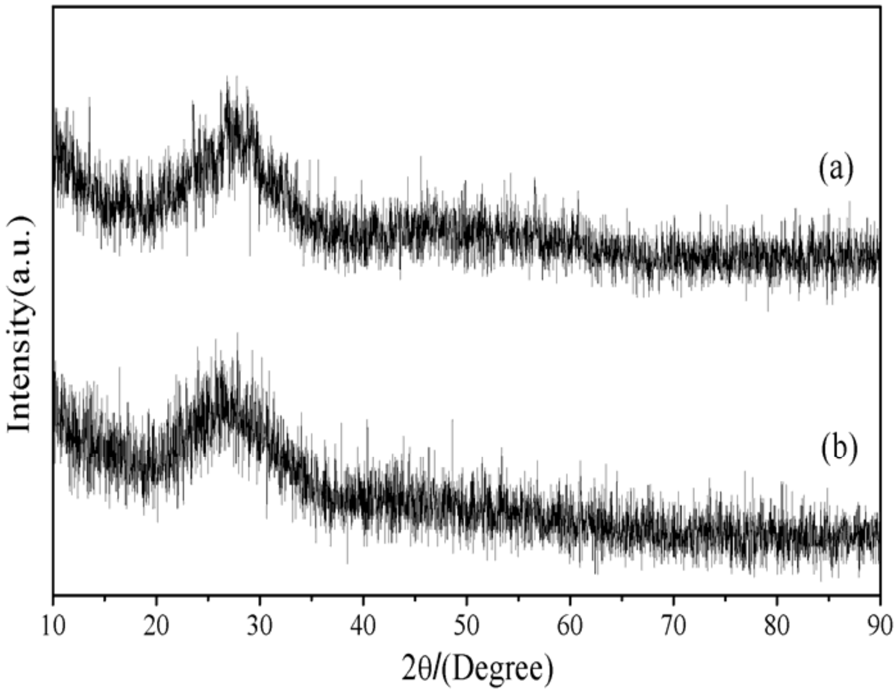

Figure 4.4 XRD patterns of: (a) nano glass frit powders prepared by sol-gel process; (b) micron glass frit powders prepared by the melt cooling route.

As mentioned before, as an important parameter, the glass transition temperature determines largely the quality of the front metallization contact, and in turn affects the photovoltaic performance of the silicon solar cells. To observe the T_g of the glass frit, the DSC curve of the glass frit sample was recorded, as shown in the upper right corner of **Figure 4.3**. It can be seen that the T_g of the glass frit powders was 376°C.

Figure 4.5 shows the SEM micrograph of the glass frit powders prepared by the sol-gel process. It is demonstrated that the mean size of the glass frit powders prepared by the sol-gel process was much smaller than that of the glass frit powders prepared by the conventional melt cooling route. The mean size of the former powders was about 100 nm, while that of the latter was about 0.5-2μm, as illustrated in the previous chapter. As mentioned above, it could be deduced that the silver front contact paste formulated using the nano glass frit powders tends to form a better front contact, which in turn leads to better solar cell performance, which would be identified by the later photovoltaic performance measurement.

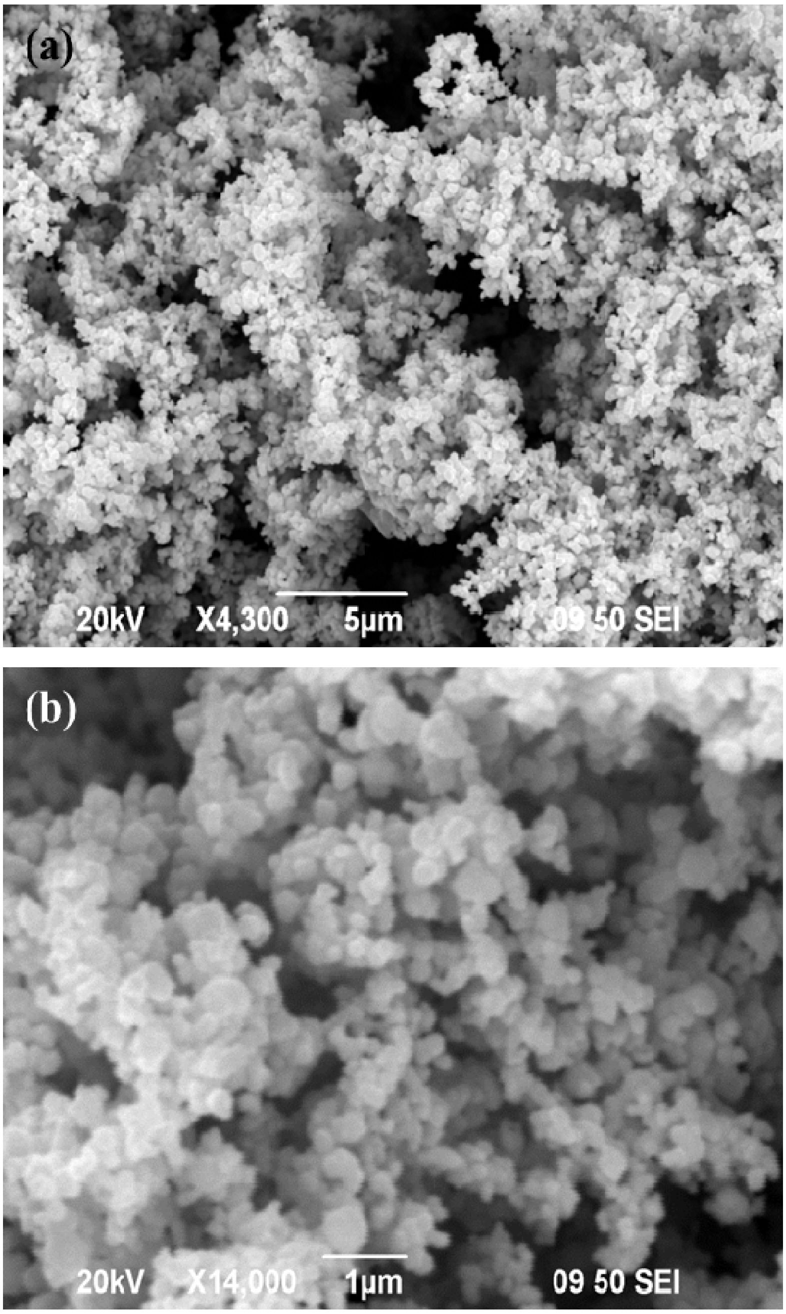

Figure 4.5 SEM micrographs of the nano glass frit powders prepared by sol-gel method, (a) low resolution, (b) high resolution

4.3.3 Wetting behavior and etching effect of nano glass frit

As discussed before, the ability of wetting and etching through the SiN_x layer and reacting with silicon wafer are the key properties for an effective glass frit powder in silver front contact paste for crystalline silicon solar cells. To determine the wetting behavior and etching effect during high temperature, the test glass paste containing the nano glass frit was prepared. Specifically, the test paste was prepared by mixing the as-developed nano glass frit powders, and organic vehicles (terpineol and ethyl celluloses) at a certain ratio in ethyl alcohol. Then the contents were concentrated in a rotary evaporator at about 40°C, and finalized by a three-roller-mill grinder. Subsequently, the glass paste was deposited on a silicon wafer with SiN_x layer deposited using plasma-enhanced chemical vapor deposition, followed by firing process in a tube furnace at 800°C for ten minutes. Finally the glass fingers were obtained. To determine the wetting behavior and etching effect of the glass frit, the key point which should be taken into consideration is the cross-section microstructure of the contact interface of glass fingers and silicon wafer.

Here the interface of the glass front contact from the test glass paste is characterized. **Figure 4.6** shows the SEM micrographs of the glass fingers deposited by screen printing on silicon wafer with SiN_x layer: **(a)** top view; and **(b)** cross-section image. It is noticed from **Figure 4.6 (a)** that the nano glass frit wetted SiN_x layer and silicon wafer surface homogenously during high temperature. Besides, small metal precipitates and a few pores were observed on the silicon emitter interface, as shown in **Figure 4.6 (b)**. As mentioned in previous chapter, all these are typical characteristics of the glass frit for silver front contact paste for crystalline silicon solar cells. Therefore, the experimental results demonstrated that the nano glass frit powders has acceptable wetting behavior and etching effect for application in the silver front contact paste for crystalline silicon solar cells.

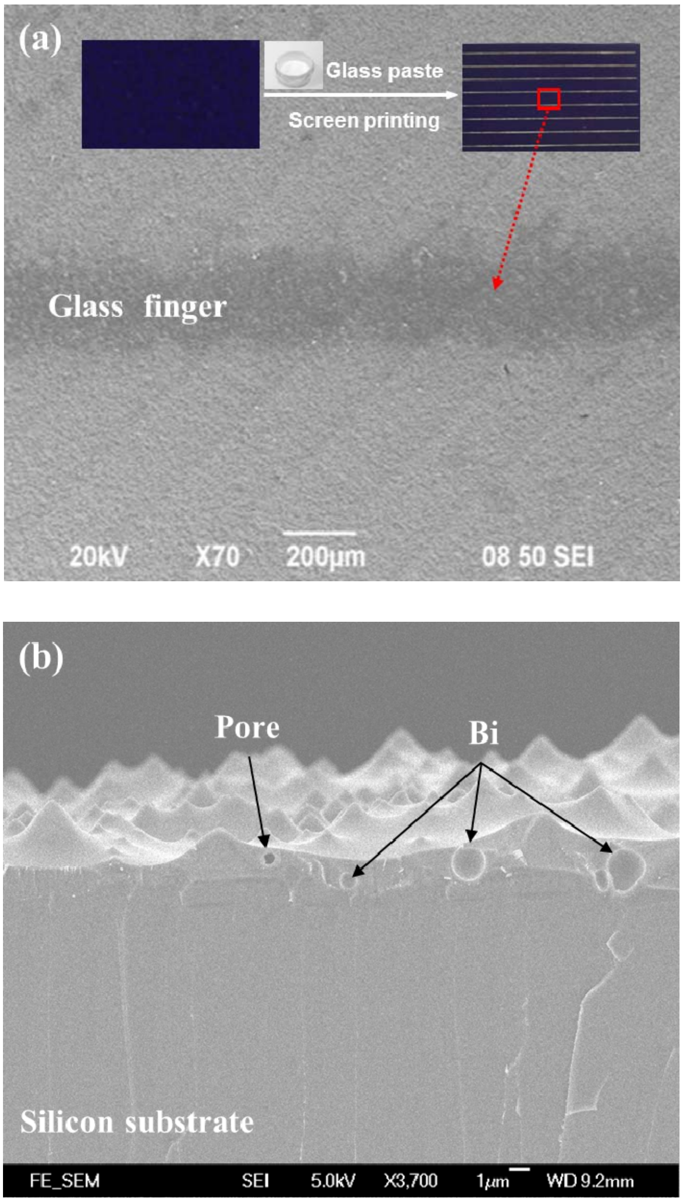

Figure 4.6 SEM images of the glass fingers deposited on a silicon wafer with SiN_x coating layer by screen-printing after the firing process: (a) top view; and (b) cross-section image; small metal precipitates and a few pores were observed on the silicon wafer interface, which are typical features for glass frit for silver front contact paste, demonstrating its efficient wetting behavior and etching effect on SiN_x coating and silicon wafers.

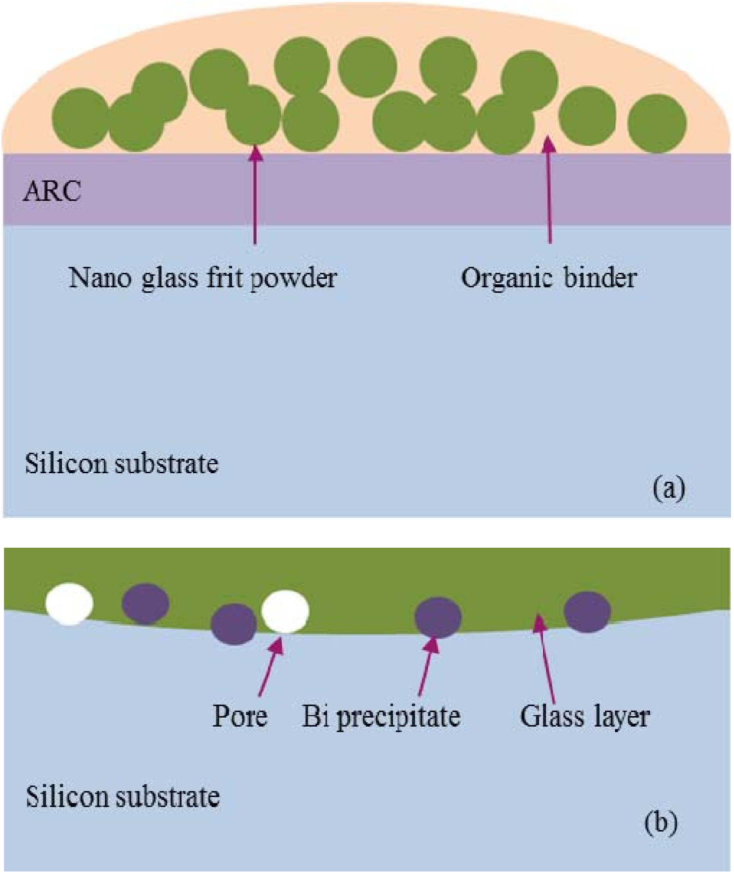

Figure 4.7 Schematic diagrams of the glass finger consisting of the nanosized glass frit powders and inorganic binder deposited by screen-printing on silicon substrate with SiN_x coating: (a) before firing process, (b) after firing process

To explain this issue clearly, a model is presented, as shown in **Figure 4.7** to explain in detail the mechanism of reactions between the nano glass frit powders and SiN_x layer and silicon wafer. Before the firing process, the glass finger consisting of the as-prepared nano glass frit powders and organic vehicles is deposited on silicon substrate with SiN_x layer by screen-printing, as shown in **Figure 4.7 (a)**. During high temperature heat treatment, the nano glass frit gets fluid soon to wet and etch the SiN_x layer and silicon wafer. Similar to the analysis in previous chapter, it is assumed that the resulted productions should be small Bi precipitates and the few pores should be related to the release of N_2 during the redox reactions, as shown in **Figure 4.7 (b)**.

4.3.4 Effect on PV performance

As mentioned above, the silver front contact paste containing glass frit powders with smaller mean size tends to resulting in higher photovoltaic performance of crystalline silicon solar cells. To determine the effect of the as-prepared nano glass frit powders on PV performance of silicon solar cells, the silver front contact paste containing the nano glass frit was prepared (denoted as paste A). Subsequently, the *I-V* characteristics of the crystalline silicon solar cells fabricated from Paste A were measured.

In previous chapter, the spherical micron silver particles were prepared by the chemical reduction method. Herein the silver front contact paste was prepared by mixing the as-prepared nano glass frit powders, silver particles and organic vehicles at the ratio of 4/80/16 (wt%) in ethyl alcohol, which was concentrated in a rotary evaporator. The specific composition of the silver paste is shown in **Table 4.3**. Silver electrodes from the paste A were formed by screen-printing the paste on crystalline silicon wafers with a SiN_x coating layer, followed by a firing process in a conveyor infrared furnace.

For comparison, a reference silver paste sample (denoted as paste B) containing the micron glass frit prepared by the conventional melt cooling route was also prepared with the same composition ratio of the paste A. The specific composition of the silver paste B is shown in **Table 4.3**. Silver fingers from the paste B were also formed by screen-printing on silicon wafers. Schematic diagrams of the two kinds of silver fingers before firing process were presented, as shown in **Figure 4.8**. From **Figure 4.8**, it is evident to see that the only difference between these two silver fingers is the glass frit source, i.e. one is nano glass frit while the other is the micron glass frit.

Table 4.3 Compositions of the as-prepared silver pastes containing different glass frit

Paste ID	Silver particles	Glass frit	Organic vehicle	Ratio
A	As-prepared	Nano glass	ethyl celluloses + terpineol	80/4/16
B	As-prepared	Micron glass	ethyl celluloses + terpineol	80/4/16

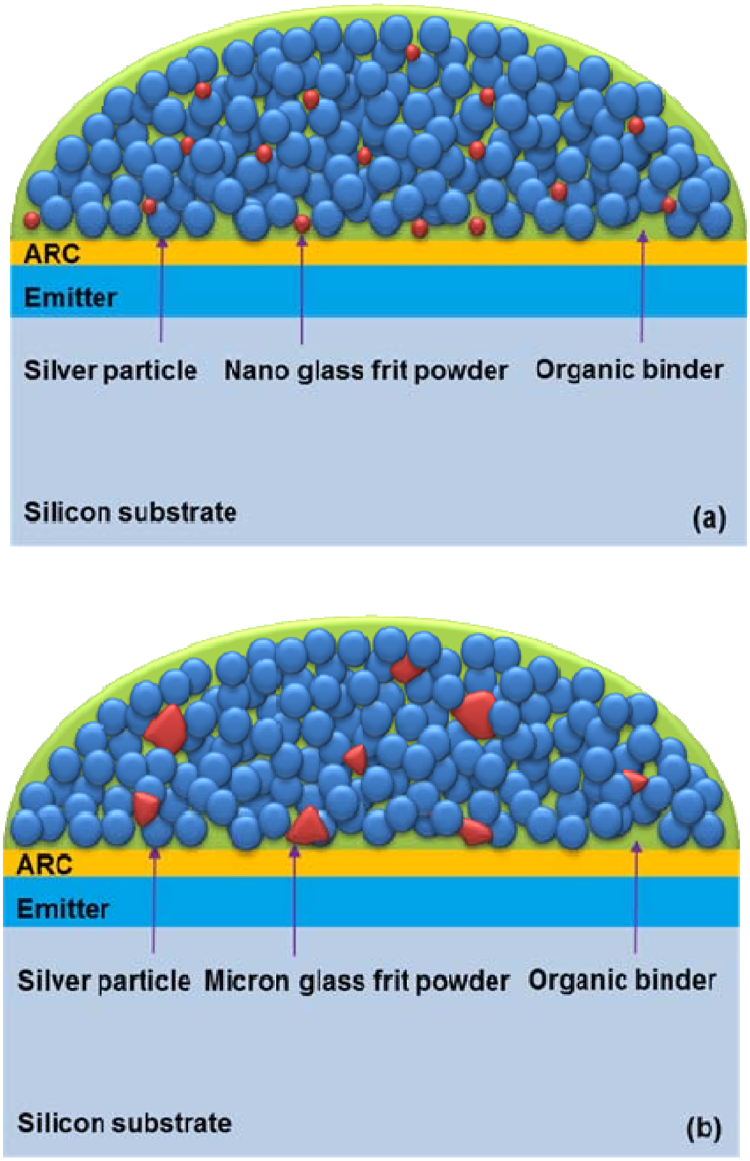

Figure 4.8 Schematic diagrams of the printed silver fingers before firing process: (a) containing nano-glass frit powders prepared by sol-gel process; (b) containing micron glass frit powders prepared by melt cooling route.

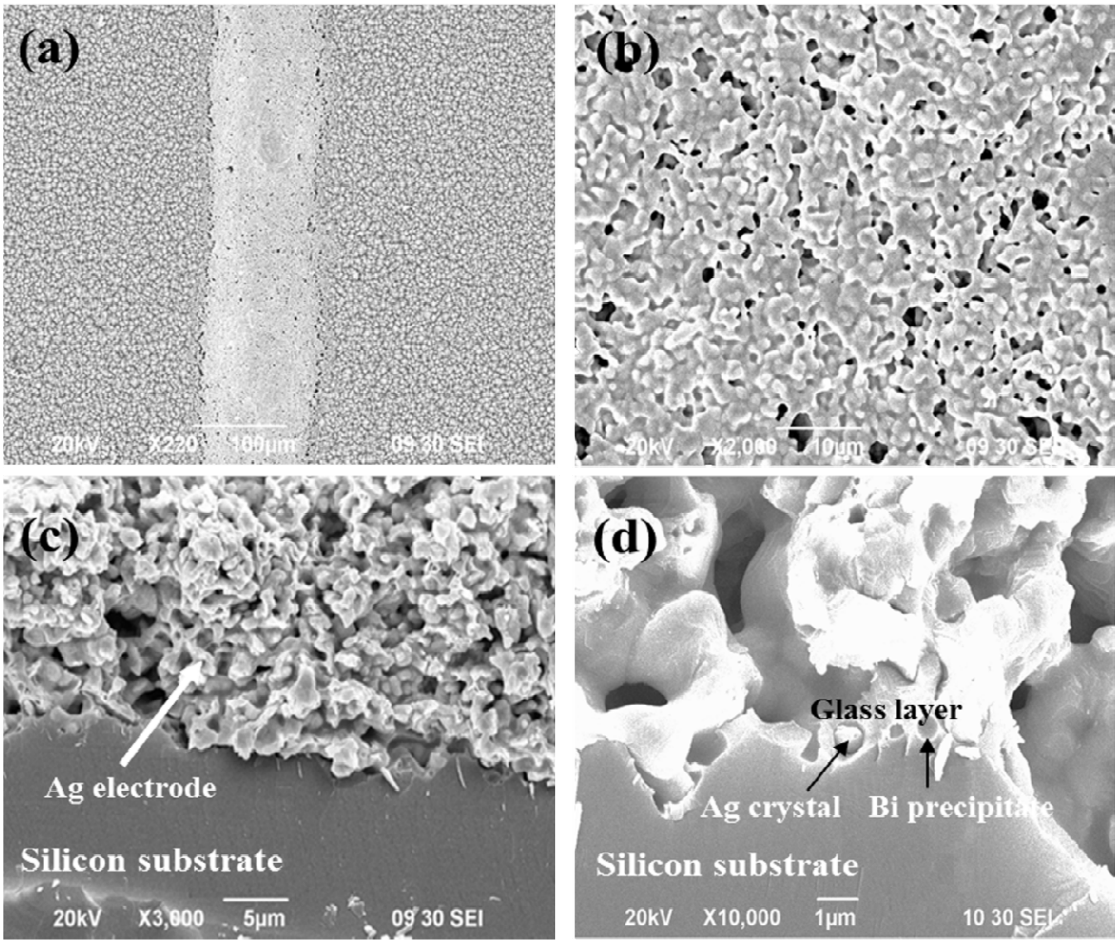

Figure 4.9 SEM images of the silver electrodes formed by screen-printing the silver paste containing the as-prepared Bi-based nano glass frit on silicon substrate, followed by firing process, exhibiting excellent sintering behavior.

Here we observed the morphology of the thick film contact on silicon wafer based on the paste A containing the as-prepared nano glass frit. **Figure 4.9** shows the SEM top view of the silver electrode **(a, b)**, and cross-section images **(c, d)**. It is noticed that the silver thick film was dense and homogenous, either from the top view and the cross-section view. Besides, all the typical features could be found at the silicon emitter interface, including Bi-precipitates, small silver crystallites, and a thin glass layer. Overall, the paste A exhibits excellent sintering behavior, and preliminarily acceptable characteristics for application of crystalline silicon solar cells.

The photovoltaic performances of the fabricated crystalline silicon solar cells based on the two kinds of silver pastes were shown in **Figure 3.12**. It can be seen that the fabricated silicon solar cell based on paste A generated an open-circuit voltage (V_{oc}) of 620mV, a short-circuit current density (J_{sc}) of 34.2mA/cm^2, a fill factor (FF) of 74.1% and a conversion efficiency (E_{ff}) of 15.7%. These are improved results compared with those resulting from the silicon solar cell based on paste B (V_{oc} = 615mV, J_{sc} = 33.8mA/cm^2, FF = 70.5%, E_{ff} = 14.6%).

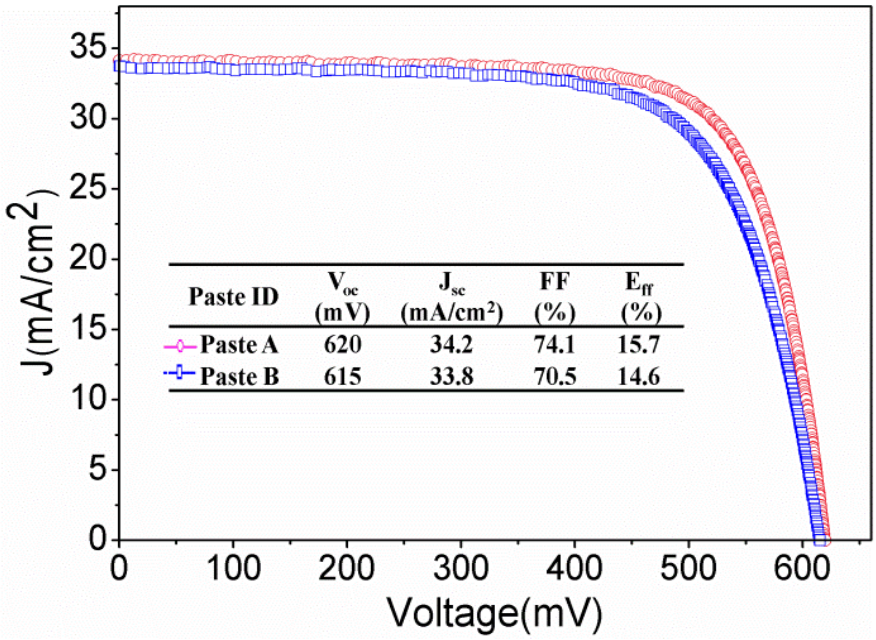

Paste ID	V_{oc} (mV)	J_{sc} (mA/cm^2)	FF (%)	E_{ff} (%)
Paste A	620	34.2	74.1	15.7
Paste B	615	33.8	70.5	14.6

Figure 4.10 Current-voltage (*I*-*V*) curves of the fabricated silicon solar cells using paste A and paste B on C_z single crystalline silicon wafers under AM 1.5 (1000W/m^2)

The fabricated crystalline silicon solar cells based on the paste A containing the as-prepared nano glass frit as an inorganic binder exhibited higher electrical conversion efficiency compared with that of the solar cell fabricated resulting from the conventional micron glass frit powders. All other factors being equal except for the glass frit in this work, this improvement should be attributed to the better metallization contact resulting from the nano glass frit powders with small size and high purity. Therefore, it can be concluded that good front metallization contact can be achieved by using the as-prepared nano glass frit powders as an inorganic binder in the silver front contact paste. Besides, this work presented an experimental case for synthesizing nano glass frit with low glass transition temperature and its application in silver front contact paste for crystalline silicon solar cells. Moreover, this work can provide useful information for synthesizing nano glass frit powders using the sol-gel method.

4. 4 Conclusions

In summary, a novel nano glass frit with low glass transition temperature (376°C) for making silver front contact paste of crystalline silicon solar cells has been developed by the sol-gel method from a multicomponent gel in the Bi_2O_3-SiO_2-B_2O_3-Al_2O_3-ZnO system. In this wok, ethyl orthosilicate, aluminum nitrate nonahydrate, bismuth(III) nitrate pentahydrate, zinc nitrate hexahydrate and boric acid were used as the metal precursor. According to the thermal analysis of the xerogel, the temperature of 500°C was selected for heat treatment to obtain glass frit powders, which was further identified by the XRD result. From the XRD, it is demonstrated that the xerogel was completely converted into amorphous state glass frit. Besides, to determine the wetting behavior and etching effect during high temperature, the test glass paste containing the as-prepared nano glass was prepared, and deposited on silicon wafer, followed by a firing process. The experiments indicated that the nano glass frit exhibited excellent wetting behavior and etching effect. Furthermore, the fabricated crystalline silicon solar cells based on the silver paste containing the nano glass frit exhibited better photovoltaic performances than those of the solar cell fabricated resulting from the conventional micron glass frit powders. This improvement should be attributed to the better metallization contact resulting from the nano glass frit powders with small size and high purity. Therefore, it can be concluded that good front metallization contact can be achieved by using the as-prepared nano glass frit powders as an inorganic binder in the silver front contact paste. Besides, this work presented an experimental case for synthesizing nano glass frit with low glass transition temperature and its application in silver front contact paste for crystalline silicon solar cells. Moreover, this work can provide useful information for synthesizing nano glass frit powders using the sol-gel method.

References

[1] M.M. Hilali, A. Rohatgi, and B. To A review and understanding of screen-printed contacts and selective- emitter formation. *14th workshop on crystalline silicon solar cells and modules*, Colorado, USA. 8-11 Augest. 2004

[2] K.K. Hong, S.B. Cho1, J.Y. Huh, H.J. Park, and J.W. Jeong, Role of PbO-Based Glass Frit in Ag Thick-Film Contact Formation for Crystalline Si Solar Cells. *Metals and Materials International*, 2009. **15**: 307-12.

[3] B. Sopori, V. Mehta, P. Rupnowski, J. Appel, M. Romero, H. Moutinho, D. Domine, B. To, R. Reedy, M. Al-Jassim, A. Shaikh, N. Merchant, C. Khadilkar, D. Carlson, and M. Bennet, *Proc. 17th Workshop on Crystalline Silicon Solar Cells & Modules: Materials and Processes*, Vail, Colorado, 2007. 93.

[4] J.H. Kim, H.Y. Koo, Y.N. Ko, and Y.C. Kang, Characteristics of Bi-based glass frit having similar mean size and morphology to those of silver powders at high firing temperatures. *Journal of Alloys and Compounds*, 2010. 497: 259-66.

[5] J. Hoornstra, G. Schubert, K. Broek, F. Granek, and C. LePrince, Lead free metallisation paste for crystalline silicon solar cells: from model to results. *in: Proceedings of the 31st IEEE Photovotaic Specialists Conference*, Florida, 2005. 651-54.

[6] M. Bahr, S. Kim, S. Sridharan, C. Khadilkar, J. Lossen, and S. Dauwe, On lead and cadmium free metallizations for industrial solar cells and modules. *in: Proceedings of the 21st European Photovoltaic Solar Energy Conference*, Dresden, Germany, 2006. 859-64.

[7] Y. Zhang, Y. Yang, J. Zheng, W. Hua, and G. Chen, Thermal properties of glass frit and effects on Si solar cells. *Materials Chemistry and Physics*, 2009. 114: 319-22.

[8] J. H. Kim, H. Y. Koo, Y.N. Ko, and Y.C. Kang, Characteristics of Bi-based glass frit having similar mean size and morphology to those of silver powders at high firing temperatures. *Journal of Alloys and Compounds*, 2010. 497: 259-66.

[9] Jeon SJ, Koo SM, Hwang SA. Optimization of lead- and cadmium-free front contact silver paste formulation to achieve high fill factors for industrial screen-printed Si solar cells. Sol Energy Mater Sol Cells. 2009;93:1103-9.

[10] R.L. Siqueira, O. Peitl, and E.D. Zanotto, Gel-derived SiO_2-CaO-Na_2O-P_2O_5 bioactive powders: Synthesis and in vitro bioactivity. *Materials Science and Engineering C*, 2011. **31**: 983-91.

[11] S. Tabatabaei, A. Shukohfar, R. Aghababazadeh, and A. Mirhabibi, Experimental study of the synthesis and characterisation of silica nanoparticles via the sol-gel method. *Journal of Physics: Conference Series*, 2006. **26**: 371-74.

[12] L. Zhang, J.C.C. Chan, and H. Eckert, Novel sol-gel synthesis of sodium aluminophosphate glass based on aluminum lactate. *Chemistry of Materials*, 2003. **15**: 2702-10.

[13] D. Baciu, and J. Simitzis, Synthesis and characterization of a calcium silicate bioactive glass. *Journal of Optoelectronics and Advanced Materials*, 2007. **9**: 3320-24.

[14] X.Q. Gao, J. He, L. Deng, and H.N. Cao, Synthesis and characterization of functionalized rhodamine B-doped silica nanoparticles. *Optical Materials*, 2009. **31**: 1715-19.

[15] M. Taira, and M. Yamaki, Preparation of SiO_2-Al_2O_3 glass powders by the sol-gel process for dental applications. Journal of materials science: materials in medicine, 1995. **6**: 197-200.

CHAPTER 5 NANOPARTICLES AIDED SILVER FRONT CONTACT PASTE

5.1 Introduction

As mentioned before, the silver front contact paste for crystalline silicon solar cells usually contains three principal constituents: silver particles, glass frit powders, and organic binder. Among them the silver particles are the only component to conduct electrons. Typically, silver particles represent 70-85% in weight of the paste with a mixture of various shaped particles (predominantly spherical). Currently, most of the commercially available silver particles for silver front contact pastes are micrometer grade, of which the peak firing temperature is near 850°C. In fact, the high temperature is harmful to the minority carrier life time in silicon wafer. Therefore, it is necessary to develop a low-firing-temperature silver front contact paste, reducing the temperature as low as possible. In the past years, silver nanoparticles have gained great attention for application in conductive paste, inks and adhesives for electronic devices due to their low sintering temperature and high conductivity [1]. Moon et al. studied the thermal property of silver nanoparticles for their application in low-temperature interconnect, and found that the silver nanoparticles showed obvious sintering effect at much low temperature than the melting point (T_m) of silver bulk material [2]. Park et al. reported that the printed silver thick film resulting from the silver paste prepared using silver nanoparticles showed high conductivity although it was sintered at low temperature [3]. Besides, one-dimensional (1-D) silver materials, such as nanorods, nanotubes and nanowires have drawn much attention for their unique electronic performance and great potential application in conductive paste for electronic devices [4-6]. It was reported that silver nanowires improved the system containing micron silver particles by a small amount addition, in which silver nanowires tend to act as bridges to form linkages between micron silver particles, increasing the contact opportunities of particles **[7]**. Therefore, it could be preliminarily deduced that the crystalline silicon solar cells fabricated using silver front contact paste containing silver nanoparticles tend to show better sintering behaviour and higher photovoltaic performance than those of solar cells resulting from silver paste containing single micron silver particles. As far as we know, there is few study on the application of silver nanoparticles in silver paste for crystalline silicon solar cells. Thus, the goal of this study is to synthesize silver nanoparticles and study their application in silver front contact paste. The synthesis mechanisms of silver nanoparticles will be studied in detail. Besides, the effect of silver nanoparticles on the sintering behaviour of micron silver particles, as well as on the photovoltaic performances of the fabricated crystalline silicon solar cells will be investigated in this chapter.

5.2 Experiment materials and equipment

5.2.1 Experiment materials

All the materials used in the experiments are listed in **Table 5.1.**

Table 5.1 Experiment materials

Name	Remark	Manufactory
Silver nitrate	AR.	China National Pharmaceutical Group Industry Corporation Ltd

Ammonia	AR. 28+%	Xilong Chemical Co., Ltd
Ethylene glycol	EG, AR.	Xilong Chemical Co., Ltd
Polyvinylpyrrolidone	AR. PVP40 , MW= 40000	Xilong Chemical Co., Ltd
Anhydrous ethyl alcohol	AR.	Xilong Chemical Co., Ltd
Acetone	AR.	Tianjin Fuchen Chemical Reagent Factory
Hydrochloric acid	AR.	Tianjin Fuchen Chemical Reagent Factory
Nitric acid	AR.	Tianjin Chemical Reagent Ltd.
Acetic acid	AR.	Tianjin Chemical Reagent Ltd.
$H_2PtCl_6 \cdot 6H_2O$	AR.	China National Pharmaceutical Group Industry Corporation Ltd
Ethylene glycol	AR.	Xilong Chemical Co., Ltd
Terpineol	AR.	Xilong Chemical Co., Ltd

5.2.2 Equipment

All the equipment used in the experiments is listed in **Table 5.2.**

Table 5.2 Equipment list

Name of instrument	Instrument model	Manufactory
Rotary evaporator	RE-52	Shanghai Yarong Biochemical Apparatus Factory
Semi-automatic screen	SYP2230	Shenzhen Qiaopai Screen

printing machine		Machine Factory
Electric heating air-blowing drier	101-2	SHANGHAI WUYANGSHAN Shanghai Guangdi Instruments Equipment Co., Ltd
Magnetic Stirring Apparatus	78-1	Changzhou Aohua Instruments Equipment Co., Ltd
Electric heating mantle	EM 100	Electromantle, England
Ultrasonic generator	KQ3200E	Kunshan Ultrasonic Electronic Equipment co., ltd
Electronic balance	ES120	Shenzhen Zhicheng Electronic Balance Co., Ltd
Laboratory pH meter	PHB-5	Shanghai Hongji Instruments Equipment Co., Ltd
All-directional planetary ball mill	PMQW0.4L	Nanjing Shunchi Technology Development Co. Ltd
Oilless vacuum pump	AP-550V	Institute of Microelectronics of Chinese Academy of sciences
Three-roller mill	S65	Changzhou Wujin Xingye Mechanical Equipment Co., Ltd

5. 3 Preparation of silver nanospheres by solvothermal method

5.3.1 Experiments

Among the current methods of synthesizing silver nanoparticles, the liquid solution-based chemical process is regarded as practical for its many advantages, such as easy operation, less experimental apparatus, and easy to scale up for industirliazation[8-14]. As a common liquid solution-based method, solvothermal synthesis has been widely used for synthesizing nanomaterial[15, 16]. The size, shape, and distribution of nanoparticles can be well controlled and altered by changing the experimental parameters, including reaction time, reaction temperature, and agent type. The size and morphology of silver nanoparticles are important for their application for producing silver paste. In this work, we try to synthesize silver nanoparticles using the solvothermal method, and study the size, shape and growth control for their application in silver front contact paste for crystalline silicon solar cells. **Figure 5.1** shows the reaction principles for synthesizing silver nanoparticles at the optimal experimental condition.

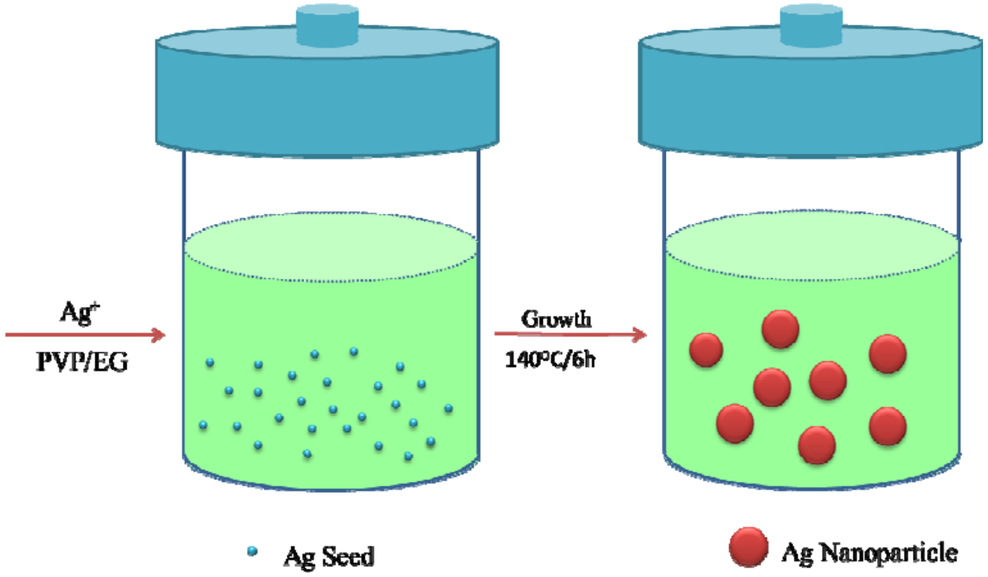

Figure 5.1 Schematic diagram of the reaction principle for synthesizing silver nanoparticles by the solvothermal method at the optimal experimental condition

Specifically, silver nitrate ($AgNO_3$), ethylene glycol (EG) and polyvinylpyrrolidone (PVP) were used as the metal precursor, reducing agent and dispersant, respectively. In a typical experiment, there are four steps for synthesizing silver nanoparticles in our work as follows: 0.085g $AgNO_3$ was dissolved in 10ml EG and the solution A was obtained. 0.1g PVP was dissolved in 10ml EG at 60 °C under vigorous stirring and the solution B was obtained. Then solution B was added into the solution A drop by drop under stirring, obtaining the solution C. Next the solution C was transferred to an autoclave. Subsequently, the autoclave was placed in a constant temperature oven for 6 hours. After 6 hours, the oven was cooled down to room temperature naturally. The final silver nanoparticles were obtained after centrifugation, washing and vacuum oven drying.

5.3.2 Morphology

The morphology of the as-prepared silver nanoparticles was observed by the scanning electron microscopy. **Figure 5.2** is the FESEM image of the silver nanoparticles synthesized by the solvothermal method under the optimal experimental condition, using silver nitrate as the metal source, ethylene glycol as the reducing agent and PVP as the dispersant agent. From the FESEM, it is demonstrated that the size of the silver particles is spherical in shape, with an average size of 50nm, which agreed well with the calculation result from X-ray diffraction.

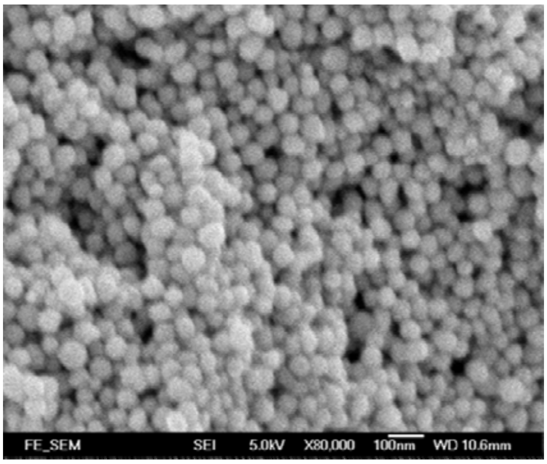

Figure 5.2 FESEM micrograph of the silver nanoparticles synthesized by the solvothemal process.

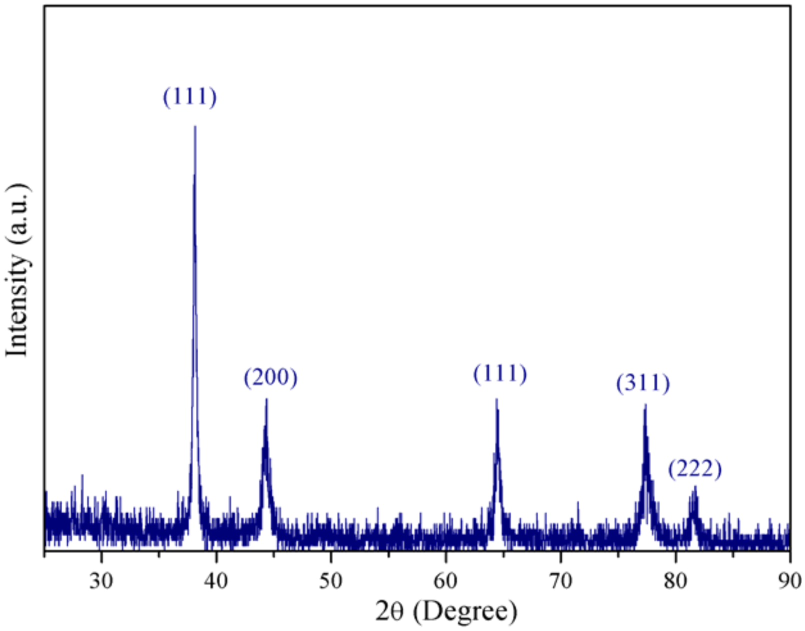

Figure 5.3 XRD pattern of the silver nanoparticles synthesized by the solvothermal method.

Figure 5.3 shows the x-ray diffraction pattern of the as-prepared silver nanoparticles synthesized by the solvothermal method. The index process of the diffraction pattern was done and the *Miller indices* for each peak were identified. There are five peaks found in the diffraction pattern, which are identical to those of the FCC silver. Besides, there are no crystallographic impurities. It is noticed that the diffraction peaks were broad, indicating the size of silver nanoparticles is small. More accurately, the grain size of the average sliver nanoparticles was calculated by the Debye-Scherrer formula **[17]**:

$$D = 0.9\lambda/\beta\cos\theta \qquad (1)$$

where λ represents the wave length of X-ray, β is the full width at half maximum of the diffraction peak (FWHM), θ is the diffraction angle and D is the diameter size of silver nanoparticles. The calculated results were shown in **Table 5.3**. The value of interplanar spacing (d) is calculated using the Bragg's Law **[18]**:

$$2d\sin\theta = n\lambda \qquad (2)$$

Table 5.3 X-ray parameters of the as-prepared silver nanoparticles

2θ	**d**	**hkl**	**FWHM**	**D(nm)**
38.102	2.360	111	0.254	36
44.315	2.042	200	0.365	24
64.534	1.443	220	0.184	61
77.414	1.232	311	0.200	58
81.560	1.179	222	0.217	62

5.3.3 Theoretical approach

(1) The relationship between T_m and silver particle size

As a basic physical parameter, the melting temperature (T_m) of a material is fundamental and important for its applications. In fact, T_m varies depending to a large extent on the surface-to-volume ratio of the material. Specifically, in bulk system, the surface-to-volume ratio and the curvature of the surface are so small that the surface effects on T_m can be negligible. However, for nanoparticles the effects cannot be disregarded, because the surface-to-volume and the curvature of the surface become significant large. In this case, T_m depends significantly on particle size.

The surface effects have been explained by thermodynamics theory [19] and have been verified experimentally [20]. For a sphere the size-dependent melting temperature could be expressed by the following equation [21]:

$$T_m/T_0 = 1 - 2\gamma_{sl}/\Delta H_m r \qquad (3)$$

where T_m is the melting point of a spherical particle with radius r, T_0 is the melting temperature of the bulk, γ_{sl} is the solid-liquid interfacial energy, and ΔH_m is the bulk latent fusion heat. For silver nanoparticles, the calculated results from equation (3) are shown in **Table 5.4** and **Figure 5.4**. It can be seen that the melting point of silver nanoparticles increases sharply with the particle size when the size is less than 50nm. After that the cure becomes flat. When the size is larger than 100nm, the melting point is close to T_0.

For this unique behavior, silver nanoparticles exhibit excellent sintering behavior for application in silver paste. Therefore it is a good way to introduce silver nanoparticles into silver front contact paste for crystalline silicon solar cells as a sintering aid.

Table 5.4 Melting point of silver particles as a function of diameter

D/nm	2	5	10	25	50	75	100	125	150	175	200
T_m/℃	83	478	689	844	901	920	930	936	940	943	945

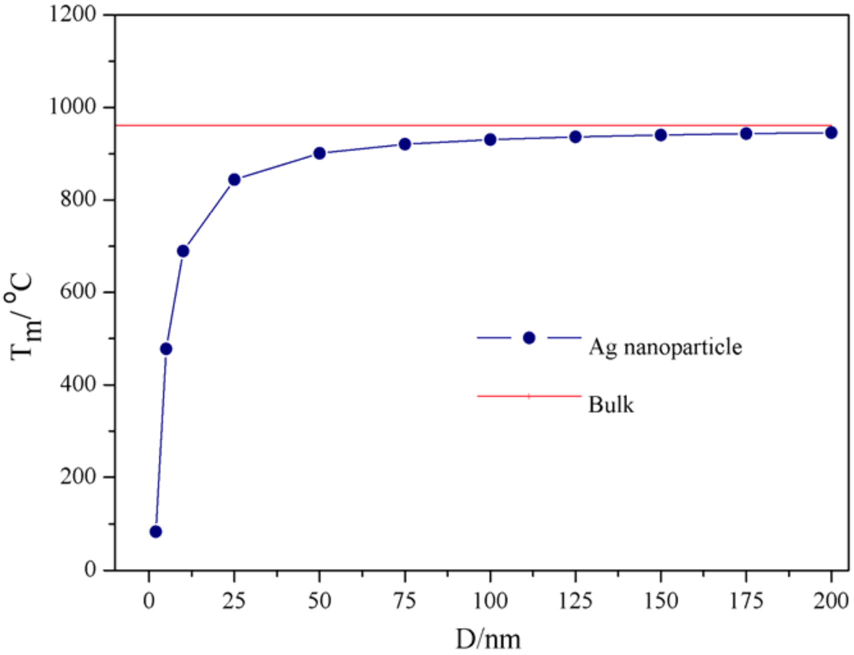

Figure 5.4 Melting point of silver nanoparticles as a function of diameter size

(2) Sintering mechanism of silver particles

As mentioned above, the melting point of silver particles decreases with the size, which is significant for their application in conductive thick films. During high temperature firing process, the silver nanoparticles melt and even vaporize, which is favorable to the sintering of micron silver particles. This can be explained by the mass-diffusion transport mechanism. Based on thermodynamics theory, during the sintering process, the driving force of the mass diffusion is the chemical potential difference **[22]**.

The surface chemical potential of silver nanoparticles is much higher than that of micron silver particles. Thus, during firing process, the flow transfers from the silver nanoparticles to the necks of micron silver particles. This process not only contributes to the sintering of silver particles, but also reducc the pores. **Figure 5.5** shows the sintering process of silver particles. It can be seen that better thick film with less pores can be obtained by adding silver nanoparticles.

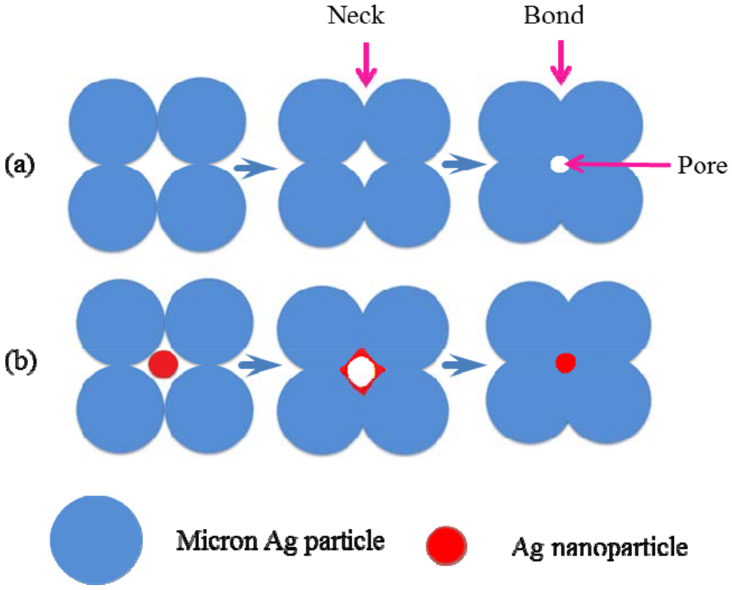

Figure 5.5 Model structure of the sintering process of the silver particles: (a) micron silver particles (b) silver nanoparticles aided micron particles.

5.3.4 Effect on PV performance

As what discussed above, it can be preliminarily deduced that the silver front contact paste containing silver nanoparticles tends to have a better front metallization contact and this in turn leads to better performance of solar cells. To determine the effect of the as-prepared silver nanoparticles on PV performance of silicon solar cells, the silver paste containing the silver nanoparticles was prepared (denoted as paste A). Subsequently, the *I-V* characteristics of the crystalline silicon solar cells fabricated using Paste A were measured.

In our previous chapter, the micron silver particles and lead-free glass frit powders were prepared by the chemical reduction method and conventional melting route, respectively. Herein the silver paste was prepared by mixing the mixture of micron and nano silver particles (ratio of micron particles: nanoparticles in weight was 70:10), glass frit powders, and organic vehicles with the ratio of 80/4/16. Thus the silver paste consisting of 70:10/4/16 was prepared by rotary evaporation method. The specific composition of the silver paste was shown in **Table 5.5**. Silver electrodes from the paste A were formed by screen-printing the paste on crystalline silicon wafers with SiN_x coating layer, followed by a firing process in a conveyor infrared furnace.

For comparison, a reference silver paste (denoted as paste B) based on single micron silver particles was also prepared with the same composition ratio of the paste A. The specific composition of the silver paste B was shown in **Table 5. 5**. Silver fingers from paste B were also formed by screen-printing on silicon wafers. Schematic diagrams of the two kinds of silver fingers before firing process were presented, as shown in **Figure 5.6**. From **Figure 5.6**, it is evident to see that the only difference between these two silver fingers is that the former contains silver nanoparticles as a sintering aid.

Table 5.5 Compositions of silver front contact paste with the as-prepared silver nanoparticles (A), and without nanoparticles (B)

Paste ID	Silver particles	Glass frit	Organic vehicle	Ratio
A	Nanoparticle aided	Bi-based	ethyl celluloses + terpineol	70/10/4/16
B	Micron	Bi-based	ethyl celluloses + terpineol	80/4/16

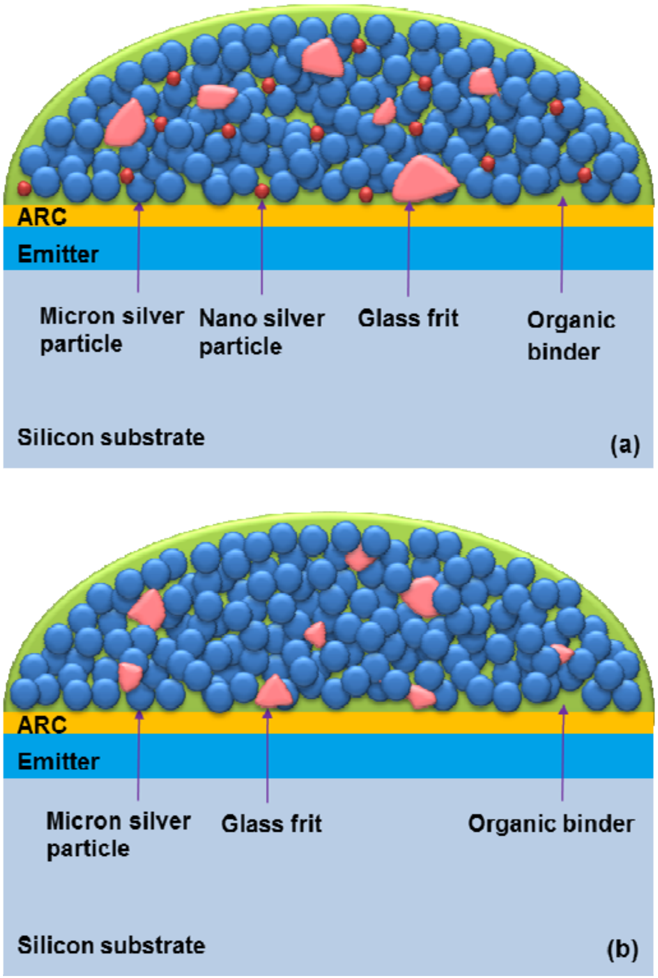

Figure 5.6 Schematic diagrams of the printed silver fingers before firing treatment: (a) containing hybrid of micron silver particles and silver nanoparticles; (b) containing single micron silver particles

Here we observed the surface structure of the silver thick films formed using the paste A and pate B, under the same sintering process, as shown in **Figure 5.7**. It can be seen that the silver thick film fabricated resulting the silver paste containing silver nanoparticles exhibits denser structure (**Figure 5.7(a)**) than that of thick film based on silver paste containing single micron silver particles (**Figure 5.7(b)**). The experimental results demonstrated that the silver nanoparticles, which were added as a sintering aid into the silver paste, promoted sintering of silver particles and promoted pore shrinkage and elimination of the thick film. All these should be attributed to the unique nano-effect of silver nanoparticles.

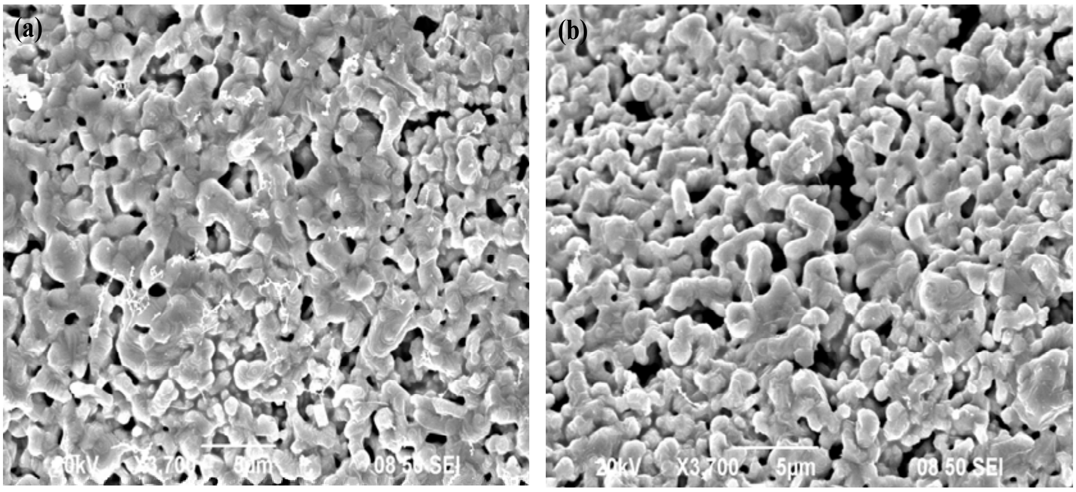

Figure 5.7 SEM morphologies of the surfaces of the silver thick films: (a) fabricated using hybrid micron silver particles and silver nanoparticles; (b) fabricated using single micron silver particles

The photovoltaic performances of the fabricated crystalline silicon solar cells resulting from the silver paste A and paste B were shown in **Figure 5.8**. It can be seen that the fabricated silicon solar cell based on paste A containing the as-prepared silver nanoparticles generated an open-circuit voltage (V_{oc}) of 622mV, a short-circuit current density (J_{sc}) of 34.6mA/cm^2, a fill factor (FF) of 74.8% and a conversion efficiency (E_{ff}) of 16.1%. These are improved results compared with those resulting from the solar cell based on the silver paste B containing single micron silver particles (V_{oc} = 618mV, J_{sc} = 34.3mA/cm^2, FF = 72.5%, E_{ff} = 15.4%). The fabricated crystalline silicon solar cell containing the silver nanoparticles exhibited higher electrical conversion efficiency compared with that of the solar cell fabricated resulting from the conventional silver paste containing single micron silver particles. All other factors being equal except for the addition of silver nanoparticles as a sintering aid in paste A. Therefore, this improvement should be attributed to the better thick film resulting from silver nanoparticles, which not only improve the compactness of thick film, but also increase the line conductivity of silver electrodes. It can be concluded that good front metallization contact can be achieved by using the as-prepared silver nanoparticles as an additive in the silver paste.

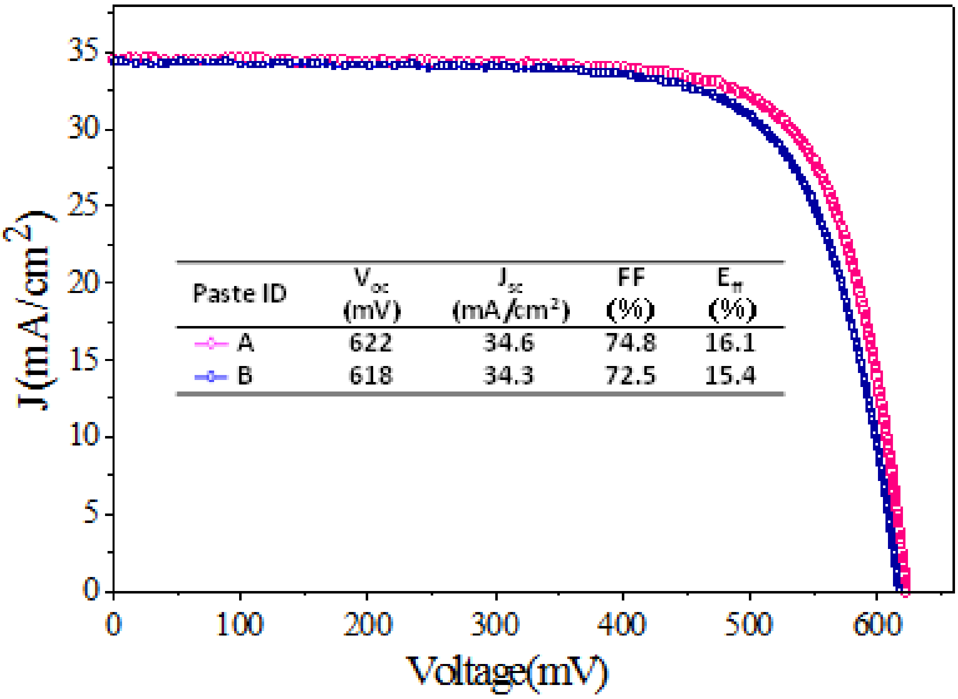

Paste ID	V_{oc} (mV)	J_{sc} (mA/cm^2)	FF (%)	E_{ff} (%)
A	622	34.6	74.8	16.1
B	618	34.3	72.5	15.4

Figure 5.8 I-V performances of the fabricated crystalline silicon solar cells based on different silver pastes under AM 1.5 (1000W/m^2)

5. 4 Preparation of silver nanowires by solvothermal method

5.4.1 Experiments

In the previous section, we prepared silver nanoparticles by the solvothermal method. In this study, we still used solvothermal method to prepare silver nanowires. The difference is that $H_2PtCl_6 \cdot 6H_2O$ as crystal-seeds was added into the reduction system. Specifically, the silver nanowires were prepared by reducing silver nitrate in ethylene glycol, using Pt nanoparticles as crystal seeds, and PVP as protective agent. Besides, the experimental parameters were adjusted and optimized to obtain high quality silver nanowires, including the concentration, reagent dosage, reaction time and temperature, and so on. Furthermore, the size, shape and growth control have been studied for better understanding of the synthesis mechanism of silver nanowires by solvothermal method. **Figure 5.9** indicates the reaction principles for synthesizing silver nanowires at the optimal experimental condition in this thesis.

In a typical experiment, there are four steps for synthesizing silver nanowires in our work as follows: 0.425 g of silver nitrate ($AgNO_3$) was dissolved in 15 mL of ethylene glycol (EG) and the solution A was obtained. A small amount of $H_2PtCl_6 \cdot 6H_2O$ and 0.275 g of PVP were dissolved in 15 mL of EG at 60 °C under vigorous stirring and the solution B was obtained. Then solution B was added into the solution A drop by drop under stirring, and the solution C was obtained. Next the solution C was transferred to an autoclave. Subsequently, the autoclave was placed in a constant temperature oven for 6 hours. After 6 hours, the oven was cooled down to room temperature naturally. The final silver nanoparticles were obtained after centrifugation, washing and vacuum oven dry.

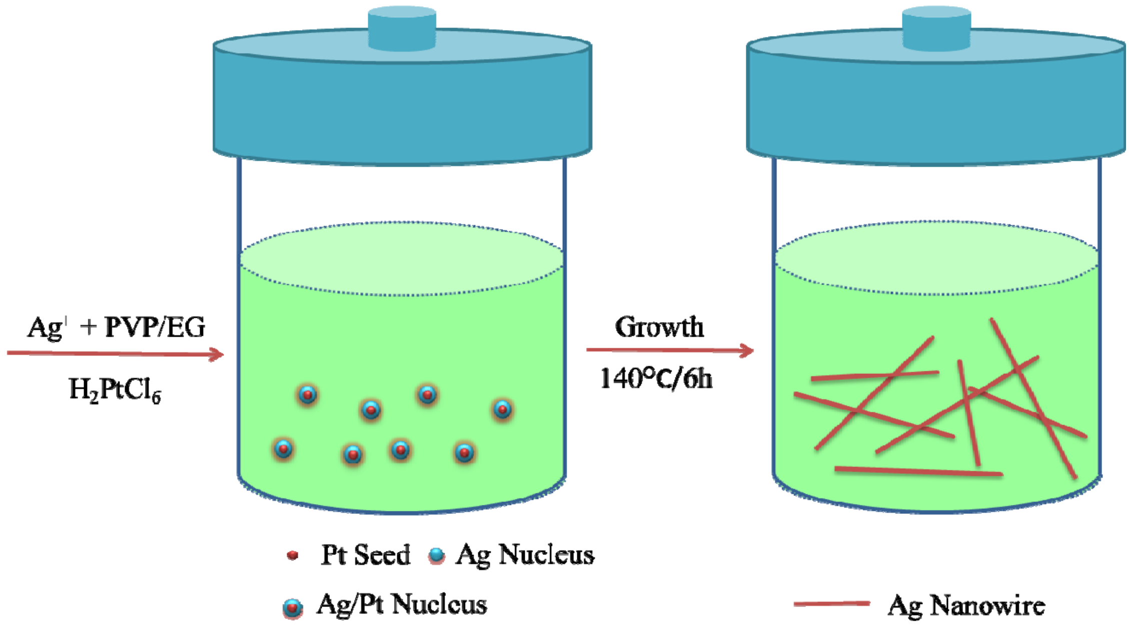

Figure 5.9 Schematic diagram of the reaction principle for synthesizing silver nanowires by solvothermal method at the optimal experimental condition

5.4.2 Morphology

The morphology of the as-prepared silver nanowires was observed by the scanning electron microscopy. **Figure 5.10** shows the SEM images of the silver nanowires synthesized by solvothermal method under the optimal experimental condition, using silver nitrate as the metal source, ethylene glycol as the reducing agent, PVP as the dispersant agent and Pt nanoparticles as crystal seeds. From the SEM, it is demonstrated that the silver nanowires were 100nm to 200nm wide and 0.5μm to 4μm long. It was reported that Pt seeds play a crucial role in the anisotropic growth of silver nanoparticles [23]. Sun et al. prepared 1-D silver nanomaterials using soft solution process with the addition of $PtCl_2$, and indicated that Pt nanoparticles was formed first and then served as nucleation for growth of silver nanoparticles [24].

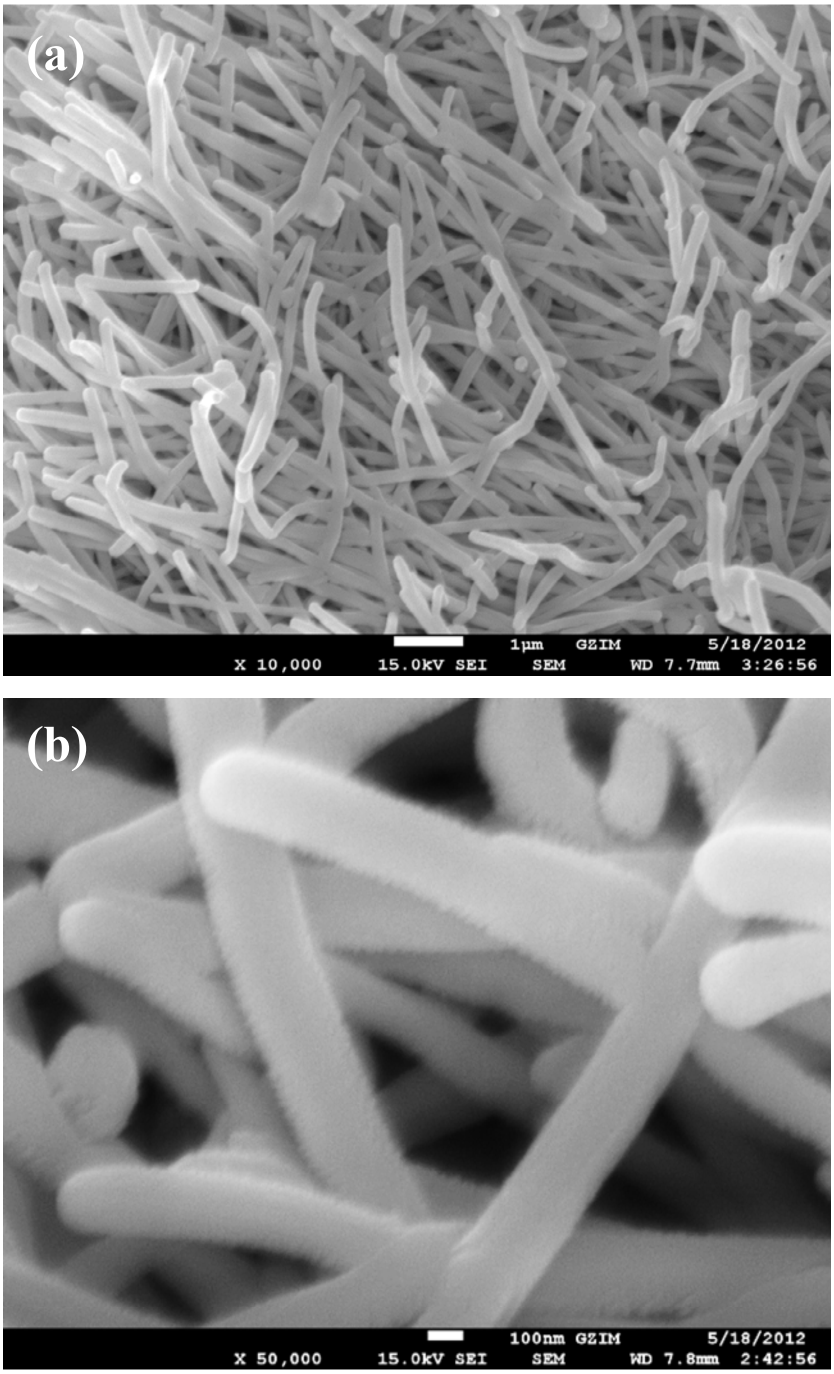

Figure 5.10 SEM micrographs of the silver nanowires prepared by solvothermal process: (a) low resolution, and (b) high resolution

5.4.3 Effect on PV performance

As discussed above, it can be preliminarily deduced that the silver front contact paste containing silver nanowires tends to have a better front metallization contact and this in turn leads to better performance of solar cells. To determine the effect of the as-prepared silver nanowires on PV performance of silicon solar cells, the silver paste containing the silver nanowires was prepared (denoted as paste C). Subsequently, the *I-V* characteristics of the fabricated crystalline silicon solar cells formed using Paste C were measured.

In our previous chapter, the micron silver particles and lead-free glass frit powders were prepared by chemical reduction method and conventional melting route, respectively. Herein the silver paste was prepared by mixing the mixture of micron silver particles and silver nanowires (ratio of micron particles: nanowires in weight was 70:10), glass frit powders, and organic vehicles with the ratio of 80/4/16. Thus the silver paste consisting of 70:10/4/16 was prepared by rotary evaporation method. The specific composition of the silver paste C is shown in **Table 5. 6**.

Table 5.6 Composition of the silver paste C containing the as-prepared silver nanowires synthesized by solvoerthermal method

Paste ID	Silver particles	Glass frit	Organic vehicle	Ratio
C	Nanowires aided	Bi-based	ethyl celluloses + terpineol	70/10/4/16

Silver electrodes from the paste C were formed by screen-printing the paste on crystalline silicon wafers with SiN_x coating layer, followed by a firing process in a conveyor infrared furnace at the same firing condition for solar cells based on paste A and paste B in previous section. The schematic diagram of the silver fingers containing silver nanowires before firing process is presented, as shown in **Figure 5.11**.

The photovoltaic performances of the fabricated crystalline silicon solar cells resulting from the silver paste C containing the as-prepared silver nanowires are shown in **Figure 5.12**. It can be seen that the fabricated silicon solar cell based on paste C generated an open-circuit voltage (V_{oc}) of 621mV, a short-circuit current density (J_{sc}) of 34.3mA/cm^2, a fill factor (FF) of 74.1% and a conversion efficiency (E_{ff}) of 15.8%. These are improved results compared with those resulting from the silicon solar cell based on the silver paste B (V_{oc} = 618mV, J_{sc} = 34.3mA/cm^2, FF = 72.5%, E_{ff} = 15.4%). All other factors being equal except for the addition of silver nanowires as an additive in paste C. Therefore, this improvement should be attributed to the unique electronic property and bridge-effect of the one-dimensional (1-D) nanostructures. It can be concluded that good front metallization contact can be achieved by using the as-prepared silver nanowires as an additive in the silver paste.

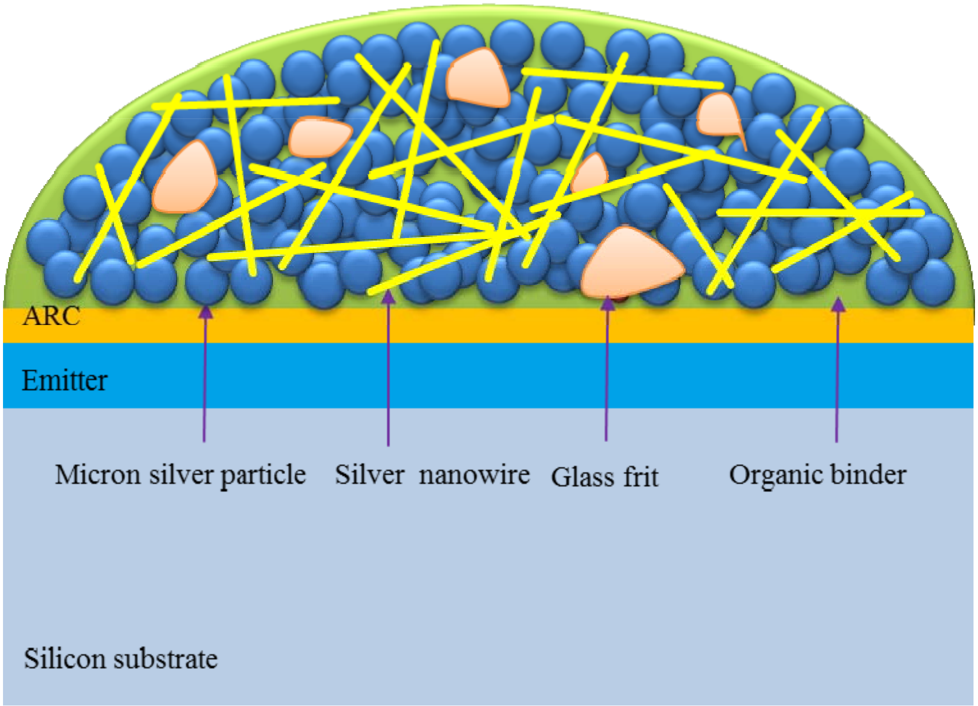

Figure 5.11 Schematic diagram of the printed silver finger containing hybrid micron silver particles and silver nanowires before firing treatment

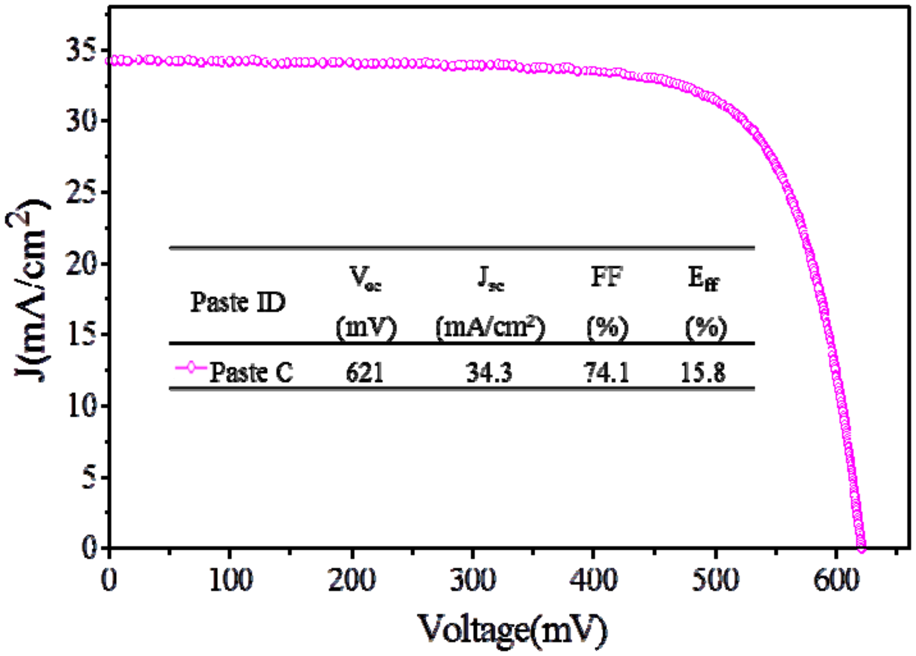

Figure 5.12 I-V performance of the crystalline silicon solar cell based on silver paste C containing the as-prepared silver nanowires under AM 1.5 (1000W/m^2)

5. 5 Conclusions

Spherical silver nanoparticles (SSNPs)-aided silver paste was developed using the SSNPs as a sintering aid. High-dispersive SSNPs were prepared by the solvothemal method, using silver nitrate as the metal source, ethylene glycol as the reducing agent and PVP as the dispersant agent. From the FESEM, it is demonstrated that the silver particles was spherical in shape, with an average size of 50nm, which agreed well with the calculation result from X-ray diffraction. The silver pastes composed of micron silver particles (70 wt%), the SSNPs with an average size of 50nm (10 wt%), lead free glass frit (4 wt%) and organic vehicle (16 wt%) were screen-printed on single crystalline silicosilicon wafers with SiN_x antireflective coating, followed by firing and tests. The experimental results demonstrated that the SSNPs with high surface energy are favor to the sintering of micron silver particles. Moreover, the size and numbers of pores in the silver thick films were reduced due to the SSNPs's unique sintering behavior, contributing to denser conductive network. In the current-voltage measurement, the fabricated solar cell based on the SSNPs-aided silver paste showed higher conversion efficiency (16.1%) than that (15.4%) resulting from the reference sample (solar cell containing no SSNPs).

Moreover, silver nanowires (SNWs)-aided silver pastes were also developed by adding the SNWs into micron silver particles. The SNWs were prepared by reducing $AgNO_3$ with ethylene glycol in the presence of seeds and PVP. Pt nanoparticles as crystal-seeds play a crucial effect on the anisotropic growth of silver nanowires. From the SEM, it is demonstrated that the silver nanowires were 100nm to 200nm wide and 0.5μm to 4μm long. The silver pastes composed of micron silver particles (70 wt%), SNWs (100nm to 200nm wide and 0.5μm to 4μm long, 10 wt%), lead free glass frit (4 wt%) and organic vehicle (16 wt%) were screen-printed on single crystalline silicon wafers with SiNx antireflective coating, followed by firing process and test. The fabricated solar cells based on the SNWs-aided paste generated an open-circuit voltage (V_{oc}) of 621mV, a short-circuit current density (J_{sc}) of 34.3mA/cm^2, a fill factor (FF) of 74.1% and a conversion efficiency (E_{ff}) of 15.8%. This improvement could be attributed to unique electronic property and bridge-effect of the one-dimensional (1-D) metal nanostructures.

References

[1] J.C. Lin, and C.Y. Wang, Effects of surface treatment of silver powder on the rheology of its thick-film paste. *Materials Chemistry and Physics*, 1996. **45**:136-44.

[2] K.S. Moon, H. Dong, R. Maric, S. Pothukuchi, A. Hunt, Y. Li, and C.P. Wong, Thermal behavior of silver nanoparticles for low-temperature inter connect applications . *Journal of Electronics Materials*. 2005. **34**: 168-75.

[3] K. Park, D. Seo, and J. Lee, Conductivity of silver paste prepared from nanoparticles. *Colloids and Surface A: Physicochemical and Engineering Aspects*, 2008. **313-314**: 351-54.

[4] D.L. Chen, and L. Gao, Large-scale growth and end-to-end assembly of silver nanorods by PVP-directed polyol process. *Journal of Crystal Growth*, 2004. **264**: 216-22.

[5] Y. Wu, J. Xiang, C. Yang, W. Lu, and C.M. Lieber, Single-crystal metallic nanowires and metal/semiconductor nanowire heterostructures. *Nature*, 2004. 430: 61-65.

[6] J. I. Pascual, J. Mendez, J. Gomez-Herrero, A.M. Baro, N. Garcia, U. Landman, W.D.Luedtke, E.N. Bogachek, and H.P.Cheng, Properties of metallic nanowires-from conductance quantization to localization. *Science*, 1995. **267**: 1793-95.

[7] C. Chen, L. Wang, R.L. Li, G.H. Jiang, H.J. Yu, and T. Chen, Effect of silver nanowires on electrical conductance of system composed of silver particles. *Journal of Materials Science*, 2007. **42**: 3172-76.

[8] L. Guo, J. Nie, B. Du, Z. Peng, B. Tesche, and K. Kleinermanns, Thermo responsive polymer stabilized silver nanoparticles. *Journal of Colloid and Interface Science*, 2008. **319**: 175-81.

[9] J. Yang, J.Y. Lee, and H. Too, Core-shell Ag-Au nanoparticles from replacement reaction in organic medium. *Journal of Physical Chemistry B*, 2005. **109**: 19208-12.

[10] J.L.H. Chau, M.K. Hsu, C.C. Hsieh, and C.C. Kao, Microwave plasma synthesis of silver nanopowders. *Materials Letters*, 2005. **59**:905-08.

[11] M.Z. Si, Y. Fang, J.L. Peng, and P.X. Zhang, Nano-silver colloids prepared by electrolysis and research on its SERS activity. *Spectroscopy and Spectral Analysis*, 2007. 27: 948-52.

[12] Z.H. Liu, Z.Y. Liu, Q.H. Li, H.P. Wu, and D.M. Zhang, Morphology control of microsized spherical silver powder prepared by spray pyrolysis. *The Chinese Journal of Nonferrous Metals*, 2007: 17: 149-55.

[13] J. Keskinen, P. Ruuskanen, M. Karttunen, and S.P. Hannula, Synthesis of silver powder using a mechanochemical process. *Applied Organometallic Chemistry*, 2001. 15: 393-95.

[14] Y. Zhou, L. Hao, Y. Hu, Y. Zhu, and Z. Chen, Synthesis of nanowires and coral-shaped nanostructures of Ag by an ultraviolet photo-reduction technique at room temperature. *Chemistry Letters*, 2001, **30**: 1192-93.

[15] S.H. Yu, Y. S. Wu, J. Yang, Z. H. Han, Y. Xie, Y. T. Qian and X. M. Liu, A novel solventothermal synthetic route to nanocrystalline CdE (E = S, Se, Te) and morphological control. *Chemistry of Materials*, 1998. **10**: 2309-12.

[16] J. Yang, C. Xue, S.H. Yu, J.H. Zeng, and Y.T. Qian, General synthesis of semiconductor chalcogenide nanorods by using the monodentate ligand n-butylamine as a shape controller. *Angewandte Chemie International Edition*, 2002. **41**: 4697-700.

[17] B.D. Cullity, *Elements of X-Ray Diffraction*, 2nd edn. Addison-Wesley publishing company Inc., MA, 1978

[18] T. Theivasanthi, and M. Alagar, X-Ray Diffraction Studies of Copper Nanopowder. *Archives of Physics Research*, 2010. **1**: 112-17.

[19] C. R. M. Wronski, The size dependence of the melting point of small particles of tin. *British Journal of Applied Physics*, 1967. **18**: 1731-37

[20] T. Bachels, H.-J. Güntherodt, and R. Schäfer, Melting of Isolated Tin Nanoparticles. *Physical Review Letters*, 2000. 85: 1250-53.

[21] P.R. Couchman, and W.A. Jesser, Thermodynamic theory of size dependence of melting temperature in metals. *Nature*, 1977. **269**: 481-83.

[22] M. N. Rahaman, Ceramic processing and sintering, Dekker, New York, 1969. P389.

[23] M. Tsuji, K. Matsumoto, P. Jiang, R. Matsuo, X.L. Tang, and K.S.N. Kamarudin, Roles of Pt seeds and chloride anions in the preparation of silver nanorods and nanowires by microwave-polyol method, Colloids and Surfaces A-Physicochemical and Engineering Aspects, 2008. **316**: 266-77.

[24] Y.G. Sun, Y.D. Yin, B.T. Mayers, T. Herricks, and Y.N. Xia, Uniform silver nanowires synthesis by reducing $AgNO_3$ with ethylene glycol in the presence of seeds and poly(vinyl pyrrolidone). *Chemistry of Materials*, 2002. **14**: 4736-45.

[25] Y.G. Sun, B. Gates, B. Mayers, and Y.N. Xia, Crystalline Silver Nanowires by Soft Solution Processing. *Nano Letter,* 2002. **2**: 165-68.

CHAPTER 6 DEVELOPMENT OF HIGH-DISPERSIVE SILVER PARTICLES BY POLYOL PROCESS

6.1 Introduction

It is well known that conductive silver thick films have been used extensively in the front metallization contact in crystalline silicon solar cells due to their good electricity and solderability. For most of the commercial crystalline silicon solar cells, the silver thick film metallization is formed by screen-printing silver pastes on silicon wafers, followed by a firing process. As mentioned before, the silver front contact paste for crystalline silicon solar cells usually contains three principal constituents: silver particles, glass frit powders, and organic binder. Among them silver particles as the conductive phase represent 70-85% in weight of the paste with a mixture of various shaped particles in micro-size meter (predominantly spherical).

As previously mentioned, for better understanding and development of high-performance silver paste for crystalline silicon solar cells, all the functional raw materials (silver particles and glass frit) would be prepared in our study. In the previous chapter, the spherical micron silver particles with an average size of 1.2μm for silver front contact paste for crystalline silicon solar cells were prepared by the traditional liquid-phase chemical reduction method. However, the only drawback is that there is, to a small degree, agglomeration behavior between the silver particles, although the PVP as a protective agent was added into the reduction system. But for this reason, the silver thick film based on the slightly agglomerated silver particles exhibited not very good continuity, with a few big pores. The *I-V* measurement of the fabricated solar cells also indicated the inferiority of the silver particles prepared by the conventional chemical reduction method. To develop high-performance silver front contact paste for crystalline silicon solar cells, the agglomeration of silver particles should be overcome, which is also the goal of this study.

In fact, the dispersibility of silver particles in silver paste plays a key role in improving the photovoltaic performance of silicon solar cells due to its great influences on the screen printability and sintering of silver paste. It was reported that silver particles with high dispersibility are required for silver front contact paste to obtain even dense screen-printed thick film after sintering process **[1, 2]**. Guo et al. investigated the dispersibility effect of silver particles on microstructure of screen-printed silver thick films and electrical property of the crystalline silicon solar cells **[3]**. In his experiment, two kinds of silver particles with different dispersibility were used to prepare the test silver paste. Then the two test pastes were screen-printed on silicon wafers, followed by firing treatment. The experimental results demonstrated that the paste containing silver particles with high dispersibility formed even denser thick film than those of tick film based on agglomerated silver particles. Therefore, it is necessary to prepare high-dispersive silver particles to develop high-performance silver front contact paste for crystalline silicon solar cells.

Although many there are many reports on synthesis of silver particles and their application in silver paste, including silver front contact paste for silicon solar cells, most of the products are usually prepared by chemical reduction method, which tends to leads to agglomeration. Therefore, the goal of this study is to synthesize high dispersive silver particles by polyol process, and study their effects on photovoltaic performance of crystalline silicon solar cells. Moreover, for narrow fingers deposited by screen-printing with higher aspect ratio, smaller (< 1μm) silver particles are required. Therefore, the size of silver particles would also be optimized to enhance the performance of solar cells.

6.2 Experiment materials and equipment

6.2.1 Experiment materials

All the materials used in the experiments are listed in **Table 6.1.**

Table 6.1 Experiment materials

Name	Remark	Manufactory
Silver nitrate	AR.	China National Pharmaceutical Group Industry Corporation Ltd
Ethylene glycol	EG, AR.	Xilong Chemical Co., Ltd
Polyvinylpyrrolidone	AR. PVP40 , MW= 40000	Xilong Chemical Co., Ltd
Anhydrous ethyl alcohol	AR.	Xilong Chemical Co., Ltd
Acetone	AR.	Tianjin Fuchen Chemical Reagent Factory
Hydrochloric acid	AR.	Tianjin Fuchen Chemical Reagent Factory
Nitric acid	AR.	Tianjin Chemical Reagent Ltd.
Acetic acid	AR.	Tianjin Chemical Reagent Ltd.
Ethylene glycol	AR.	Xilong Chemical Co., Ltd
Terpineol	AR.	Xilong Chemical Co., Ltd

6.2.2 Equipment

All the equipment used in the experiments is listed in **Table 6.2.**

Table 6.2 Equipment list

Name of instrument	Instrument model	Manufactory
Rotary evaporator	RE-52	Shanghai Yarong Biochemical Apparatus Factory
Electric Stirrer	JJ-1	Shanghai Meipu Instrument Co., Ltd
Semi-automatic screen printing machine	SYP2230	Shenzhen Qiaopai Screen Machine Factory
Electric heating air-blowing drier	101-2	SHANGHAI WUYANGSHAN Shanghai Guangdi Instruments Equipment Co., Ltd
Magnetic Stirring Apparatus	78-1	Changzhou Aohua Instruments Equipment Co., Ltd
Electric heating mantle	EM 100	Electromantle, England
Ultrasonic generator	KQ3200E	Kunshan Ultrasonic Electronic Equipment co., ltd
Electronic balance	ES120	Shenzhen Zhicheng Electronic Balance Co., Ltd
Laboratory pH meter	PHB-5	Shanghai Hongji Instruments Equipment Co., Ltd

All-directional planetary ball mill	PMQW0.4L	Nanjing Shunchi Technology Development Co. Ltd
Oilless vacuum pump	AP-550V	Institute of Microelectronics of Chinese Academy of sciences
Oilless compressor	EWS24	Zhejiang Jonway Machinery & Electric Manufacture Co., Ltd
Three-roller mill	S65	Changzhou Wujin Xingye Mechanical Equipment Co., Ltd
Thermostat oil bath cauldron	HH-S_1	Changzhou Aohua Instruments Equipment Co., Ltd

6. 3 Preparation of high-dispersive silver particles by polyol method

6.3.1 Theoretical approach

(1) Agglomeration mechanism

It is well known that there is a so-called capillary and surface tension force between particles in an aqueous system. Pendular liquid bridges are formed due to the capillary force, as shown in **Figure 6.1**. During the drying process, particles are bound together by the liquid bridges through a combination of capillary pressure and surface tension force until the solid bonds are formed. That is to say in the drying process, particles are agglomerated together into aggregate structures. Therefore, in the traditional chemical reduction aqueous system, silver particles are obtained, but they tend to be agglomerated in the drying process. To solve this problem, a dispersant agent, such as PVP, gelatin and oleic acid, which are usually added into the reduction systems. However, it would bring new issues for the application of silver particles in front contact paste for crystalline silicon solar cells. For example, it will reduce the solid content of silver paste, which would decrease the line conductivity of silver electrodes.

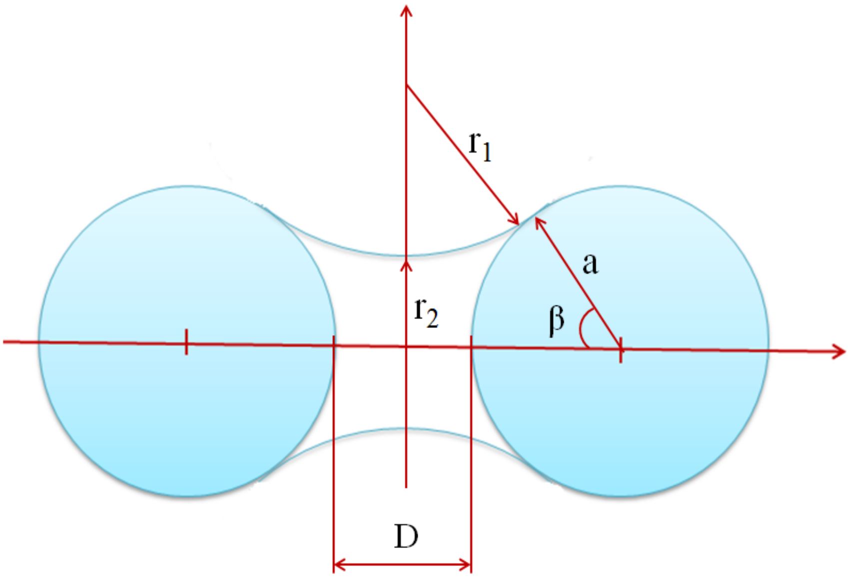

Figure 6.1 Schematic diagram of pendular liquid bridge formed by capillary and surface tension force between two spherical particles in aqueous system

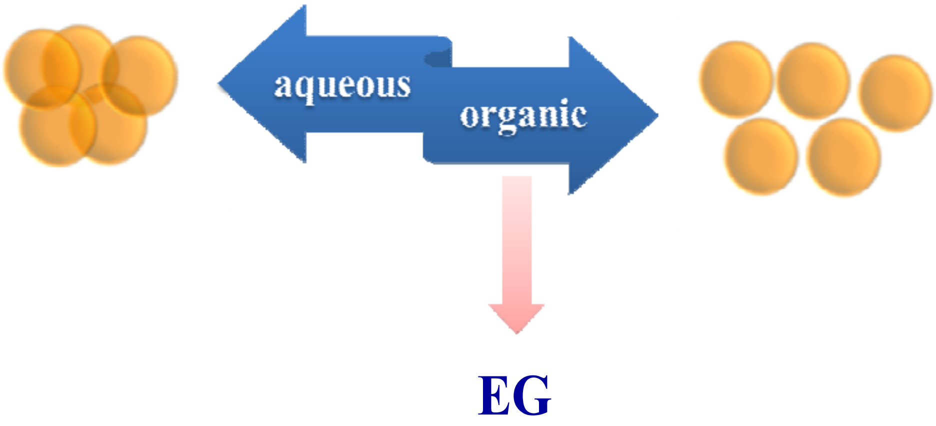

Figure 6.2 Schematic diagram of the mechanism of polyol process for preparing high-dispersive silver particles

Based on what has been mentioned above, it can be concluded that it is complicated to prepare the high-dispersive silver particles for silver front contact paste in the traditional chemical reduction aqueous system. In this section, we choose the polyol process to prepare silver particles. The main difference of these two methods is the reaction media, which are aqueous phase and organic phase, respectively, as shown in **Figure 6.2**.

(2) Polyol process

In fact, polyol process has been successfully used in preparation of metal nanoparticles or oxide materials in various shapes **[4-9]**. The biggest advantage of this method lies in its feasibility of preparing particles with mono-dispersibility. Typically, silver nanoparticles with high-dispersibility in various shapes have been reported **[10-16]**. Generally, silver particles can be obtained by reducing metal precursor by organic reducing agent, which usually serves as solvent at the same time during the polyol process. A certain amount of dispersant agent like PVP should also be added into the reduction system.

However, as far as we know, there is few study on the preparation of sub/micron silver particles by polyol process for their application in silver front contact paste for crystalline silicon solar cells. Therefore, in this work, we try to synthesis high dispersive silver particles in submicron size and study their application in silver front contact paste. Besides, a series of experiments would be carried out to optimize the products, including concentration, reaction time, reaction temperature, and so on. Moreover, the size, shape and growth control of silver particles would be studied in detail for their application in silver front contact paste.

6.3.2 Preparation

As mentioned above, the main difference between the traditional chemical reduction method and polyol process is the reaction media, aqueous phase and organic phase, respectively. In this work, we try to prepare silver particles in hot ethylene glycol, which serves as solvent and reducing agent at the same time. **Figure 6.3** shows the reaction principle for preparing silver particles by polyol process. Besides, to obtain high-dispersive silver particles with appropriate size and morphology, experimental parameters should be optimized, including concentrations of the agents, reaction time, temperature and so on.

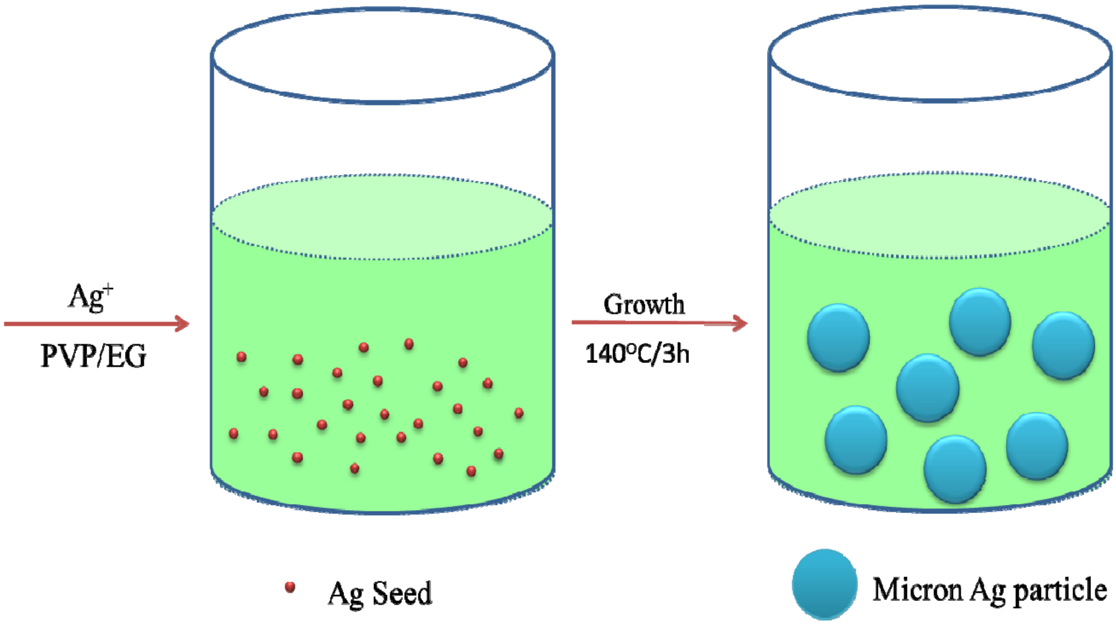

Figure 6.3 Schematic diagram of the reaction principle for synthesizing high-dispersive silver particles by polyol process at the optimal experimental condition

In a typical experiment, there are four steps for synthesizing silver particles in our work as follows:

(1) 15ml EG was refluxed in a three-necked flask at 140°C for one hour. Then 20ml EG solution of silver nitrate and PVP was added into the refluxing solution drop by drop under stirring.

(2) The final solution was further heated at 140°C for three hours after the addition ended.

(3) The solution was cooled down to room temperature naturally.

(4) The final silver particles were obtained after centrifugation, washing and drying in a vacuum oven. Subsequently, the product was used for producing silver paste.

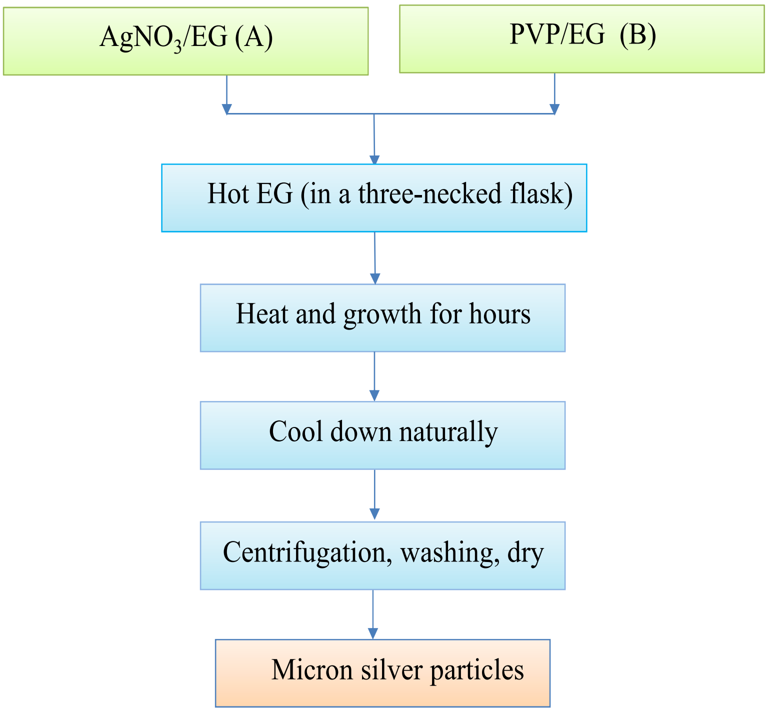

Figure 6.4 Flowchart for synthesizing submicron high-dispersive silver particles by polyol process

6.3.3 Morphology

The morphology of the as-prepared silver particles was observed by the scanning electron microscopy. **Figure 6.5** shows the SEM images of the silver particles synthesized by the polyol method under the optimal experimental condition, using silver nitrate as the metal source, ethylene glycol as the reducing agent and solvent and PVP as the dispersant agent. From the SEM, it is demonstrated that the silver particles are high-dispersive and quasi-spherical in shape, with an average size of 0.5μm.

Figure 6.6 shows the X-ray diffraction pattern of the as-prepared high-dispersive silver particles synthesized by the polyol method. The index process of the diffraction pattern was done and the *Miller indices* to each peak were identified. There are five strong peaks found in the diffraction pattern, which are identical to those of the FCC silver. And there are no crystallographic impurities. Moreover, the silver particles were well crystallized, which could be identified by the high-intensity peaks.

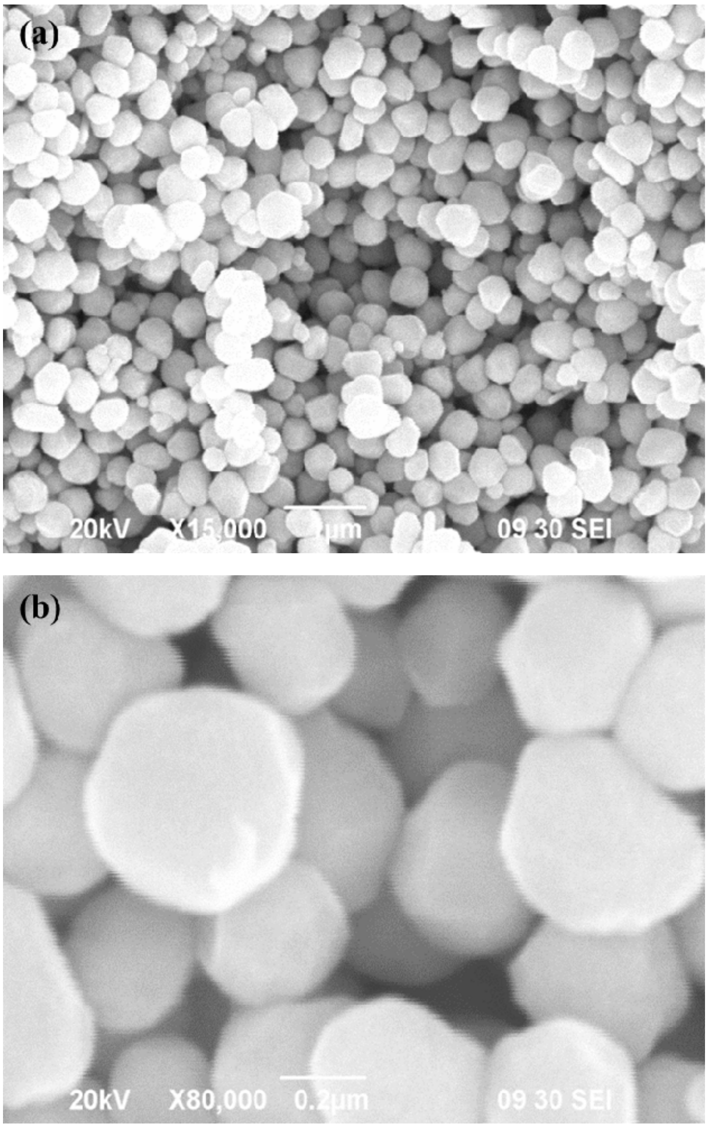

Figure 6.5 SEM micrographs of the silver particles prepared by polyol process: (a) low resolution, and (b) high resolution

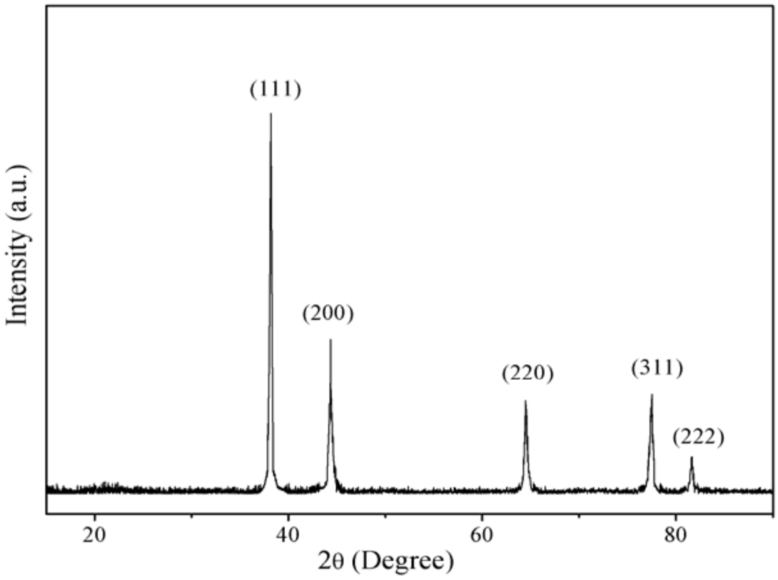

Figure 6.6 X-ray diffraction pattern of the as-prepared high-dispersive silver particles synthesized by polyol method

6.3.4 Effect on PV performance

According to what has been discussed above, it can be preliminarily deduced that the silver front contact paste resulting from the as-prepared high-dispersive silver particles tends to have a better front metallization contact and this in turn leads to better performance of solar cells. To determine the effect of the as-prepared silver particles on PV performance of silicon solar cells, the silver pastes containing the silver particles were prepared. Subsequently, the *I-V* characteristics of the fabricated crystalline silicon solar cells formed using the paste were measured.

In our previous chapter, the lead-free glass frit powders were prepared by the conventional melting route. Herein the silver pastes were prepared by mixing the as-prepared high-dispersive submicron silver particles, glass frit powders, and organic vehicles with the ratio of 80/4/16 by rotary evaporation method. The specific composition of the silver paste was shown in **Table 6.3**. Silver electrodes from the paste were formed by screen-printing the paste on crystalline silicon wafers with SiN_x coating layer, followed by a firing process in a conveyor infrared furnace.

Table 6.3 Compositions of silver paste based on the as-prepared high-dispersive silver particles synthesized by polyol process

Paste ID	Silver particles	Glass frit	Organic vehicle	Ratio
New	High-dispersive	Bi-based	ethyl celluloses + terpineol	80/4/16

As mentioned before, it is essential to obtain even dense thick film metallization to obtain high performance silicon solar cells. Therefore, it is necessary to study the sintering behavior of the as-prepared high-dispersive silver particles, and the corresponding thick film based on the silver particles. Here we observed the morphologies of the front thick film metallization formed using the silver paste containing the as-prepared high-dispersive silver particles. **Figure 6.7** shows the SEM top views of the silver electrodes **(a, b)**, and cross-section images of the front contact **(c, d)**. It is noticed that the silver thick film was even dense. Compared with the thick film (as shown in **Figure 3.12**) based on the particles synthesized by chemical reduction method, the thick film is denser, which has fewer and smaller pores. This improvement should be attributed to high dispersibility of silver particles synthesized by polyol method. Besides, Bi-precipitates and small silver crystallites, and a thin glass layer were formed, which demonstrated that the silver particles are sintered well, and an acceptable front metallization contacts were formed.

The photovoltaic performances of the crystalline silicon solar cells based on the silver paste containing the as-prepared high-dispersive silver particles are shown in **Figure 6.8**. It can be seen that the fabricated silicon solar cell generated an open-circuit voltage (V_{oc}) of 620mV, a short-circuit current density (J_{sc}) of 35.0mA/cm^2, a fill factor (FF) of 76.0% and a conversion efficiency (E_{ff}) of 16.4%. These are improved results compared with those resulting from the silicon solar cell based on the silver particles prepared by chemical reduction method, as illustrated in Chapter 3. Therefore, the developed high-dispersive silver particles are promising for its application in silver front contact paste for crystalline silicon solar cells.

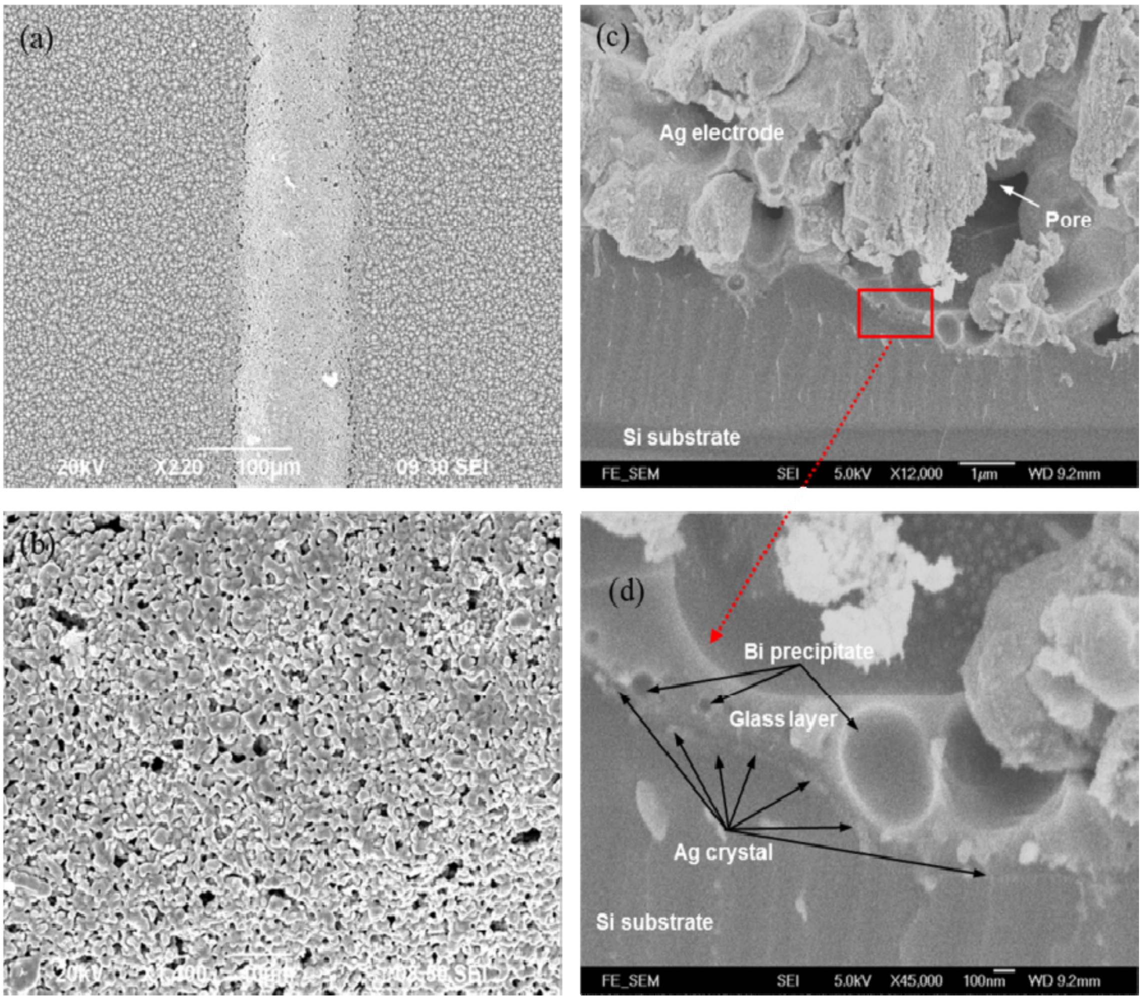

Figure 6.7 SEM images of the silver electrodes formed by screen printing the silver paste containing the as-prepared high-dispersive silver particles on silicon substrate: followed by firing process, top view of the silver electrode (a, b), and cross-section images of the front contact (c, d)

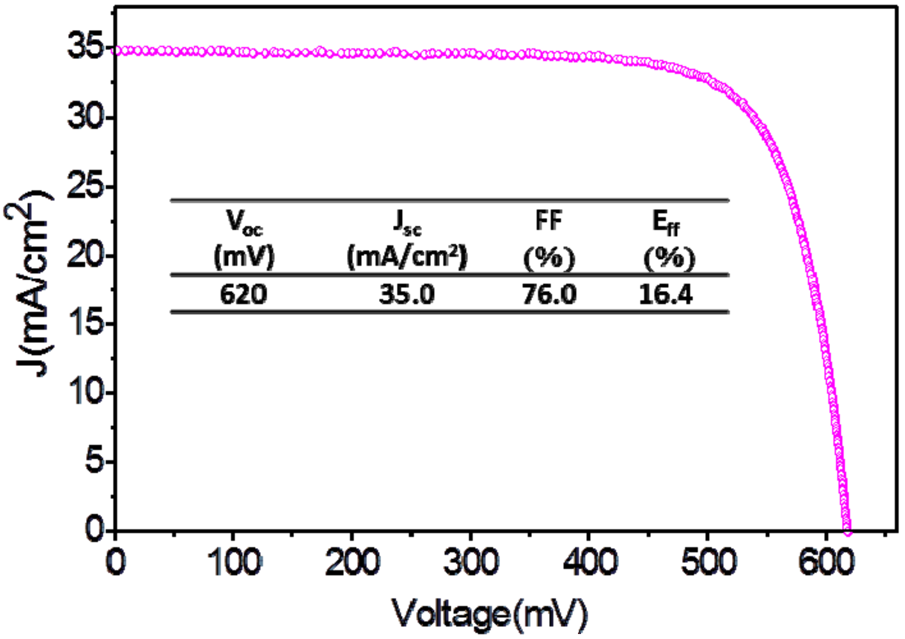

Figure 6.8 I-V performances of the fabricated crystalline silicon solar cell based on the silver paste containing the as-prepared high-dispersive silver particles under AM 1.5 (1000W/m^2)

6.4 Conclusions

The dispersibility of silver particles in silver paste plays a key role in photovoltaic performance of crystalline silicon solar cells since it greatly influences the screen printability and sintering behavior of a silver paste. To obtain high-quality thick film metallization with even dense structure and good conductivity, it is essential to overcome the agglomeration of silver particles. In this work, high-dispersive submicron silver particles were prepared by the polyol process in hot ethylene glycol. From the SEM, it is demonstrated that the silver particles are high-dispersive and quasi-spherical in shape, with an average size of 0.5μm. Experimental results demonstrated that the polyol process tends to obtain silver particles with better dispersibility compared with the aqueous reduction system. The silver paste composed of high-dispersive silver particles (80 wt%), lead free glass frit (4 wt%)

and organic vehicle (16 wt%) were screen-printed on single crystalline silicon wafers with SiNx antireflective coating, followed by a firing process. The fabricated solar cell based on the silver paste containing the as-developed high-dispersive silver particles generated a conversion efficiency of 16.4%.

References

[1] S.B. Rane, T. Seth, G.J. Phatak, D.P. Amalnerkar, and B.K. Das, Influence of surfactants treatment on silver powder and its thick films. *Materials Letters*, 2003. 57: 3096-100.

[2] J.C. Lin, and C.Y. Wang, Effects of surfactant treatment of silver powder on the rheology of its thick-film paste. *Materials Chemistry and Physics*, 1996. 45: 136-44.

[3] G. Guo, W. Gan, F. Xiang, J. Zhang, H. Zhou, H. Liu, and J. Luo, Effect of dispersibility of silver powders in conductive paste on microstructure of screen-printed front contacts and electrical performance of crystalline silicon solar cells. Journal of Materials Science: Materials in Electronics, 2011. **22**: 527-30.

[4] D. Kim, S. Jeong and J. Moon, Synthesis of silver nanoparticles using the polyol process and the influence of precursor injection. *Nanotechnology*, 2006. 17: 4019-24.

[5] C. Feldmann and H.O. Jungk, Polyol-mediated preparation of nanoscale oxide particles. *Angewante Chemie International Edition*, 2001. **40**: 359-62.

[6] Y.T. Chen, W. Zhang, B.Z. Hou, X.Q. Xu, Y.Q. Fan, Y.J. Guo, and Z.X. Zhang, Polyol process to large-scale synthesis of Cu_2O with disk-like structure. *Chinese Chemical Letters*, 2005. **16**: 245-48.

[7] G.G. Couto, J.J. Klein, W.H. Schreiner, D.H. Mosca, A.J.A. de Oliveira, and A.J.G. Zarbin, Nickel nanoparticles obtained by a modified polyol process: Synthesis, characterization, and magnetic properties. *Journal of Colloid and Interface Science*, 2007. **311**:461-68.

[8] H. Kawasaki, Y. Kosaka, Y. Myoujin, T. Narushima, T. Yonezawa and R. Arakawa, Microwave-assisted polyol synthesis of copper nanocrystals without using additional protective agents. *Chemical Communication*, 2011. **47**: 7740-42

[9] Y. Wang and K.S Kim, Large-scale polyol synthesis of single-crystal bismuth nanowires and the role of NaOH in the synthesis process. *Nanotechnology,* 2008. **19**: 265303.

[10] Y. Sun, B. Mayers, T. Herricks, and Y. Xia, Polyol synthesis of uniform silver nanowires: a plausible growth mechanism and the supporting evidence. *Nano Letters*, 2003. **3**: 955-60.

[11] S.E. Skrabalak, B.J. Wiley, M. Kim, E.V. Formo, and Y. Xia, On the polyol synthesis of silver nanostructures: glycolaldehyde as a reducing agent. *Nano letters*, 2008. **8**: 2077-81.

[12] P.Y. Silvert, R.H. Urbina, N. Duvauchelle, V. Vijayakrishnan and K.T. Elhsissen, Preparation of colloidal silver dispersions by the polyol process Part 1 -Synthesis and characterization. *Journal of Materials Chemistry,*1996. **6**: 573.

[13] A.R. Siekkinen, J.M. McLellan, J.Chen, and Y.Xia, Rapid synthesis of small silver nanocubes by mediating polyol reduction with a trace amount of sodium sulfide or sodium hydrosulfide. *Chemical Physics Letters*. 2006. **432**: 491-96.

[14] N.V. Nghia, N.N.K. Truong, N.M. Thong, and N.P. Hung, Synthesis of nanowire-shaped silver by polyol process of sodium chloride. *International Journal of Materials and Chemistry*, 2012. **2**: 75-78.

[15] A. Slistan-Grijalvaa, R. Herrera-Urbinab, J.F. Rivas-Silvac, M. Ávalos-Borjad, F.F. Castillón-Barrazad, and A. Posada-Amarillase, Assessment of growth of silver nanoparticles synthesized from an ethylene glycol-silver nitrate-

polyvinylpyrrolidone solution. *Physica E: Low-dimensional Systems and Nanostructures*, 2005. **25**: 438-48.

[16] A. R. Siekkinen, J. M. McLellan, J. Chen, Y. Xia, Rapid synthesis of small silver nanocubes by mediating polyol reduction with a trace amount of sodium sulfide or sodium hydrosulfide. *Chemical Physics Letters*, 2006. **432**: 491-96.

CHAPTER 7 CONCLUSIONS AND RECOMMENDATIONS FOR FUTURE WORK

7.1 Summary of the research results

As illustrated in Chapter 1, due to the significant shrinkage of silver paste during the firing process, it is difficult to achieve silver electrodes with high aspect ratio by screen-printing. This means that there would be high shading losses caused by a large percentage of front-side metal coverage. Besides, the inferior conductivity of the fired silver paste, which is several times lower than that of pure silver, largely limits the optimization of the metal contacts. In order to solve these problems, in this thesis, a series of new silver paste based on nanomaterials were designed. The silver nanoparticles/ nanowires with unique conductivity and sintering behavior are added into the silver paste to increase the line conductivity and obtain homogenously metallization contact, which in turn improve the performances of crystalline silicon solar cells. Besides, a lead-free nano glass frit was developed in this study and introduced into the silver front contact paste for the first time. Moreover, high-dispersive submicron silver particles were synthesized in hot ethylene glycol, which are favor to obtain high quality silver paste exhibiting good screen printability and sintering behavior.

First, for better understanding and development of a novel silver front contact paste based on nanomaterials, the preparation of conventional silver front contact pastes based on micron materials have been further developed. First of all, as the conduction phase in silver paste, micron spherical silver particles were synthesized by the chemical reduction method, using silver nitrate as the metal source, ascorbic acid as the reducing agent and PVP as the dispersant agent. The morphology and phase structure of the as-prepared silver particles were observed by the SEM and XRD, respectively. From the SEM, it is demonstrated that the silver particles are quasi-spherical in shape, with an average size of 1.2μm, which basically satisfy the requirement for application in silver front contact paste for crystalline silicon solar cells. Besides, the XRD pattern indicated that the silver particles were well crystallized with no crystallographic impurities. The only drawback is that there is, to a small degree, agglomeration behavior between the silver particles, although the PVP as a protective agent was added into the reduction system. Second, as the inorganic binder in the silver front contact paste, micron lead-free (Bi-Si-B-Al-Zn-O) glass frit powders were prepared by the conventional melting route. The amorphous state of the glass frit was identified by the result of X-ray diffraction, without any sharp peaks, and only broad peak can be found at around 28^{o}. The glass transition temperature is 385°C. Subsequently, the front contact silver pastes were prepared using the as-prepared silver particles, lead-free glass frit and organic vehicle (ethyl celluloses and terpineol) by the rotary evaporation method. For comparison, the silver pastes containing the commercial Pb-based glass frit were also prepared. The experiments indicated that the fabricated crystalline silicon solar cells containing the as-prepared Bi-based glass frit as an inorganic binder exhibited higher electrical conversion efficiency compared with that of the solar cell fabricated from the commercial lead-based glass frit. All other factors being equal except for the glass frit used in this work, this improvement should be attributed to the better metallization contact resulting from the Bi-based glass frit powder with better size distribution and lower T_g than those of the commercial Pb-based glass frit. It can be concluded that good front metallization contact of crystalline silicon solar cells can be achieved by using the as-developed Bi-based glass frit powders as an inorganic binder in the silver paste. Therefore, the as-prepared Bi-based glass frit is promising to substitute for the currently conventional Pb-based glass frit in silver front contact paste for crystalline silicon solar cells.

A new nano glass frit with low glass transition temperature (376°C) for silver front contact paste for crystalline silicon solar cells has been developed by the sol-gel method from a multicomponent gel in the Bi_2O_3-SiO_2-B_2O_3-Al_2O_3-ZnO system. In this wok, ethyl orthosilicate, aluminum nitrate nonahydrate, bismuth(III) nitrate pentahydrate, zinc nitrate hexahydrate and boric acid were used as the metal precursor. According to the thermal analysis of the xerogel, the temperature of 500°C was selected for heat treatment to obtain glass frit powders, which was further identified by the XRD result. From the XRD, it is demonstrated that the xerogel was completely converted into amorphous state glass frit. Besides, to determine the wetting behavior and etching effect during high temperature, the test glass paste containing the as-prepared nano glass was prepared, and deposited on silicon wafer, followed by a firing process. The experiments indicated that the nano glass frit exhibited excellent wetting behavior and etching effect. Furthermore, the fabricated crystalline silicon solar cells based on the silver paste containing the nano glass frit exhibited better photovoltaic performances than those of the solar cell fabricated resulting from the conventional micron glass frit powders. This improvement should be attributed to the better metallization contact resulting from the nano glass frit powders with small size and high purity. Besides, this work presented an experimental case for synthesizing nano glass frit with low glass transition temperature and its application in silver front contact paste for crystalline silicon solar cells. Moreover, this work can provide useful information for synthesizing nano glass frit powders using sol-gel method.

Besides, spherical silver nanoparticles (SSNPs)-aided silver pastes were developed using the SSNPs as a sintering aid. High-dispersive SSNPs were prepared by the solvothemal method, using silver nitrate as the metal source, ethylene glycol as the reducing agent and PVP as the dispersant agent. From the FESEM, it is demonstrated that the silver particles were spherical in shape, with an average size of 50nm, which agreed well with the calculation result from X-ray diffraction. The silver pastes composed of micron silver particles (70 wt%), the SSNPs (10 wt%), lead free glass frit (4 wt%) and organic vehicle (16 wt%) were screen-printed on single crystalline silicon wafers with SiN_x antireflective coating, followed by firing and tests. The experimental results demonstrated that the SSNPs with high surface energy are favor to the sintering of micron silver particles. Moreover, the size and numbers of pores in the silver thick films were reduced due to the SSNPs's unique sintering behavior, contributing to denser conductive network. In the current-voltage measurement, the fabricated solar cell based on the SSNPs-aided silver paste showed higher conversion efficiency (16.1%) than that (15.4%) resulting from the reference sample (solar cell containing no SSNPs).

Moreover, silver nanowires (SNWs)-aided silver pastes were also developed by adding the SNWs into micron silver particles. The SNWs were prepared by reducing $AgNO_3$ with ethylene glycol in the presence of seeds and PVP. Pt nanoparticles as crystal-seeds play a crucial effect on the anisotropic growth of silver nanowires. From the SEM, it is demonstrated that the silver nanowires were 100nm to 200nm wide and 0.5μm to 4μm long. The silver pastes composed of micron silver particles (70 wt%), SNWs (100nm to 200nm wide and 0.5μm to 4μm long, 10 wt%), lead free glass frit (4 wt%) and organic vehicle (16 wt%) were screen-printed on single crystalline silicon wafers with SiNx antireflective coating, followed by firing and tests. The fabricated solar cells based on the SNWs-aided paste generated an open-circuit voltage (V_{oc}) of 621mV, a short-circuit current density (J_{sc}) of 34.3mA/cm^2, a fill factor (FF) of 74.1% and a conversion efficiency (E_{ff}) of 15.8%. This improvement could be attributed to unique electronic property and “bridge-effect” of the one-dimensional (1-D) metal nanostructures.

Finally, high-dispersive submicron silver particles were prepared by polyol process in hot ethylene glycol. From the SEM, it is demonstrated that the silver particles are high-dispersive and quasi-spherical in shape, with an average size of 0.5μm. Experimental results demonstrated that the polyol process tends to obtain silver particles with better dispersibility compared with the aqueous reduction system. The silver paste composed of high-dispersive silver particles (80 wt%), lead free glass frit (4 wt%) and organic vehicle (16 wt%) were screen-printed on single crystalline silicon wafers with SiNx antireflective coating, followed by firing process. The fabricated solar cell based on the silver paste containing the as-developed high-dispersive silver particles generated a conversion efficiency of 16.4%.

7.2 Recommendations for Future Work

For the further work of the as-developed new silver front contact pastes for crystalline silicon solar cells, it is essential to optimize the functional materials to reduce the line resistance and contact resistance as low as possible. For cost-effective silver pastes, less silver content is needed to reduce the fabrication cost of solar cells. Although silver is the best choice for the front-side paste, high price limits largely its large scale application in the world. For the long run of photovoltaic production, it is necessary to replace the expensive sliver by other cheap metal due to the limitation of silver reserves. Cooper turns out to be the most promising substitute for silver for application in metal contact for crystalline silicon solar cells due to its great advantages **[1-3]**. However, the problem is that copper with high high diffusion coefficient in Si easily diffuses too deep to P-type layer of silicon wafer. It will cause shunting of the P-N juction. Therefore, it is necessary to prevent the high diffusion of Cu by inroducing a barrier layer on copper particles. Besides, copper is easy to be oxided, loosing conductivity.

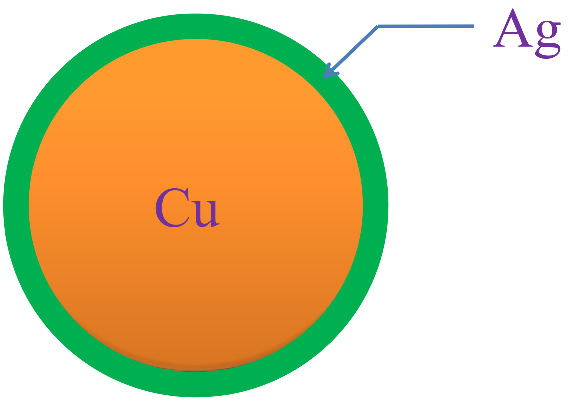

Figure 7.1 Schematic diagram of silver coated copper particles for application in front contact paste for crystalline silicon solar cells

To solve these issues, we are trying to prepare silver-coated copper particles to replace the silver particles in front contact pate. The structure of silver-coated copper particles is presented, as shown in **Figure 7.1**. The dense silver coating layer would be obtained by electroless plating method in aqueous system at room temperature. Completely removing the oxidation layer and and preventing the copper powder surface from hydrolysis are the two principle factors to obtain uniform silver/copper powders. From **Figure 7.1**, it is evident that the silver coated copper particles largely reduce the silver content in paste, at the same time satisfy the conduction requirement. This work is currently under study and will be reported in the near future.

References

[1] J. Kanga, J.S. Youb, C.S. Kangb, J.J. Pakc, and D. Kim, Investigation of Cu metallization for Si solar cells. *Solar Energy Materials & Solar Cells*, 2002. **74**: 91-96.

[2] E.J. Lee, D.S. Kim, and S.H. Lee, Ni/Cu metallization for low-cost high-efficiency PERC cells. *Solar Energy Materials & Solar Cells*, 2002. **74**:65-70.

[3] V. A. Chaudhari, and C.S. Solanki, A novel two step metallization of Ni/Cu for low concentrator c-Si solar cells. *Solar Energy Materials & Solar Cells*, 2010. **94**: 2094-2101.